Spring 1-1-2015

Osteochondral Tissue Modeling of Damage, Poroelastcity, and Remodeling in Osteoarthritis

Michael Eric Stender
University of Colorado Boulder, stender.michael@gmail.com

OSTEOCHONDRAL TISSUE MODELING OF DAMAGE, POROELASTICITY, AND REMODELING IN OSTEOARTHRITIS

by

MICHAEL ERIC STENDER

B.S., California Polytechnic State University, San Luis Obispo, 2011

M.S., California Polytechnic State University, San Luis Obispo, 2011

A thesis submitted to the

Faculty of the Graduate School of the

University of Colorado in partial fulfillment

Of the requirement for the degree of

Doctor of Philosophy

Department of Mechanical Engineering

2015

This thesis entitled:

Osteochondral tissue modeling of damage, poroelasticity, and remodeling in osteoarthritis

Written by Michael E. Stender

has been approved for the Department of Mechanical Engineering

_____

Committee Chair: Virginia L. Ferguson

_____

Richard A. Regueiro

Date: _____

The final copy of this thesis has been examined by the signatories, and we Find that both the content and the form meet acceptable presentation standards of scholarly work in the above mentioned discipline.

ABSTRACT

Osteochondral tissue modeling of damage, poroelasticity, and remodeling in osteoarthritis

Stender, Michael Eric (Ph.D. Mechanical Engineering)

Thesis directed by Associate Professor Virginia L. Ferguson

Arthritis is the most costly disability in the United States annually incurring billions of dollars in treatment costs and lost wages. Osteoarthritis, a classification of arthritis, affects articulating synovial joints (*e.g.,* hip, knee, shoulder) and results in moderate to severe pain. In extreme cases, osteoarthritis causes loss of joint mobility. Presently, there is not a clear understanding of how osteoarthritis initiates, propagates, and ultimately degrades the mechanics of healthy synovial joints. This doctoral work uses computational modeling techniques and finite element analysis to elucidate the initiation and evolution of osteoarthritis with the ultimate goal of contributing to improved clinical treatments. The first project was to develop a damage model for articular cartilage, the tissue lining the contact surfaces of synovial joints. An articular cartilage damage model was developed with the capability to model 3-D fully anisotropic damage including complete tissue tensile failure and progressive damage to critical structural elements. The second project was to develop

a model of the complete bone-cartilage unit including poroelastic material behavior (*i.e.,* solid-fluid interactions during loading of porous materials). This model demonstrated differences in poroelastic behavior between normal and osteoarthritic joint tissues and suggested that alterations in fluid flow patterns as a result of osteoarthritis may lead to increasingly diminished joint health. The final project integrated the first and second projects with a previously developed bone remodeling algorithm to study the initiation and progression behavior of osteoarthritis. This model showed that while articular cartilage damage and bone remodeling may initially as independent processes, they likely become interdependent as osteoarthritis progresses. Overall, these results improve our understanding of the *in vivo* mechanics of osteoarthritis initiation and progression and may guide future experimental and computational studies with the ultimate goal of improving clinical outcomes for osteoarthritis patients.

ACKNOWLEDGEMENTS

I would like to express my sincere gratitude to my primary research advisor Dr. Virginia L. Ferguson. Without her patience, hard work, and guidance throughout my time at CU Boulder this work would not have been possible. I would also like to sincerely thank Dr. Richard A. Regueiro for also overseeing my research and providing invaluable assistance and guidance in the development of my computational mechanics skills.

I would like thank the additional members of my dissertation committee, Dr. Dana Carpenter, Dr. Rong Long, and Dr. Franck Vernerey for contributing their time and energy to this work. Their advice and insight has proved to be extremely valuable over the course of the development of my dissertation.

During my doctoral studies, I have been very fortunate to have collaborated with a number of investigators and fellow students. I would like to thank Dr. Steve Klisch (Cal Poly, SLO) for his assistance and guidance in the development and publication of the work presented in Chapter 2. I would also like to thank Dr. Dana Carpenter (University of Colorado, Denver) for his ongoing efforts in the development and publication of the work in Chapter 4. I appreciate the opportunities I had to collaborate with my fellow Biomechanics and Biomimetics Lab members Dr. Kirsten Kinneberg-Mihalik and Dr. Brandi Briggs on their refreshingly different research projects; thank you both for letting me be a part of your work. I would also like to

thank the fellow members of the Biomechanics and Biomimetics Laboratory including Alicia, Brandi, Callie, Chelsea, Joseph, Julia, and Rachel for their friendship, kindness, and assistance. Their camaraderie in the sometimes bewildering process of graduate school was certainly one highlight of my experience at CU Boulder.

I would like to sincerely thank my wife and best friend Marissa for her unyielding support and encouragement of me throughout this endeavor. My family has been supportive throughout my many years of education. I cannot thank them enough for allowing me to get to this point. I would like to thank my friends both inside and outside of academia Drew, Kent, Kevin, Lucian, Marisa, Matt G., and Matt N. Your willingness to meet up and escape the 'real world' for a climb or a ski always keeps me smiling and motivated.

I am extremely grateful for the financial support I received, through my advisor Dr. Virginia L. Ferguson that enabled me to complete this dissertation work. This entirety of this work was made possible by NSF *CAREER* award #1055989, and the Innovative Grant Program at the University of Colorado Boulder.

Chapter 2 is reproduced, in full, from *The Journal of Biomechanical Engineering*, volume 127, issue 8 with permission from Beth Darchi. The dissertation author was the primary author of this paper and thanks co-authors Richard A. Regueiro, Stephen M. Klisch, and Virginia L. Ferguson. This work was funded by grants from the National Science Foundation (NSF), and the University of Colorado, Boulder.

Chapter 3 has been submitted for publication and is presented as it may appear in *Computer Methods in Biomechanics and Biomedical Engineering*. The dissertation was the primary author and thanks co-authors Richard A. Regueiro and Virginia L. Ferguson. This work was funded by grants from the National Science Foundation (NSF), and the University of Colorado, Boulder.

Chapter 4 will be submitted to for publication in *Biomechanics and Modeling in Mechanobiology.* The dissertation author was the primary author and thanks co-authors Richard A. Regueiro, R. Dana Carpenter, and Virginia L. Ferguson. This work was funded by grants from the National Science Foundation (NSF), and the University of Colorado, Boulder.

TABLE OF CONTENTS

LIST OF TABLES

LIST OF FIGURES

Chapter 1: Introduction

Chapter 2: A Constitutive Model of Articular Cartilage Damage

CHAPTER 1

INTRODUCTION

1.1 Background

The bone-cartilage unit, a phrase first coined by Lories & Luyten (2010), contains a large degree of structural and compositional complexity over relatively small length scales compared to traditional engineering problems. The bone-cartilage unit can be divided into six differential tissue zones defined from the articular surface as: the superficial zone of articular cartilage, the middle zone of articular cartilage, the deep zone of articular cartilage, the zone of calcified cartilage, subchondral cortical bone and trabecular bone (Figure 1). *In vivo*, the sizes and orientations of the differential tissues of the bone-cartilage unit vary with anatomical location (Ferguson *et al.*, 2003; Li & Aspden, 1997; Milz *et al.*, 1995). The variation in size and orientation of tissues in the bone-cartilage unit likely depends on loading conditions and patient-specific joint architecture. For example, the thickness of the subchondral cortical bone in the healthy human patella can vary from 100 μm to 2000 μm, and is likely thicker in regions of higher loading (Milz *et al.*, 1995; Norrdin *et al.*, 1999). Calcified cartilage thickness can also vary with location and disease state (Burr, 2004). In the human spine collagen fibril insertion angle as well as calcified cartilage thickness vary again likely due to the loading profile at a given location (Paietta *et al.*, 2013). Articular

cartilage composition, structure, and mechanical response can change based on depth from the articular surface (Aspden & Hukins, 1981; Schinagl *et al.*, 1997; Chen *et al.* 2001; Chen *et al.* 2007) and location and disease state (Mononen *et al.*, 2010, Mononen *et al.*, 2012; Temple-Wong *et al.* 2009). The variations inherent within the bone-cartilage unit coupled with the small length scales make comprehensive experimental assessment particularly challenging.

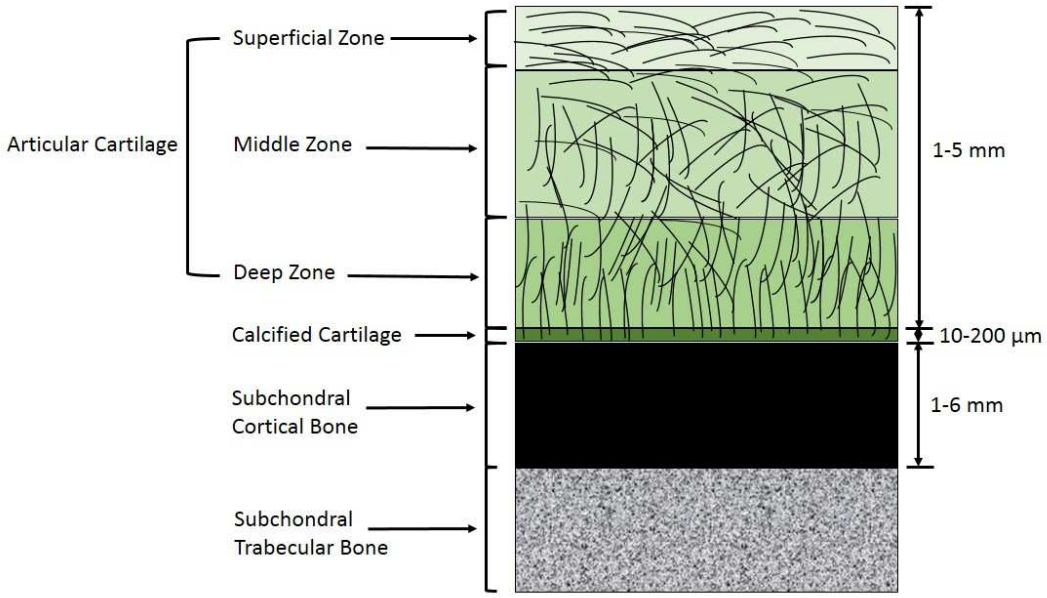

Figure 1. Illustration of an infinitesimal 2D slice of the bone-cartilage unit showing six differential tissue zones. Lines represent general orientation of type II collagen fibrils. Note the insertion of deep zone collagen fibrils into the calcified cartilage.

A primary goal of tissue engineering and other osteoarthritis treatment strategies is to regenerate surface cartilage to restore joint functionality, yet no technique has been able to successfully regenerate articular cartilage in clinical

studies (Gomoll *et al.* 2010). It is becoming increasingly apparent that the primary pathology of synovial joints, osteoarthritis, is a disease of the complete bone-cartilage unit, rather than a disease of solely articular cartilage (Brandt *et al.* 2006; Burr and Gallant 2012). Emerging osteoarthritis treatment strategies appear to focus on complete osteochondral grafts (Chan *et al.*, 2012; Gautier *et al.*, 2002) rather than replacement of one particular tissue. Contemporary tissue engineering of more complete osteochondral–mimetic units incorporating continuous material and chemical gradients (Mohan *et al.*, 2011), a calcified cartilage-like region (St-Pierre *et al.* 2012), a bone like region (Kitahara *et al.* 2008) or bilayer tissue scaffolds with differential moduli (Zhang *et al.* 2013) are increasingly popular. Although many of these osteoarthritis treatment strategies offer promising potential, there remains insufficient knowledge of the underlying mechanics of the osteochondral interface, and the complete bone-cartilage unit to successfully engineer bio-mimetic osteoarthritis treatments.

A limited amount of traditional mechanical tests have been performed with the aim of defining the mechanical response of calcified cartilage, subchondral cortical bone, and subchondral trabecular bone. Three point bending tests of 100-1000 μm thick samples of subchondral cortical and trabecular bone were used to establish elastic modulus values (Choi *et al.* 1990). Li and Aspden (1997) tested subchondral cortical bone from healthy and osteoarthritic samples in unconfined compression determining that osteoarthritic subchondral cortical bone tissue was stiffer and had a higher yield strength and apparent density compared to healthy bone. Three point

bending techniques were also applied to composite beams of subchondral cortical bone with and without a layer of calcified cartilage to determine the elastic modulus of calcified cartilage (Mente & Lewis, 1994). Furthermore, Choi *et al.* (1990) and Mente and Lewis (1994) have established that subchondral cortical bone is less stiff when compared to cortical bone. Nanoindentation studies have recently been applied to establish the micro scale indentation response of calcified joint tissues (Campbell *et al.* 2012; Ferguson *et al.*, 2003; Hauch *et al.*, 2009), yet such measurements are subject to variations in sample preparation and therefore fail to provide an absolute measurement of mechanical properties. The anisotropic properties of cortical bone have been well established at macroscopic (Reilly & Burstein 1974) and micro length scales (Fan *et al.*, 2002; Carnelli *et al.*, 2011) including post elastic micro scale behavior (Carnelli *et al.*, 2013). However, whether or not there exists an anisotropic mechanical response of subchondral cortical bone, or calcified cartilage has not been established experimentally. Further experimental work may in the future elucidate the specific mechanical responses of calcified cartilage, subchondral cortical bone, and subchondral trabecular bone.

1.2 Tissues of the Bone-Cartilage Unit

1.2.1 Articular Cartilage

Articular cartilage exists at the interface between opposing joint surfaces and provides a low-friction load-bearing surface that is essential to the overall function of the bone-cartilage unit. The solid matrix of articular cartilage is composed primarily of two mechanically relevant constituents: type II collagen fibrils and proteoglycan molecules (Maroudas *et al.*, 1980; Brocklehurst *et al.*, 1984). The collagen fibrils contribute primarily to the tensile integrity and Poisson's ratios of articular cartilage (Asanbaeva *et al.* 2008; Williams *et al.*, 2010). Proteoglycan, or glycosaminoglycan molecules impart an osmotic swelling pressure on the tissue (Maroudas *et al.* 1981; Asanbaeva *et al.*, 2007; Williams *et al.* 2010). Additional constituents make up a small volume fraction of the cartilage solid matrix including cartilage cells, or chondrocytes, additional proteins, type IV collagen fibrils, and other charged molecules (Kuettner 1992; Williamson *et al.* 2001). Patellar cartilage has been found to deform 3%-20% from equilibrium conditions after being subjected to walking and heavy loading (Eckstein *et al.*, 2006; Van de Velde, 2009). After sustained running loading, articular cartilage was found to exhibit a decrease in volume one hour following activity in all parts of the knee joint when compared to one hour prior to the run (Kersting *et al.*, 2005). During joint loading and articulation, shear strain of a magnitude of roughly 20-25% at surface decreased rapidly with depth from the articular surface to roughly

0% with no noticeable stress relaxation effects (Wong *et al.*, 2008). Despite the complex properties and mechanical response of articular cartilage, it is a tissue essential to the proper functioning of the bone-cartilage unit.

Arguably, the ability of articular cartilage to resist compressive forces developed during skeletal movement is the most essential function of the tissue. Many models have been proposed and experiments conducted with the intention of understanding the compressive resistance and inherent osmotic pressure of healthy, damaged, diseased and altered articular cartilage. Proteoglycan molecules in articular cartilage provide resistance to both compressive loading (Maroudas *et al.*, 1981; Chen *et al.*, 2007) and fluid flow (Maroudas *et al.*, 1968) and contribute to the overall capability of articular cartilage to resist compressive loads. Continuum electrochemical models of proteoglycan interactions have emerged as the primary means of modeling the compressive response and osmotic swelling pressure of the proteoglycan constituent of articular cartilage. The Donnan model which requires no assumption of molecular structure, but calculates an osmotic pressure based on the molecular fixed charge density (Overbeek, 1956) has been applied to calculate osmotic pressure in cartilage (Buschmann & Grodzinsky, 1995; Olsen *et al.*, 2004; Setton, 1998). A modification to the Donnan model was proposed by Buschmann and Grodzinsky (1995) wherein an additional term accounts for the molecular shielding of the proteoglycan molecules by adjacent proteoglycan molecules. The Poisson-Boltzmann unit cell electrochemical model which accounts for the spatially varying electrochemical forces and requires glycosaminoglycan molecule radius and

glycosaminoglycan intercharge distance as inputs has been shown to agree more closely with experimental osmotic pressure results for proteoglycans than either the Donnan, or the modified Donnan models (Buschmann and Grodzinsky 1995). Presently, the most accurate predictor of the electromechanical forces in articular cartilage is the Poisson-Boltzmann unit cell model (Buschmann & Grodzinsky 1995). Implementation of the Poisson-Boltzmann unit cell model in the context of a finite element analysis of articular cartilage is outlined by Stender *et al.*, (2012). These results provide a link between molecular scale interactions and continuum scale response essential to understanding the compressive response of articular cartilage.

Modeling of the anisotropic collagen fibril network of articular cartilage has received a great deal of attention due to the complexities, and importance of the collagen fibril network to the mechanical response of articular cartilage in tensile loading. In general, articular cartilage modeling studies that employ distinct stress constitutive equations for the collagen fibril network, rather than higher level material assumptions fall into three classes. The first class uses a discrete number of fibers defined explicitly (Bursac *et al.*, 2000; Thomas *et al.*, 2009), while the second employs a structural fiber reinforced finite element analysis (Li *et al.*, 1999; Wilson *et al.*, 2004; Wilson *et al.*, 2005). The third class of collagen fibril models implement continuum theories implementing a continuous fibril distribution (Lei & Szeri, 2006; Ateshian *et al.*, 2009; Stender *et al.*, 2012). The recent continuum theory model for the collagen fibril network of articular cartilage, developed by Shirazi *et al.*, (2011), accounts for experimentally measurable collagen fibril orientations and collagen fibril

tissue volume fraction as model input parameters and allows complete control of the spatial fiber distribution. The spatial distribution and modulus of type II collagen fibrils in articular cartilage have been shown to have significant effect on the mechanical response of articular cartilage in joint modeling studies (Mononen *et al.* 2010; Mononen *et al.*, 2012). These recent advances in collagen fibril network modeling have enabled an unprecedented capability and level of detail in collagen fibril modeling, and consequently the overall mechanics of articular cartilage.

Studies of soft biological tissues have suggested that the additional components of the solid matrix of articular cartilage, including chondrocytes, may contribute to the mechanical and electromechanical responses of articular cartilage tissue (Buschmann & Grodzinsky, 1995; Ehrlich *et al.*, 1998; Chahine *et al.*, 2005). The specific response of these additional constituents of articular cartilage, referred to here as the ground substance matrix, has not been directly determined experimentally. Previously, a Neo-Hookean material model was used to model the behavior of an individual chondrocyte (Baaijens *et al.*, 2005), and Neo-Hookean material models have been used to model the ground substance matrix of other tissues including arteries (Veress *et al.*, 2002; Holzapfel, 2006) and articular cartilage (Stender *et al.*, 2012). Stender *et al.*, (2012) showed that the inclusion of a ground substance matrix of articular cartilage helps to improve convergence properties of numerical models. Thus, the inclusion of the mechanical response of constituents other than collagen fibrils and proteoglycans appears to be a relevant and advantageous methodology.

The growth, degradation, and remodeling mechanisms of articular cartilage tissue are still not well understood today. *In vitro* culture in chemical growth factors have been observed to play a role in the matrix modulation and, consequently, the mechanical response of articular cartilage explants (Asanbaeva *et al.*, 2007; Ficklin *et al.*, 2007; Williams *et al.*, 2010; Balcom *et al.*, 2012). An initial theoretical study considered the independent growth and evolution of proteoglycan and collagen constituents in developing articular cartilage (Klisch *et al.*, 2003). Another finite element model studied the effects of differential growth triggers such as fluid velocity in unconfined compression in initiating an isotropic growth response in articular cartilage tissue (Davol *et al.*, 2007). Furthermore, a collagen fibril remodeling simulation has been conducted to determine the effect of differential loading conditions on collagen fibril orientations (Wilson *et al.*, 2006). Further work to establish relevant numerical models of articular cartilage damage may help to better understand the initiation and progression of osteoarthritis.

In vivo, articular cartilage exists as a saturated tissue and thus exhibits a poroelastic response and diffusive properties that are dependent on the permeability of the tissue when subjected to mechanical loading (Maroudas *et al.*, 1968). Additionally, articular cartilage exhibits a strain dependent permeability that was first established in a theoretical framework by Lai *et al.* (1980), and later extended to finite strain (Holmes and Mow 1990). Unlike traditional permeability studies applied to soils and other geomaterials where pore size, shape, and connectivity primarily define material permeability, the electrochemical properties of

proteoglycans provide the primary resistance to fluid flow through articular cartilage (Maroudas *et al.*, 1968). Additional studies have determined that the collagen fibril organization and the solid matrix structure may also play a role in the permeability properties of articular cartilage (Federico and Herzog 2007). The fluid pressure inside cartilage during confined compression loading has been measured experimentally using piezoelectric transducers. It was discovered that for loading durations up to 725 seconds in stress relaxation and 404 (sec) in creep loading, fluid pressure alone reacts more than 90% of the applied load (Soltz and Ateshian 1998). Experimentally, cartilage has demonstrated a decreasing permeability with increasing depth from the articular surface (Chen *et al.*, 2001, 2007; Williams *et al.*, 2010). Undoubtedly, the complex poroelastic properties of the solid matrix of articular cartilage play a significant role in joint mechanics, particularly for short (*i.e.*, less than 600 seconds) duration loading.

The determination of elastic Young's modulus of collagen fibrils in articular cartilage is complicated by the difficulty, using current methods, of experimentally measuring the elastic Young's modulus of type II collagen fibrils. Experimental testing of type I collagen fibers, that are structurally different from type II collagen fibrils, has established the elastic modulus of type I cartilage from the bovine Achilles tendon at roughly 430 MPa (Sasaki and Odajima 1996). An early estimate of the modulus of type II collagen fibrils in articular cartilage was 1-2 GPa (Elden, 1968). Because type II collagen fibril modulus cannot reliably be measured experimentally, modeling studies have sought to quantify the mechanical response of type II collagen

fibrils. Modeling studies have applied continuum mixture models fit to macroscopic mechanical tests to determine the elastic modulus of type II collagen fibrils. Lei & Szeri (2006) performed a parameter study to determine the response of differing collagen fibril orientations and estimated the true modulus of articular cartilage collagen fibrils at 625 MPa. Linear strain dependent (Li *et al.*, 1999, 2000) and viscoelastic (Wilson *et al.*, 2004; Wilson *et al.*, 2005; Julkunen *et al.*, 2008) models of independent type II collagen fibril response have also been proposed. A recent study established that the modulus of collagen fibrils in articular cartilage varied with depth increasing from the articular surface and fell between 175 MPa in the superficial layer and 422 MPa in the middle layer of newborn bovine articular cartilage (Stender *et al.*, 2012). Although there is not presently a precise consensus, estimates of the type II collagen fibril modulus in articular cartilage generally fall between 75 and 654 MPa (Farquhar *et al.*, 1990; Schwartz *et al.*, 1994; Soulhat *et al.*, 1999; Shirazi and Shirazi-Adl 2005; Lei & Szeri, 2006; Quinn and Morel 2007; Stender *et al.*, 2012). Molecular computational modeling studies have suggested that type II collagen fibrils are capable of attaining large deformations between 15% and 45% (Buehler, 2007; Buehler & Ackbarow, 2008; Gautieri *et al.*, 2011). An additional molecular modeling study examined the failure behavior of collagen fibrils showing that structural fibril parameters such as fibril length, fibril diameter, and cross link density had an effect on fibril failure properties in uniaxial stress in tension (Tang *et al.*, 2010). An experimental study using self-assembled uncrosslinked type I collagen fibers found fiber failure strains between 24% and 68% strain (Pins *et al.*, 1995).

There currently exists no concise description of the failure behavior or the failure strain of type II collagen fibrils.

1.2.2 Calcified Cartilage

Another tissue that is critical for the mechanical function of the bone-cartilage unit is calcified cartilage. Calcified cartilage forms a transitional zone that exists between articular cartilage and the subchondral bone at the osteochondral interface. The calcification of cartilage tissue is due to the deposition of calcium salts in the extracellular matrix resulting in a calcified tissue that is composed primarily of 3 constituents; 1) inorganic molecules including hydroxyapatite, 2) collagen fibrils, and 3) other organic molecules (Scherft 1968). It has been hypothesized that the insertion and anchoring of deep zone articular cartilage collagen fibrils into calcified cartilage helps to provide mechanical robustness at the osteochondral interface between unmineralized and mineralized tissue (Benninghoff, 1925; Aspden & Hukins, 1981; Paietta *et al.*, 2013). It has been observed that the thickness of the zone of calcified cartilage varies with location in the human spine (Paietta *et al.*, 2013) and in human Patellae (Milz *et al.*, 1995) likely depending on the loading conditions at specific anatomical sites. Hwang *et al.* (2010) studied the development of calcified cartilage tissue in 1-3 week old bovine samples finding that calcification takes place only in the deep zone of articular cartilage and results in a stiffer tissue post calcification. Subchondral bone remodeling has been observed to extend into the zone of calcified cartilage, specifically in areas of higher loading in equine carpal bones (Norrdin *et*

al., 1999). Although calcified cartilage appears to be of critical importance to the function of the osteochondral interface, it is not possible to separate the calcified cartilage from subchondral bone (Mente and Lewis 1994) making conventional mechanical tests impossible. Additionally, calcified cartilage tissue has a small thickness (10-200 μm) and an irregular geometry (Paietta *et al.*, 2013) making it very difficult to harvest samples appropriate for mechanical testing. Because of these difficulties, independent study of the mechanical properties of calcified cartilage is not possible using conventional methodology.

Researchers currently believe the elastic modulus of calcified cartilage to be roughly an order of magnitude less than the modulus of subchondral bone, or 0.32 GPa (Mente and Lewis 1994). In Mente and Lewis (1994), the modulus of calcified cartilage was determined by testing beam samples of only subchondral bone and composite beams of subchondral bone and attached calcified cartilage in three point bending. Linear elastic beam theory was used to calculate the modulus of subchondral bone from 3 point bending force vs. displacement curves. Additionally, linear elastic composite beam theory was applied to calculate calcified cartilage modulus by including subchondral bone modulus and calcified cartilage thickness as input parameters. By solving for the unknown of the calcified cartilage elastic modulus, the linear elastic modulus of calcified cartilage was determined. Although this study uses a clever methodology to determine calcified cartilage elastic modulus, linear elastic material behavior with the absence of any yield criteria, anisotropy, or post-yield

material behavior is an unlikely approximation of calcified cartilage and subchondral bone properties.

Nanoindentation has been applied to attempt to quantify the mechanical and structural properties of the bone-cartilage unit including calcified cartilage tissue (Ferguson *et al., 2003;* Gupta *et al.*, 2005; Hauch *et al.*, 2009; Campbell *et al.*, 2012). However, these methods lack a fundamental absolute quantification of the mechanical properties of calcified cartilage.

1.2.3 Subchondral and Trabecular Bone

Subchondral cortical and trabecular bone are stiff calcified tissues that transmit joint loads to weight bearing bones and permit robust mechanical function in the skeleton. Subchondral cortical bone lies adjacent to both the zone of calcified cartilage and subchondral trabecular bone providing a stiff underlying structure of the bone-cartilage unit. With remodeling and in osteoarthritis blood vessels are able to penetrate into subchondral cortical bone tissue and into calcified cartilage (Hwang *et al.*, 2008). In the healthy bone-cartilage unit, blood vessels promote and regulate cellular activity by transferring nutrients and signal molecules to cells and removing waste products. In general, subchondral cortical bone is considered to be similar to cortical bone in structure with longitudinal osteon structures that appear to lie parallel to the articular surface. Subchondral bone is the stiffest material in the bone-cartilage unit. However, the elastic modulus of subchondral cortical bone has been shown to be lower than that of cortical bone from the diaphysis of a bone (Choi *et al.*,

1990; Mente & Lewis 1994). Additionally it has been shown that subchondral cortical bone modulus depends on anatomical location (Choi *et al.*, 1990). Cortical bone from the diaphysis of a bone has been shown to exhibit fatigue, creep and eventual failure due to cyclical loading, with differential fracture surfaces from failure in tension or compression (Caler & Carter, 1989; Patten *et al.*, 1994). *In vivo*, subchondral cortical bone is a hydrated tissue and thus, is subject to poroelastic effects (Cowin 1999). Presently, no specific information on the permeability of isolated subchondral cortical bone is available in the literature. However, values for cortical bone permeability are well established (Cowin 1999; Baroud *et al.*, 2004) including spatial variations in flow (Uh & Watson, 2013). For the bone-cartilage unit the permeability of subchondral bone may play a greater role in exchange and/or pressurization of fluid across the osteochondral interface, rather than in the deformations of the subchondral cortical bone. The interactions of fluids in the bone-cartilage unit are not well understood and are likely to play an important role in the physiological functions of the region not only with regards to mechanical loading, but also cell nutrition and health.

Trabecular bone is a spongy, highly porous (pore size scale ~1mm) type of bone found at the ends long bones and in flat irregular bones. In the context of this study, subchondral trabecular bone is trabecular bone that directly supports the subchondral cortical bone beneath a joint surface. Trabecular bone continuum mechanical properties have been shown to be mildly anisotropic, and highly dependent on anatomical location in ultimate strength as well as modulus (Keaveny *et al.*, 2001). The yield strength of trabecular bone in compression depends on tissue

density while yield behavior in tension is independent of density and anatomical site (Kopperdahl and Keaveny 1998; Morgan and Keaveny 2001). Trabecular bone demonstrates creep behavior typical of metals and ceramics, and cyclic fatigue in compression that can lead to failure at sub yield stresses (Bowman *et al.*, 1994). Finite element modeling has been applied to trabecular bone modeling the complexities inherent with the structure of trabecular bone using "high resolution" finite element models that explicitly model the structure of experimental samples (Niebur *et al.*, 1999; Niebur *et al.*, 2000). To eliminate the complications and computational expense associated with high resolution trabecular bone models, the studies in this dissertation will assume a continuum solid matrix model for trabecular bone. The continuum assumption for trabecular bone has been discussed in detail by Harrigan *et al.* (1988) concluding that further than 3-5 trabeculae away from an interface, a continuum model is appropriate. Due to the high porosity of trabecular bone, intratrabecular permeability (fluid flow through the structure rather than through actual tissue) is anisotropic and depends on anatomical location (Nauman, Fong, and Keaveny 1999). Trabecular bone and its associated porous anisotropic structure is the final tissue in the bone-cartilage unit that transfers load applied to the articular surface to the rest of a long bone and the body.

1.3 Arthritis, the Primary Pathology of the Bone-Cartilage Unit

Arthritis is an extremely painful, debilitating, and expensive condition affecting millions of patients and costing billions of dollars annually in the United

States alone. Two types of arthritis, osteoarthritis and rheumatoid arthritis are the primary pathologies affecting synovial joints. Osteoarthritis is a progressive condition where the tissues of the bone-cartilage unit, including subchondral cortical bone and articular cartilage, break down over time resulting in a loss of joint function and severe pain. Osteoarthritis can occur in any joint, but is most common in the hands, neck, lower back, hips, and knees. Rheumatoid arthritis is an autoimmune disease that principally attacks synovial joints, resulting in the destruction of articular cartilage and leading to the degradation of the bone-cartilage unit, potentially debilitating pain, and loss of joint function. Osteoarthritis is a complex disease, and presently besides extreme traumatic injury to tissues of the bone-cartilage unit, the precise trigger, or sequence of triggers, that lead to osteoarthritis is not well understood. Studies of osteoarthritis are often capable only of examining the differences between a healthy control group and an osteoarthritic group(s) and thus, only the resulting effects, and not the precise causes of osteoarthritis are well understood. Increasingly, osteoarthritis is being viewed as a disease of the entire bone-cartilage unit rather than a disease or condition of any single tissue of the bone-cartilage unit (Burr, 2004; Brandt *et al.*, 2006; Burr & Gallant, 2012). The changes observed with osteoarthritis within joint tissues can be divided into two categories the first being compositional, or chemical changes in the constituents of joint tissues, and a second category that can be described by changes in the structure or form of tissues in the joint. Different studies have shown that variations in either or both of these categories can have profound effect in the load carrying capability of a healthy

joint (Li *et al.*, 1999; Hwang *et al.*, 2008; Sniekers *et al.*, 2008; Temple-Wong *et al.*, 2009). In general, there exist two pathways to arthritis the first being traumatic injury that either directly injures joint tissues, or an injury that dramatically changes the loading of a joint such (Figure 2.)

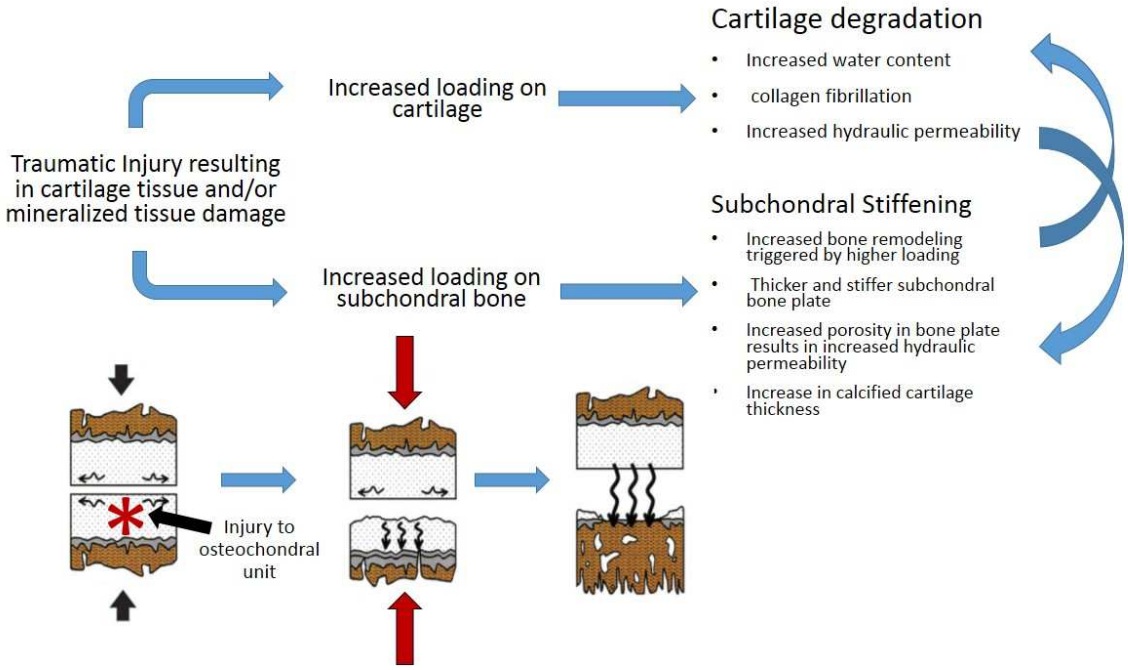

Figure 2. Diagram showing the progression of osteoarthritis following a traumatic injury that severely damages joint tissue, and/or alters the pattern of loading in a synovial joint. Images modified from Hwang *et al.* (2008).

The second form of osteoarthritis induction and propagation can be attributed to long term degradation resulting from sub threshold impulse loading (Radin *et al.*, 1972) wherein osteoarthritis progresses slowly rather than in a single traumatic event (Figure 3.)

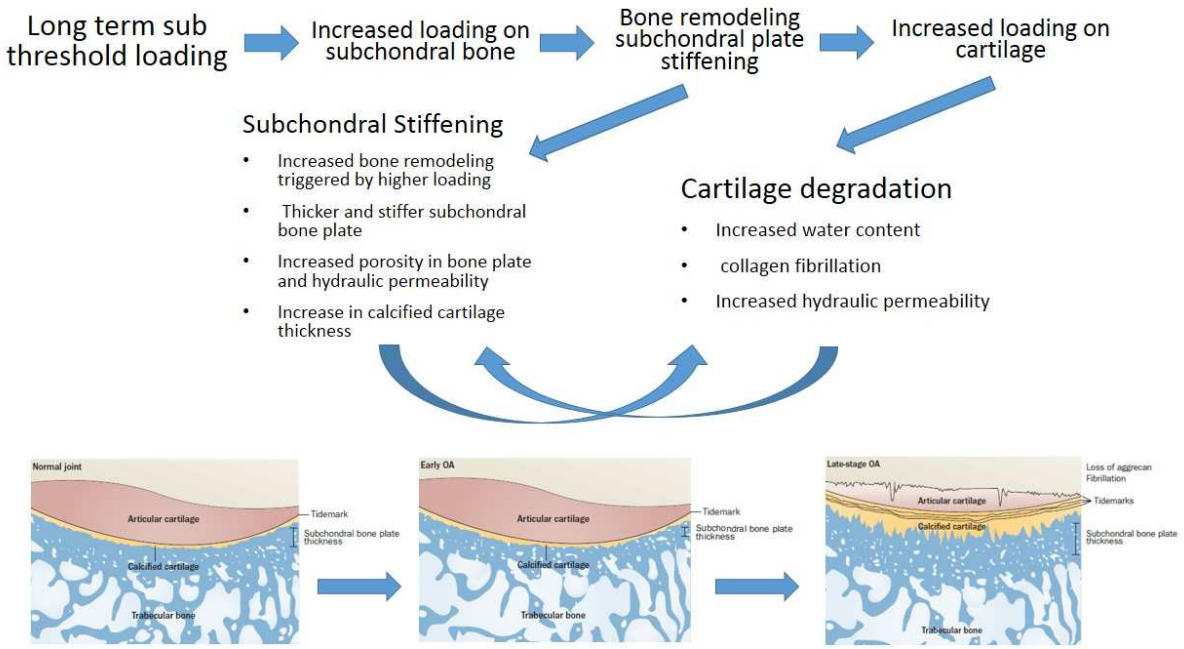

Figure 3. Pathway of osteoarthritis progression in the absence of a traumatic initiating event for osteoarthritis. Images modified from Burr and Gallant (2012).

The changes and evolution of joint structures with the onset and progression of osteoarthritis are complex. To better understand early onset arthritis, one study looked at the short term (2-14 weeks post osteoarthritis induction) effects of osteoarthritis induction on mice knees finding that the subchondral bone plate initially thins relative to healthy joints (up to 4 weeks) and then increases in thickness (up to 14 weeks) (Botter *et al.*, 2008). Another study observed increases in mineral content and thickness of calcified cartilage with osteoarthritis, and an increased rate of subchondral bone turnover such that the subchondral cortical bone becomes thicker and stiffer (Burr, 2004). Because subchondral and trabecular bone remodeling occurs at a much greater capacity, rate, and degree compared to articular cartilage, it has been hypothesized that for non-traumatic osteoarthritis, changes in

bone may antedate cartilage damage and degradation (Goldring and Goldring 2010). In a canine model of induced osteoarthritis, initial subchondral cortical bone thinning and increased bone plate porosity were observed at 10 and 20 weeks post-induction (Sniekers *et al.*, 2008). Additionally, increased bone porosity, a 'more textured surface,' and increased osteoclast resorption pits indicating increased remodeling activity were observed in human femoral heads from patients with osteoarthritis (Li *et al.*, 1999). Importantly, the hydraulic conductance of arthritic osteochondral tissue was measured as 2,700 times greater than that of healthy patients while subchondral plate only hydraulic conductance increased three fold with osteoarthritis compared to healthy samples (Hwang *et al.*, 2008; Mastbergen & Lafeber, 2011). The experimentally observed thickening of the subchondral plate and increase in calcified cartilage thickness can increase articular cartilage stresses and potentially causing damage resulting in further subchondral bone remodeling, thus altering the function of the healthy bone-cartilage unit. Following traumatic injury, markedly greater shear deformations have been measured partially due to altered synovial fluid composition that can be partially restored with the addition of hyaluronan (Wong *et al.*, 2010). Additionally, focal cartilage defects which can result from traumatic injury or surgical treatment have been shown to increase both strain adjacent to and opposing defects and magnitudes of steady state sliding forces (Gratz *et al.*, 2009). The alterations of normal tissue strains, sliding force magnitudes, and synovial fluid compositions may all contribute to accelerated tissue wear and degradation leading to osteoarthritis. Furthermore, an increase in hydraulic permeability can decrease

the pore fluid pressure held in the tissues of the bone-cartilage unit, forcing the solid skeletons of bone-cartilage unit tissues to carry additional loads potentially leading to additional remodeling and/or bone-cartilage unit tissue damage.

Molecular signaling between cells in articular cartilage and bone cells is possible in the healthy bone-cartilage unit, (Arkill & Winlove 2008). With the progression of osteoarthritis, the frequency of molecular signaling between articular cartilage and subchondral bone cells increases potentially due to the increased hydraulic conductance of the bone-cartilage unit (Hwang *et al.,* 2008; Lories and Luyten 2010). Human knee joints from healthy and osteoarthritic samples have been compared to study the compositional changes of articular cartilage with osteoarthritis. Osteoarthritic samples demonstrated a higher overall water content, and a decrease in proteoglycan content throughout all layers (Brocklehurst *et al.*, 1984;Temple-Wong *et al.*, 2009) which results in decreased compressive stiffness. Hwang *et al.* (2008) showed that in osteoarthritis, vascular canals can penetrate calcified cartilage, and eventually articular cartilage greatly increasing the permeability of the bone-cartilage unit. During osteoarthritis, progressive fibrillation of collagen fibrils which results in decreased mechanical integrity of collagen fibrils, a loss of organization of the collagen fibril network, and cartilage thickening starting at the surface and progressing into deeper layers and with increased severity has been observed (Temple-Wong *et al.*, 2009). In human patellar cartilage, early arthritis is characterized by a decrease in proteoglycan content and a loss of collagen network organization while late stage arthritis sees a decrease in overall collagen and

glycosaminoglycan content (Temple-Wong *et al.,* 2009; Saarakkala *et al.*, 2010). A comprehensive modeling study has yet to incorporate directly the effects of osteoarthritis in the context of a high precision poroelastic model, or a model incorporating the effects of tissue injury and damage.

A great deal of work has been done in the development of appropriate constitutive material models for soft biological materials such as tendon, ligament, arteries, and cartilage. However, only recently have constitutive material damage models for soft biological tissues emerged as an area of interest and study in finite element analysis. Typically, damage formulations for fibril reinforced composite material models of soft biological tissues develop ground matrix specific damage parameters for the ground matrix and independent damage parameters for the fibril network of the tissue (Calvo *et al.*, 2007; Weisbecker *et al.*, 2012), or solely for the fibril network (Gajewski *et al.*, 2013; Weisbecker *et al.*, 2012). In comparison to experimental tensile tests of the human aorta, a model accounting for accumulated damage of solely the fiber constituent (*i.e.*, no damage in the ground matrix of the tissue) showed better agreement with experimental data compared to a combined ground matrix and fibril model (Calvo *et al.*, 2007; Weisbecker *et al.*, 2012). Calvo *et al.* (2007) implemented a model wherein a minimum strain energy must be reached in order to incur damage, while Weisbecker *et al.* (2012) and Gajewski *et al.* (2013) do not include a minimum strain energy threshold for damage initiation. The development relevant damage models for articular cartilage would enable the

simulation of the initiation and progression behavior of osteoarthritis; an extremely difficult process to assess experimentally.

1.4 Finite Element Modeling and Techniques

1.4.1 Contact Modeling in Finite Element Analysis

Fundamental to full joint or partial joint finite element simulations is the inclusion of the geometrically nonlinear effects of contact between opposing surfaces. Within a finite element solution, a contact constraint can be exactly enforced using a Lagrange multiplier solution. Many traditional computational contact solutions are based on an augmented Lagrange method, where penalty terms are added to the Lagrange method to calculate contact properties (Cook *et al.*, 1979). Traditionally, contact formulations are enforced using a node-on-segment formulation where nodes in one surface are restricted from penetrating surfaces of the adjacent contacting surface which can result in locking in certain geometric situations, or finite deformations as often encountered in joint contact analysis. Additional improvements to the traditional finite element contact framework include segment-to-segment, or "mortar" contact which has been developed (Puso & Laursen, 2004; Laursen *et al.*, 2012) for finite deformations and large sliding. Mortar contact has demonstrated the potential to eliminate the locking issues associated with node-to-segment contact. The ability to model finite deformation contact and large sliding is an essential capability to appropriately simulate many finite element joint simulations.

The analysis of joint contact conditions presents an additional contact complication with the necessity of biphasic contact when modeling saturated contacting tissues *in vivo*. A Lagrange multiplier based method for two dimensional, small strain, biphasic contact has been developed by Donzelli and Spilker (1998), and extended to three dimensions by Yang and Spilker (2007), and finite deformations with large sliding by Chen *et al.*, (2005). Recently, a biphasic contact implementation that allows finite deformation, large sliding, and automatic enforcement of free draining outside of contact surfaces was developed for the free, open source finite element code FEBio (Ateshian *et al.*, 2010, Mass *et al.*, 2013). Two key features of the FEBio biphasic contact capability are the ability to automatically enforce a free draining boundary condition on contacting surfaces outside of the contacting region, and the capability to model tangential fluid flow at free surfaces. A comparison between default contact methods in ABAQUS, a modified Python/ABAQUS biphasic contact method, and FEBio determined that either FEBio or the Python/ABAQUS method could effectively simulate biphasic contact as seen in joints *in vivo* (Galbusera *et al.*, 2012). These recent developments in the finite deformation, large sliding, and biphasic contact formulations enable improved methods with which to evaluate with unprecedented precision joint contact problems *in vivo*.

1.4.2 Full Joint Finite Element Models

Full joint finite element models provide unparalleled insight into the precise mechanics of synovial joints. Full joint finite element models have been proposed as

a means of studying the responses of synovial joints to various loading scenarios and material formulations. Although not always explicitly stated, all of the full or partial joint models described below incorporate the bone-cartilage unit either through explicit modeling, or assumptions made within the context of the model. The first example of a joint contact model was done by Hirsch (1944) who applied a Hertzian contact formulation to two contacting elastic spheres. The emergence of finite element analysis allowed additional, more precise study of joint mechanics. Brown *et al.*, (1984) studied the static effects of subchondral stiffening due to surgical implants in the osteochondral region finding that subchondral implants stiffened the subchondral region and increased cartilage stresses. Another joint study (Eberhardt *et al.*, 1990) investigated the effects of differing joint geometry and included a deformable model for bone. One model took into account realistic joint geometry to study the equilibrium response of knee ligaments to various loading conditions (Bendjaballah *et al.*, 1997). A complete human knee joint model developed from computed tomography (*i.e.*, CT) scans (Donahue *et al.*, 2002) examined the effects of including subchondral cortical bone as deformable rather than rigid. Donahue *et al.* (2002) determined that the rigid assumption for bone had a less than 2% change in any contact variable in a complete knee joint model. A human hip joint model was used to determine the changes in contact pressure distributions with different hip joint geometries (Anderson *et al.*, 2010). The effects of poroelasticity were studied in a plane strain finite element model (Ferguson *et al.*, 2000) investigating the hip joint in long duration (~10,000 second) loading. The effect of different cartilage thickness in a full joint contact model was

studied by Li *et al.* (2001). Many early models were limited in size and complexity by a finite computational capability, and lack of understanding of joint tissues and thus, neglected a complete high fidelity study with the most accurate constitutive, contact, and poroelastic formulations of the osteochondral tissues.

Contemporary full joint models have taken advantage of increasing computational capacity and the current experimental base of knowledge to gain insight in joint behavior from increasingly complex joint models. The effects of different press fit tolerances and positioning on osteochondral implants was studied in a strain dependent permeability poroelastic model by Wu *et al.* (2002) who found that anything less than a perfect implant would adversely affect cartilage strain during physiological loading. Peña *et al.* (2007) studied the gait cycle of a knee with differing cartilage material properties in a solid phase only model assuming rigid bone. An anisotropic collagen fibril model was incorporated into a knee joint to study the effects of collagen fibril distributions on joint response (Shirazi *et al.*, 2008). Arguably, full joint models studying the effects of osteochondral defects demonstrate the best modeling treatments of the complete bone-cartilage unit currently available in the literature. A full knee joint model developed to explicitly model calcified cartilage, subchondral bone, trabecular bone, and cortical bone with linear elastic material models determined the effect of various hypothesized osteochondral defects, yet neglected poroelastic modeling of the tissues (Shirazi & Shirazi-Adl, 2009). Another model sought to include the effects of loading a joint using physically relevant muscle loading for a typical gait cycle (Adouni *et al.*, 2012). Vahdati and

Wagner (2009) simulated the effects of including a permeable layer of calcified cartilage distal to articular cartilage finding that calcified cartilage permeability had a negligible effect on steady-state stress, strain, and pore pressure measures, but did affect the transient response. Differential collagen fibril orientations resulting from injury, biology, and osteoarthritis were examined during impact loading in a poroelastic joint model by (Mononen *et al.*, 2012, 2011). Despite numerous contemporary full joint computational models, the precise behavior of the bone-cartilage unit still presents a frontier for investigation.

Near neighbor problems to full joint contact models also may provide insight and guidance in the development of improved joint modeling methods. For example, the insertions of tendons and ligaments into bone represent a material and compositional gradient somewhat similar to the bone-cartilage unit. Analytical two dimensional models of experimentally determined collagen fiber distributions at the bone tendon interface have indicated that the collagen fiber orientation serves to minimize stress concentrations and minimize interface mass (Thomopoulos *et al.*, 2006). However, experimental and analytical models of the tendon to bone interface suggest that the transition from tendon to bone occurs over longer length scales, and is less abrupt compared to the osteochondral interface in synovial joints (Genin *et al.*, 2009). A poroelastic model of tissue engineered constructs demonstrated that the addition of a "gel-bone" interface region similar to the bone-cartilage unit introduces inhomogeneous mechanical fields in the scaffold. Although the models described above do not comprehensively capture the behavior of the bone-cartilage unit *in vivo*,

because of assumptions made in boundary conditions and/or material properties that do not comprehensively reflect the *in vivo* behavior of the bone-cartilage unit, they do provide reasonable bounds for the mechanical properties of joint contact.

1.5 Innovation & Motivation for This Research

Despite the progress in bone-cartilage unit tissue characterization and material modeling work currently available in the literature, advancements in computational capability, and improvements in biomechanics modeling techniques, there still remains much insight to be gained from improved modeling studies of the complete bone-cartilage unit. Although the osteochondral interface, calcified cartilage, and subchondral bone plate tissues have been proven to be permeable, (Hwang *et al.*, 2008), there exists no bone-cartilage unit model that accounts for the effects of fluid flow between all the tissues of the bone-cartilage unit. Although the material properties and mechanical behavior of articular cartilage have been shown to be depth-dependent and inhomogeneous, (Aspden & Hukins, 1981b; Schinagl *et al.*, 1997; Asanbaeva, *et al.*, 2007; Chen, 2007; Klein, *et al.*, 2007; Williams *et al.*, 2010) a model incorporating the depth dependent osmotic pressures, collagen fibril distributions, permeability and porosity seen experimentally in articular cartilage has yet to be implemented. Although subchondral bone, trabecular bone, and cortical bone have all been proven to deform elastically, (Mente & Lewis, 1994; Niebur *et al.*, 2000; Carnelli *et al.*, 2011) almost all full joint models available in the literature treat these materials as rigid. Although articular cartilage has been shown to incur damage

resulting in mechanical degradation (Weightman, 1976; Weightman *et al.*, 1978; Jeffrey *et al.*, 1997; Bellucci & Seedhom, 2002; Lin, 2004; Bush *et al.*, 2005), no model has incorporated the anisotropic physically relevant effects of articular cartilage damage. Therefore, this study seeks to elucidate the functional mechanisms of load transfer across the bone-cartilage unit in healthy and osteoarthritic tissues through novel constitutive modeling and finite element analysis methods.

The overall objective of this work is to develop an improved understanding of the functional load transfer through the bone-cartilage unit in order to better understand the progression and initiation of osteoarthritis. This goal will be accomplished *via* three aims with each aim integrating together towards the ultimate goal. First, a thermodynamically consistent constitutive model of articular cartilage damage will be developed to create an unprecedented capability for modeling articular cartilage damage consistent with osteoarthritis. Second, a fully poroelastic and deformable finite element model of the bone-cartilage unit will shed light on the precise functional mechanics, including fluid flow paths throughout the bone-cartilage unit under healthy and with osteoarthritic tissue permeabilities. This complete poroelastic bone-cartilage unit model will be used to better understand time dependent loading, cell nutrition, tidemark advancement, and the consequences of increasing permeabilities in all tissues of the bone-cartilage unit observed to occur experimentally with osteoarthritis. Finally, the first and second aims will be combined with an established bone remodeling algorithm to create an evolutionary model of osteoarthritis including all tissues of the bone-cartilage unit. The previously

developed articular cartilage damage model from the first aim, and bone remodeling will capture the long term time dependent response of the bone-cartilage unit to mechanical loading. This complete evolutionary computational model of osteoarthritis will demonstrate how osteoarthritis initiates and progresses over time *in vivo* enabling researchers to more precisely develop treatments and prevention strategies for osteoarthritis. Combined, the three primary aims of this work serve to better inform future researchers, as well as experimental and computational studies with the ultimate goal of eliminating the pain, disability, and cost of osteoarthritis.

1.6 References

1. Adouni, M., A. Shirazi-Adl, and R. Shirazi 2012 Computational Biodynamics of Human Knee Joint in Gait: From Muscle Forces to Cartilage Stresses. Journal of Biomechanics 45(12): 2149–2156.
2. Anderson, Andrew E., Benjamin J. Ellis, Steve A. Maas, and Jeffrey A. Weiss 2010 Effects of Idealized Joint Geometry on Finite Element Predictions of Cartilage Contact Stresses in the Hip. Journal of Biomechanics 43(7): 1351–1357.
3. Arkill, K.P., and C.P. Winlove 2008 Solute Transport in the Deep and Calcified Zones of Articular Cartilage. Osteoarthritis and Cartilage 16(6): 708–714.
4. Asanbaeva, Anna, Koichi Masuda, Eugene J.-M. A. Thonar, Stephen M. Klisch, and Robert L. Sah 2007 Mechanisms of Cartilage Growth: Modulation of Balance between Proteoglycan and Collagen *in Vitro* Using Chondroitinase ABC. Arthritis & Rheumatism 56(1): 188–198.

5. Aspden, R. M., and D. W. L. Hukins 1981a Collagen Organization in Articular Cartilage, Determined by X-Ray Diffraction, and Its Relationship to Tissue Function. Proceedings of the Royal Society B: Biological Sciences 212(1188): 299–304.
6. 1981bCollagen Organization in Articular Cartilage, Determined by X-Ray Diffraction, and Its Relationship to Tissue Function. Proceedings of the Royal Society B: Biological Sciences 212(1188): 299–304.
7. Ateshian, Gerard A., Steve Maas, and Jeffrey A. Weiss 2010 Finite Element Algorithm for Frictionless Contact of Porous Permeable Media Under Finite Deformation and Sliding. Journal of Biomechanical Engineering 132(6): 061006.
8. Ateshian, Gerard A., Vikram Rajan, Nadeen O. Chahine, Clare E. Canal, and Clark T. Hung 2009 Modeling the Matrix of Articular Cartilage Using a Continuous Fiber Angular Distribution Predicts Many Observed Phenomena. Journal of Biomechanical Engineering 131(6): 061003.
9. Baroud, G., R. Falk, M. Crookshank, S. Sponagel, and T. Steffen 2004 Experimental and Theoretical Investigation of Directional Permeability of Human Vertebral Cancellous Bone for Cement Infiltration. Journal of Biomechanics 37(2): 189–196.
10. Bendjaballah, M. Z., A. Shirazi-Adl, and D. J. Zukor 1997 Finite Element Analysis of Human Knee Joint in Varus-Valgus. Clinical Biomechanics 12(3): 139–148.

11. Botter, S.M., G.J.V.M. van Osch, J.H. Waarsing, *et al.* 2008 Cartilage Damage Pattern in Relation to Subchondral Plate Thickness in a Collagenase-Induced Model of Osteoarthritis. Osteoarthritis and Cartilage 16(4): 506–514.
12. Bowman, Steven M., Tony M. Keaveny, Lorna J. Gibson, Wilson C. Hayes, and Thomas A. McMahon 1994 Compressive Creep Behavior of Bovine Trabecular Bone. Journal of Biomechanics 27(3): 301–310.
13. Brandt, K. D., E. L. Radin, P. A. Dieppe, and L. Van De Putte 2006 Yet More Evidence That Osteoarthritis Is Not a Cartilage Disease. Annals of the Rheumatic Diseases 65(10): 1261–1264.
14. Brocklehurst, R., M. T. Bayliss, A. Maroudas, *et al.* 1984 The Composition of Normal and Osteoarthritic Articular Cartilage from Human Knee Joints. J Bone Joint Surg Am 66: 95–106.
15. Brown, Thomas D., Eric L. Radin, R. Bruce Martin, and David B. Burr 1984Finite Element Studies of Some Juxtarticular Stress Changes due to Localized Subchondral Stiffening. Journal of Biomechanics 17(1): 11–24.
16. Buehler, Markus J 2007 Molecular Nanomechanics of Nascent Bone: Fibrillar Toughening by Mineralization. Nanotechnology 18(29): 295102.
17. Buehler, Markus J., and Theodor Ackbarow 2008 Nanomechanical Strength Mechanisms of Hierarchical Biological Materials and Tissues. Computer Methods in Biomechanics and Biomedical Engineering 11(6): 595–607.
18. Burr, D 2004 Anatomy and Physiology of the Mineralized Tissues: Role in the Pathogenesis of Osteoarthrosis. Osteoarthritis and Cartilage 12: 20–30.

19. Burr, David B., and Maxime A. Gallant 2012 Bone Remodelling in Osteoarthritis. Nature Reviews Rheumatology 8(11): 665–673.

20. Bush, P, P Hodkinson, G Hamilton, and A Hall 2005 Viability and Volume of Bovine Articular Chondrocytes Changes Following a Single Impact and Effects of Medium Osmolarity. Osteoarthritis and Cartilage 13(1): 54–65.

21. Calvo, B., E. Peña, M. A. Martinez, and M. Doblaré 2007 An Uncoupled Directional Damage Model for Fibred Biological Soft Tissues. Formulation and Computational Aspects. International Journal for Numerical Methods in Engineering 69(10): 2036–2057.

22. Campbell, Sara E., Virginia L. Ferguson, and Donna C. Hurley 2012 Nanomechanical Mapping of the Osteochondral Interface with Contact Resonance Force Microscopy and Nanoindentation. Acta Biomaterialia 8(12): 4389–4396.

23. Carnelli, Davide, Riccardo Lucchini, Matteo Ponzoni, Roberto Contro, and Pasquale Vena 2011 Nanoindentation Testing and Finite Element Simulations of Cortical Bone Allowing for Anisotropic Elastic and Inelastic Mechanical Response. Journal of Biomechanics 44(10): 1852–1858.

24. Carnelli, D., P. Vena, M. Dao, C. Ortiz, and R. Contro 2013 Orientation and Size-Dependent Mechanical Modulation within Individual Secondary Osteons in Cortical Bone Tissue. Journal of The Royal Society Interface 10(81): 20120953–20120953.

25. Chan, E. F., I.-L. Liu, E. J. Semler, *et al.* 2012 Association of 3-Dimensional Cartilage and Bone Structure with Articular Cartilage Properties in and Adjacent

to Autologous Osteochondral Grafts after 6 and 12 Months in a Goat Model. Cartilage 3(3): 255–266.

26. Chen, S 2007 Depth-Dependent Compressive Properties of Normal Aged Human Femoral Head Articular Cartilage: Relationship to Fixed Charge Density. Osteoarthritis and Cartilage 9(6): 561–569.
27. Cowin, S. C. 1999 Bone Poroelasticity. Journal of Biomechanics 32(3): 217–238.
28. Eckstein, F., M. Hudelmaier, and R. Putz 2006 The Effects of Exercise on Human Articular Cartilage. Journal of Anatomy 208(4): 491–512.
29. Federico, Salvatore, and Walter Herzog 2007 The Effect of Collagen Fibres on Permeability of Articular Cartilage. *In* Proceedings of the 31st Annual Meeting of the American Society of Biomechanics. http://www.asbweb.org/conferences/2007/149.pdf, accessed September 30, 2013.
30. Ferguson, S. J., J. T. Bryant, R. Ganz, and K. Ito 2000 The Influence of the Acetabular Labrum on Hip Joint Cartilage Consolidation: A Poroelastic Finite Element Model. Journal of Biomechanics 33(8): 953–960.
31. Ferguson, Virginia L., Andrew J. Bushby, and Alan Boyde 2003 Nanomechanical Properties and Mineral Concentration in Articular Calcified Cartilage and Subchondral Bone. Journal of Anatomy 203(2): 191–202.
32. Ficklin, Timothy, Gregory Thomas, James C. Barthel, *et al.* 2007 Articular Cartilage Mechanical and Biochemical Property Relations before and After *in Vitro* Growth. Journal of Biomechanics 40(16): 3607–3614.

33. Gajewski, Tomasz, Hannah Weisbecker, Gerhard A. Holzapfel, and Tomasz Lodygowski 2013 Implementation of a Hyperelastic Model for Arterial Layers Considering Damage and Distributed Collagen Fiber Orientations. http://www.ikb.poznan.pl/tomasz.gajewski/cad.put.poznan.pl/TG/cmm2013_gajewski_weisbecker_holzapfel_logydowski.pdf, accessed October 31, 2013.
34. Galbusera, Fabio, Maxim Bashkuev, Hans-Joachim Wilke, Aboulfazl Shirazi-Adl, and Hendrik Schmidt 2012 Comparison of Various Contact Algorithms for Poroelastic Tissues. Computer Methods in Biomechanics and Biomedical Engineering: 1–12.
35. Gautier, E., D. Kolker, and R. P. Jakob 2002 Treatment of Cartilage Defects of the Talus by Autologous Osteochondral Grafts. Journal of Bone & Joint Surgery, British Volume 84(2): 237–244.
36. Gautieri, Alfonso, Simone Vesentini, Alberto Redaelli, and Markus J. Buehler 2011 Hierarchical Structure and Nanomechanics of Collagen Microfibrils from the Atomistic Scale Up. Nano Letters 11(2): 757–766.
37. Genin, Guy M., Alistair Kent, Victor Birman, *et al.* 2009 Functional Grading of Mineral and Collagen in the Attachment of Tendon to Bone. Biophysical Journal 97(4): 976–985.
38. Goldring, Mary B., and Steven R. Goldring 2010 Articular Cartilage and Subchondral Bone in the Pathogenesis of Osteoarthritis: Articular Cartilage and Subchondral Bone. Annals of the New York Academy of Sciences 1192(1): 230–237.

39. Gomoll, Andreas H., Henning Madry, Gunnar Knutsen, *et al.* 2010 The Subchondral Bone in Articular Cartilage Repair: Current Problems in the Surgical Management. Knee Surgery, Sports Traumatology, Arthroscopy 18(4): 434–447.
40. Gratz, Kenneth R., Benjamin L. Wong, Won C. Bae, and Robert L. Sah 2009 The Effects of Focal Articular Defects on Cartilage Contact Mechanics. Journal of Orthopaedic Research 27(5): 584–592.
41. Gupta, H.S., S. Schratter, W. Tesch, *et al.* 2005 Two Different Correlations between Nanoindentation Modulus and Mineral Content in the Bone–cartilage Interface. Journal of Structural Biology 149(2): 138–148.
42. Harrigan, Timothy P., Murali Jasty, Robert W. Mann, and William H. Harris 1988 Limitations of the Continuum Assumption in Cancellous Bone. Journal of Biomechanics 21(4): 269–275.
43. Hauch, K.N., M.L. Oyen, G.M. Odegard, and T.L. Haut Donahue 2009 Nanoindentation of the Insertional Zones of Human Meniscal Attachments into Underlying Bone. Journal of the Mechanical Behavior of Biomedical Materials 2(4): 339–347.
44. Holmes, M. H., and V. C. Mow 1990 The Nonlinear Characteristics of Soft Gels and Hydrated Connective Tissues in Ultrafiltration. Journal of Biomechanics 23(11): 1145–1156.
45. Hosseini, S.M., W. Wilson, K. Ito, and C.C. van Donkelaar 2014 A Numerical Model to Study Mechanically Induced Initiation and Progression of Damage in Articular Cartilage. Osteoarthritis and Cartilage 22(1): 95–103.

46. Hull, M. L. 2002 A Finite Element Model of the Human Knee Joint for the Study of Tibio-Femoral Contact. Journal of Biomechanical Engineering 124(3): 273.
47. Hwang, Jennifer, Won C. Bae, Wendy Shieu, *et al.* 2008 Increased Hydraulic Conductance of Human Articular Cartilage and Subchondral Bone Plate with Progression of Osteoarthritis. Arthritis & Rheumatism 58(12): 3831–3842.
48. Hwang, J., E. M. Kyubwa, W. C. Bae, *et al.* 2010 *In Vitro* Calcification of Immature Bovine Articular Cartilage: Formation of a Functional Zone of Calcified Cartilage. Cartilage 1(4): 287–297.
49. Jeffrey, Janet E., L. Anne Thomson, and Richard M. Aspden 1997 Matrix Loss and Synthesis Following a Single Impact Load on Articular Cartilage *in Vitro*. Biochimica et Biophysica Acta (BBA)-General Subjects 1334(2): 223–232.
50. Julkunen, Petro, Rami K. Korhonen, Walter Herzog, and Jukka S. Jurvelin 2008 Uncertainties in Indentation Testing of Articular Cartilage: A Fibril-Reinforced Poroviscoelastic Study. Medical Engineering & Physics 30(4): 506–515.
51. Kersting, Uwe G., Johann J. Stubendorff, Matthias C. Schmidt, and Gert-Peter Brüggemann 2005 Changes in Knee Cartilage Volume and Serum COMP Concentration after Running exercise1. Osteoarthritis and Cartilage 13(10): 925–934.
52. Kitahara, Sota, Koichi Nakagawa, Robert L. Sah, *et al.* 2008 *In Vivo* Maturation of Scaffold-Free Engineered Articular Cartilage on Hydroxyapatite. Tissue Engineering Part A 14(11): 1905–1913.

53. Klein, Travis J., Manu Chaudhry, Won C. Bae, and Robert L. Sah 2007 Depth-Dependent Biomechanical and Biochemical Properties of Fetal, Newborn, and Tissue-Engineered Articular Cartilage. Journal of Biomechanics 40(1): 182–190.
54. Klisch, Stephen M., Silvia S. Chen, Robert L. Sah, and Anne Hoger 2003 A Growth Mixture Theory for Cartilage With Application to Growth-Related Experiments on Cartilage Explants. Journal of Biomechanical Engineering 125(2): 169.
55. Kopperdahl, David L., and Tony M. Keaveny 1998 Yield Strain Behavior of Trabecular Bone. Journal of Biomechanics 31(7): 601–608.
56. Laursen, Tod A., Michael A. Puso, and Jessica Sanders 2012 Mortar Contact Formulations for Deformable–deformable Contact: Past Contributions and New Extensions for Enriched and Embedded Interface Formulations. Computer Methods in Applied Mechanics and Engineering 205-208: 3–15.
57. Lei, Fulin, and Andras Z. Szeri 2006 The Influence of Fibril Organization on the Mechanical Behaviour of Articular Cartilage. Proceedings of the Royal Society A: Mathematical, Physical and Engineering Sciences 462(2075): 3301–3322.
58. Li, Baohua, and Richard M. Aspden 1997 Mechanical and Material Properties of the Subchondral Bone Plate from the Femoral Head of Patients with Osteoarthritis or Osteoporosis. Annals of the Rheumatic Diseases 56(4): 247–254.
59. Li, Baohua, Deborah Marshall, Martin Roe, and Richhard M. Aspden 1999The Electron Microscope Appearance of the Subchondral Bone Plate in the Human Femoral Head in Osteoarthritis and Osteoporosis. Journal of Anatomy 195(1): 101–110.

60. Li, Guoan, Orlando Lopez, and Harry Rubash 2001 Variability of a Three-Dimensional Finite Element Model Constructed Using Magnetic Resonance Images of a Knee for Joint Contact Stress Analysis. Journal of Biomechanical Engineering 123(4): 341.
61. Li, L. P., M. D. Buschmann, and A. Shirazi-Adl 2000 A Fibril Reinforced Nonhomogeneous Poroelastic Model for Articular Cartilage: Inhomogeneous Response in Unconfined Compression. Journal of Biomechanics 33(12): 1533–1541.
62. Li, L. P., J. Soulhat, M. D. Buschmann, and A. Shirazi-Adl 1999 Nonlinear Analysis of Cartilage in Unconfined Ramp Compression Using a Fibril Reinforced Poroelastic Model. Clinical Biomechanics 14(9): 673–682.
63. Lima, Eric G., Robert L. Mauck, Shelley H. Han, *et al.* 2004 Functional Tissue Engineering of Chondral and Osteochondral Constructs. Biorheology 41(3): 577–590.
64. Lories, Rik J., and Frank P. Luyten 2010 The Bone–cartilage Unit in Osteoarthritis. Nature Reviews Rheumatology 7(1): 43–49.
65. Maroudas, A., M. T. Bayliss, and M. F. Venn 1980 Further Studies on the Composition of Human Femoral Head Cartilage. Annals of the Rheumatic Diseases 39(5): 514–523.
66. Mastbergen, S. C., and F. P. J. G. Lafeber 2011 Changes in Subchondral Bone Early in the Development of Osteoarthritis. Arthritis & Rheumatism 63(9): 2561–2563.

67. Mente, P. L., and J. L. Lewis 1994 Elastic Modulus of Calcified Cartilage Is an Order of Magnitude Less than that of Subchondral Bone. Journal of Orthopaedic Research 12(5): 637–647.

68. Milz, S., F. Eckstein, and R. Putz 1995 The Thickness of the Subchondral Plate and Its Correlation with the Thickness of the Uncalcified Articular Cartilage in the Human Patella. Anatomy and Embryology 192(5): 437–444.

69. Mohan, Neethu, Nathan H. Dormer, Kenneth L. Caldwell, *et al.* 2011 Continuous Gradients of Material Composition and Growth Factors for Effective Regeneration of the Osteochondral Interface. Tissue Engineering Part A 17(21-22): 2845–2855.

70. Mononen, M. E., P. Julkunen, J. Töyräs, *et al.* 2010 Alterations in Structure and Properties of Collagen Network of Osteoarthritic and Repaired Cartilage Modify Knee Joint Stresses. Biomechanics and Modeling in Mechanobiology 10(3): 357–369.

71. Mononen, M.E., M.T. Mikkola, P. Julkunen, *et al.* 2012 Effect of Superficial Collagen Patterns and Fibrillation of Femoral Articular Cartilage on Knee Joint mechanics—A 3D Finite Element Analysis. Journal of Biomechanics 45(3): 579–587.

72. Morgan, Elise F., and Tony M. Keaveny 2001 Dependence of Yield Strain of Human Trabecular Bone on Anatomic Site. Journal of Biomechanics 34(5): 569–577.

73. Nauman, Eric A., K. E. Fong, and T. M. Keaveny 1999 Dependence of Intertrabecular Permeability on Flow Direction and Anatomic Site. Annals of Biomedical Engineering 27(4): 517–524.

74. Niebur, G. L., M. J. Feldstein, J. C. Yuen, T. J. Chen, and T. M. Keaveny 2000 High-Resolution Finite Element Models with Tissue Strength Asymmetry Accurately Predict Failure of Trabecular Bone. Journal of Biomechanics 33(12): 1575–1583.

75. Norrdin, R. W., C. E. Kawcak, B. A. Capwell, and C. W. McIlwraith 1999 Calcified Cartilage Morphometry and Its Relation to Subchondral Bone Remodeling in Equine Arthrosis. Bone 24(2): 109–114.

76. Olsen, S., A. Oloyede, and C. Adam 2004 A Finite Element Formulation and Program to Study Transient Swelling and Load-Carriage in Healthy and Degenerate Articular Cartilage. Computer Methods in Biomechanics and Biomedical Engineering 7(2): 111–120.

77. Paietta, Rachel C., Evalina L. Burger, and Virginia L. Ferguson 2013 Mineralization and Collagen Orientation throughout Aging at the Vertebral Endplate in the Human Lumbar Spine. Journal of Structural Biology. http://linkinghub.elsevier.com/retrieve/pii/S1047847713002177, accessed October 15, 2013.

78. Peña, Estefanía, Begoña Calvo, Miguel Angel Martínez, and Manuel Doblaré 2007 Effect of the Size and Location of Osteochondral Defects in Degenerative

Arthritis. A Finite Element Simulation. Computers in Biology and Medicine 37(3): 376–387.

79. Puso, Michael A., and Tod A. Laursen 2004 A Mortar Segment-to-Segment Contact Method for Large Deformation Solid Mechanics. Computer Methods in Applied Mechanics and Engineering 193(6): 601–629.

80. Radin, EricL, IgorL Paul, and Robert M Rose 1972 Role of Mechanical Factors in Pathogenesis of Primary Osteoarthritis. The Lancet 299(7749): 519–522.

81. Saarakkala, S., P. Julkunen, P. Kiviranta, *et al.* 2010 Depth-Wise Progression of Osteoarthritis in Human Articular Cartilage: Investigation of Composition, Structure and Biomechanics. Osteoarthritis and Cartilage 18(1): 73–81.

82. Sasaki, Naoki, and Shingo Odajima 1996 Elongation Mechanism of Collagen Fibrils and Force-Strain Relations of Tendon at Each Level of Structural Hierarchy. Journal of Biomechanics 29(9): 1131–1136.

83. Scherft, J. P. 1968 The Ultrastructure of the Organic Matrix of Calcified Cartilage and Bone in Embryonic Mouse Radii. Journal of Ultrastructure Research 23(3): 333–343.

84. Schinagl, Robert M., Donnell Gurskis, Albert C. Chen, and Robert L. Sah 1997 Depth-Dependent Confined Compression Modulus of Full-Thickness Bovine Articular Cartilage. Journal of Orthopaedic Research 15(4): 499–506.

85. Shirazi, R., and A. Shirazi-Adl 2009 Computational Biomechanics of Articular Cartilage of Human Knee Joint: Effect of Osteochondral Defects. Journal of Biomechanics 42(15): 2458–2465.

86. Shirazi, R., A. Shirazi-Adl, and M. Hurtig 2008 Role of Cartilage Collagen Fibrils Networks in Knee Joint Biomechanics under Compression. Journal of Biomechanics 41(16): 3340–3348.

87. Shirazi, R., P. Vena, R. L. Sah, and S. M. Klisch 2011 Modeling the Collagen Fibril Network of Biological Tissues as a Nonlinearly Elastic Material Using a Continuous Volume Fraction Distribution Function. Mathematics and Mechanics of Solids 16(7): 706–715.

88. Sniekers, Yvonne H, Femke Intema, Floris PJG Lafeber, *et al.* 2008 A Role for Subchondral Bone Changes in the Process of Osteoarthritis; a Micro-CT Study of Two Canine Models. BMC Musculoskeletal Disorders 9(1): 20.

89. Soltz, Michael A., and Gerard A. Ateshian 1998 Experimental Verification and Theoretical Prediction of Cartilage Interstitial Fluid Pressurization at an Impermeable Contact Interface in Confined Compression. Journal of Biomechanics 31(10): 927–934.

90. Stender, Michael E., Christopher B. Raub, Kevin A. Yamauchi, *et al.* 2012 Integrating qPLM and Biomechanical Test Data with an Anisotropic Fiber Distribution Model and Predictions of TGF- ß1 and IGF-1 Regulation of Articular Cartilage Fiber Modulus. Biomechanics and Modeling in Mechanobiology. http://link.springer.com/10.1007/s10237-012-0463-y, accessed April 20, 2013.

91. St-Pierre, Jean-Philippe, Lu Gan, Jian Wang, *et al.* 2012 The Incorporation of a Zone of Calcified Cartilage Improves the Interfacial Shear Strength between *in*

Vitro-Formed Cartilage and the Underlying Substrate. Acta Biomaterialia 8(4): 1603–1615.

92. Tang, Y., R. Ballarini, M. J. Buehler, and S. J. Eppell 2010 Deformation Micromechanisms of Collagen Fibrils under Uniaxial Tension. Journal of The Royal Society Interface 7(46): 839–850.

93. Temple-Wong, M.M., W.C. Bae, M.Q. Chen, *et al.* 2009 Biomechanical, Structural, and Biochemical Indices of Degenerative and Osteoarthritic Deterioration of Adult Human Articular Cartilage of the Femoral Condyle. Osteoarthritis and Cartilage 17(11): 1469–1476.

94. Thomas, Gregory C., Anna Asanbaeva, Pasquale Vena, Robert L. Sah, and Stephen M. Klisch 2009 A Nonlinear Constituent Based Viscoelastic Model for Articular Cartilage and Analysis of Tissue Remodeling Due to Altered Glycosaminoglycan-Collagen Interactions. Journal of Biomechanical Engineering 131(10): 101002.

95. Thomopoulos, Stavros, Juan P. Marquez, Bradley Weinberger, Victor Birman, and Guy M. Genin 2006 Collagen Fiber Orientation at the Tendon to Bone Insertion and Its Influence on Stress Concentrations. Journal of Biomechanics 39(10): 1842–1851.

96. Vahdati, Ali, and Diane R. Wagner 2009 Influence of Calcified Cartilage Zone Permeability in Mechanical Behavior of Articular Cartilage: A Finite Element Study. *In.* http://www.simulia.com/academics/research_pdfs/4_2011-04-08_163753_Vahdati%20SBC%202009.pdf, accessed October 3, 2013.

97. Van de Velde, Samuel K. 2009 Analysis of Tibiofemoral Cartilage Deformation in the Posterior Cruciate Ligament-Deficient Knee. The Journal of Bone and Joint Surgery (American) 91(1): 167.

98. Weisbecker, Hannah, David M. Pierce, Peter Regitnig, and Gerhard A. Holzapfel 2012 Layer-Specific Damage Experiments and Modeling of Human Thoracic and Abdominal Aortas with Non-Atherosclerotic Intimal Thickening. Journal of the Mechanical Behavior of Biomedical Materials 12: 93–106.

99. Williams, Gregory M., Kristin J. Dills, Christian R. Flores, *et al.* 2010 Differential Regulation of Immature Articular Cartilage Compressive Moduli and Poisson's Ratios By *in Vitro* Stimulation with IGF-1 and TGF-β1. Journal of Biomechanics 43(13): 2501–2507.

100. Wilson, W., C.C. van Donkelaar, B. van Rietbergen, and R. Huiskes 2005 A Fibril-Reinforced Poroviscoelastic Swelling Model for Articular Cartilage. Journal of Biomechanics 38(6): 1195–1204.

101. Wilson, W., C.C. van Donkelaar, B. van Rietbergen, K. Ito, and R. Huiskes 2004 Stresses in the Local Collagen Network of Articular Cartilage: A Poroviscoelastic Fibril-Reinforced Finite Element Study. Journal of Biomechanics 37(3): 357–366.

102. Wilson, W, N Driessen, C Vandonkelaar, and K Ito 2006 Prediction of Collagen Orientation in Articular Cartilage by a Collagen Remodeling Algorithm. Osteoarthritis and Cartilage 14(11): 1196–1202.

103. Wong, Benjamin L., Won C. Bae, Kenneth R. Gratz, and Robert L. Sah 2008 Shear Deformation Kinematics during Cartilage Articulation: Effect of Lubrication, Degeneration, and Stress Relaxation. Molecular & Cellular Biomechanics: MCB 5(3): 197.

104. Wong, B.L., S.H. Chris Kim, J.M. Antonacci, C. Wayne McIlwraith, and R.L. Sah 2010 Cartilage Shear Dynamics during Tibio-Femoral Articulation: Effect of Acute Joint Injury and Tribosupplementation on Synovial Fluid Lubrication. Osteoarthritis and Cartilage 18(3): 464–471.

105. Wu, J. Z., W. Herzog, and E. M. Hasler 2002 Inadequate Placement of Osteochondral Plugs May Induce Abnormal Stress-Strain Distributions in Articular Cartilage-Finite Element Simulations. Medical Engineering & Physics 24(2): 85–97.

106. Zhang, Wei, Jialin Chen, Jiadong Tao, *et al.* 2013 The Promotion of Osteochondral Repair by Combined Intra-Articular Injection of Parathyroid Hormone-Related Protein and Implantation of a Bi-Layer Collagen-Silk Scaffold. Biomaterials 34(25): 6046–6057.

CHAPTER 2

An Equilibrium Constitutive Model of Anisotropic Cartilage Damage to Elucidate Mechanisms of Damage Initiation and Progression

2.1 Abstract

Traumatic injuries and gradual wear-and-tear of articular cartilage that can lead to osteoarthritis have been hypothesized to result from tissue damage to articular cartilage. In this study, a previous equilibrium constitutive model of articular cartilage was extended to a constitutive damage articular cartilage (CDAC) model. In particular, anisotropic collagen fibril damage and isotropic glycosaminoglycan damage were considered in a 3-D formulation. In the CDAC model, time dependent effects such as viscoelasticity and poroelasticity were neglected, and thus all results represent the equilibrium response after all time dependent effects have dissipated. The resulting CDAC model was implemented in two different finite element models. The first simulated uniaxial tensile loading to failure, while the second simulated spherical indentation with a rigid indenter displaced into a bi-layer articular cartilage sample. Uniaxial tension to failure simulations were performed for three collagen fibril Lagrangian failure strain (*i.e.*

the maximum elastic collagen fibril strain) values of 15%, 30%, and 45% while spherical indentation simulations were performed with a collagen fibril Lagrangian failure strain of 15%. Glycosaminoglycan damage parameters were held constant for all simulations. Our results indicated that the equilibrium post-yield tensile response of articular cartilage and the macroscopic tissue failure strain are highly dependent on collagen fibril Lagrangian failure strain. The uniaxial tensile response consisted of an initial nonlinear ramp region due to the recruitment of intact fibrils followed by a rapid decrease in tissue stress at initial collagen fibril failure, as a result of collagen fibril damage which continued until ultimate tissue failure. In the spherical indentation simulation, damage to both the collagen fibril and glycosaminoglycan constituents was located only in the superficial zone and near the articular surface with tissue thickening following unloading. Spherical indentation simulation results are in agreement with published experimental observations. Our results indicate that the proposed CDAC model is capable of simulating both initial small magnitude damage as well as complete failure of articular cartilage tissue. The results of this study may help to elucidate the mechanisms of articular cartilage tissue damage that initiate and propagate osteoarthritis.

2.2 Introduction

Injuries to articular cartilage (AC) can range from debilitating to undetectable, yet there is currently a limited understanding of the mechanisms that result in AC injuries and the long term consequences of damage *in vivo*. The AC solid matrix is

composed primarily of type II collagen (COL) fibrils and glycosaminoglycan (GAG) molecules (Maroudas *et al.*, 1980; Brocklehurst *et al.*, 1984). The COL fibrils contribute primarily to tissue integrity under uniaxial tensile loading (Asanbaeva *et al.* 2008) and Poisson's ratios of AC in unconfined compression (Kiviranta *et al.*, 2006; Ficklin *et al.*, 2007; Williams *et al.*, 2010). GAG molecules impart an osmotic swelling pressure on the tissue that counteracts compressive loading (Maroudas *et al.* 1981; Asanbaeva *et al.*, 2007; Williams *et al.* 2010) and imparts a prestress on COL fibrils (Maroudas, 1976; Thomas *et al.*, 2009). Additionally, molecular level covalent and non-covalent interactions between GAG molecules and COL fibrils have an effect on the mechanical response of AC (Asanbaeva *et al.*, 2008; Thomas *et al.*, 2009). Additional constituents make up a small volume fraction of the cartilage solid matrix including cartilage cells, or chondrocytes, additional proteins, type IV COL fibrils, and other charged molecules and macromolecules (Kuettner 1992; Williamson *et al.* 2001). Thus, the gross mechanical response of AC is derived from a superposition of individual constituent specific responses and subtle interactive effects between constituents that depend on the applied loading condition.

Despite the demanding mechanical function of AC, it has poor intrinsic healing capability likely due to avascularity and low cell count (Buckwalter & Mankin, 1998). AC is subject to varying degrees of traumatic injury and/or progressive degeneration that can result in osteoarthritis (OA) as observed in animal and human studies (Noyes & Stabler, 1989; Curl *et al.*, 1997; Botter *et al.*, 2008; Temple-Wong *et al.*, 2009). AC injuries as a result of overloading have been observed to result in cell death

and a decrease in the capability of AC to resist subsequent loading (Wong, *et al.*, 2010; Novakofski *et al.*, 2014). Due to the complexity of AC, and the difficulty in experimentally assessing constituent specific damage, relatively little is known about the consequences of AC injuries, particularly when injuries do not result in macroscopically visible AC damage.

Experimental studies of OA often aptly examine the differences between a healthy control group and an osteoarthritic group and thus, the resulting effects rather than the precise causes of OA are quantified experimentally. For example, variations in biochemical composition of AC with OA such as increased water content and decreased GAG content have been quantified (Maroudas & Venn, 1977; Brocklehurst *et al.*, 1984;Temple-Wong *et al.*, 2009). In human patellar cartilage, early OA is characterized by decreased GAG content and loss of COL fibril network organization, while late stage OA shows decreased COL content (Saarakkala *et al.*, 2010). With OA, progressive fibrillation of COL fibrils, which results in decreased mechanical integrity of COL fibrils, a loss of COL fibril network organization, and AC thickening has been observed to start at the surface and progress into deeper layers (Temple-Wong *et al.*, 2009; Cotofana *et al.*, 2012). With OA and degeneration, AC has been observed to undergo both compositional and structural changes that lead to a decreased mechanical integrity and a progressive lessening of AC functionality.

The aim of this work is to expand on contemporary experimental studies using a computational model to better understand AC degradation and injury. Previous computational approaches have been implemented to study the characteristics of

damage in COL fibril reinforced soft tissues other than AC that are not experimentally measurable or prohibitively difficult to measure experimentally. Recent stochastic finite strain models for fibril reinforced soft tissues have been proposed without extensive validation (Rodriguez *et al.*, 2006; Calvo, *et al.*, 2007; Rodriguez *et al.*, 2008). Other studies have proposed constituent-based continuum damage models of aortic tissues including only damage to the fibrillar network (Gajewski *et al.*, 2013) and damage to the nonfibrillar network and/or the tissue ground matrix (Weisbecker *et al.*, 2012; Famaey,*et al.*, 2013) with varying degrees of validation. Also, while one study proposed a constitutive model specific to AC including damage to the ground matrix and the COL fibril constituents without experimental validation, this study was only 2-D (Hosseini, *et al.*, 2014). Therefore, the primary objective of this paper is to improve upon current models and expand our understanding of AC degradation by developing a 3-D AC specific constitutive damage articular cartilage (CDAC) model. This model is capable of highly anisotropic COL fibril damage (*i.e.* damage in any number of discrete COL fibril directions), and an isotropic GAG molecule damage formulation that captures GAG molecule leeching and cleaving as a result of deformation. To provide a validation of the results of the CDAC model, results from a spherical indentation simulation will be compared to experimental observations from similar loading scenarios of COL fibril damage and denaturation (Hollander *et al.*, 1995) and the locations of GAG molecule leeching and/or cleaving (Rolauffs *et al.*, 2010).

2.3 Materials and Methods

Preliminaries

The right Cauchy-Green deformation tensor, $\mathbf{C}$, is defined as

$$\mathbf{C} = \mathbf{F}^{\mathrm{T}}\mathbf{F} \tag{1}$$

where $\mathbf{F}$ is the deformation gradient tensor. The Lagrangian strain tensor, $\mathbf{E}$, is defined as

$$\mathbf{E} = \frac{1}{2}(\mathbf{C} - \mathbf{I}) \tag{2}$$

where $\mathbf{I}$ is the identity tensor. The directional Lagrangian strain implemented in this work to define COL fibril constituent material behavior is calculated as

$$E_N = \mathbf{N} \cdot (\mathbf{EN}) \tag{3}$$

where $\mathbf{N}$ is a unit normal direction vector in the reference configuration and $(\cdot)$ is the dot product operator. Note that the vector and tensor operations required to calculate E_N return a scalar for the value of E_N in a direction, N. The second Piola-Kirchhoff stress tensor, $\mathbf{S}$, and the Cauchy stress tensor, $\mathbf{T}$, can be related *via* a push forward operation as shown below

$$\mathbf{T} = \frac{1}{J}\mathbf{F}\mathbf{S}\mathbf{F}^{\mathrm{T}} \tag{4}$$

where $J = det\mathbf{F}$ is the determinant of the deformation gradient tensor. The second Piola-Kirchhoff stress tensor for a Green elastic material (eventually with damage) can be derived from the Helmholtz free energy function per unit reference volume, ψ, using the following relationship

$$\mathbf{S} = 2\frac{\partial \psi}{\partial \mathbf{C}} \tag{5}$$

Similarly, the fourth order material elasticity tensor in the reference configuration, $\mathbb{C}$, is derived as

$$\mathbb{C} = 2\frac{\partial \mathbf{S}}{\partial \mathbf{C}} \tag{6}$$

For this study, a previous equilibrium constitutive model of AC (Stender *et al.*, 2012) is extended to include damage to COL and GAG constituents. In the previous model, the mechanical response of AC is assumed to be a superposition of responses from an anisotropic COL fibril network, GAG molecules, and a ground substance matrix (MAT). Any viscoelastic effects are neglected. All constituents are hypothesized to be linked directly to the solid matrix. Thus, COL, GAG, and MAT constituents all experience the same deformation, **F**, when loaded. The total solid matrix stress without damage is reported as a sum of COL, GAG, and MAT constituent stresses *via* a stress balance hypothesis. As in Stender *et al.,* (2012), this CDAC model is developed for newborn (1-3 week old) bovine AC from the patellofemoral groove because of an existing comprehensive set of biomechanical, biochemical, and theoretical properties available for that specific tissue source (Williams *et al.*, 2010; Stender *et al.*, 2012). Currently, there is not a similar comprehensive set of data available for other AC in mature or aging tissues. For a more complete summary of this previous model of AC, and a discussion of the results, refer to Stender *et al.* (2012).

Anisotropic Collagen Fibril Damage Model

The COL fibril Helmholtz free energy function per unit reference volume, ψ^{COL}, is proposed to be a function of the true COL fibril Helmholtz free energy function per unit reference volume, $\breve{\psi}^{COL}$, and a dimensionless COL fibril damage parameter, d_N^f,

$$\psi^{COL} = \breve{\psi}^{COL}\left[1 - d_N^f\right] \tag{7}$$

where $0 \leq d_N^f \leq 1$in direction N. Note that here the damage parameter d_N^f represents the percent degradation of COL fibril material (damage is independent of loading) in direction N; (*e.g.*, $d_N^f = 0$ implies no fibril damage while $d_N^f = 1$ is 100% degraded fibril elastic strain energy). Note that equation (7) is a 1-D relation in direction N, that is later integrated over a unit sphere at each material point while allowing d_N^f to vary based on direction, thus allowing for 3-D anisotropic COL fibril damage. The COL fibril damage parameter, d_N^f, is not to be confused with damage in ductile polycrystalline metals that is associated with void nucleation, growth, and coalescence, requiring the damage to be represented in the kinematics, as well as thermodynamics (see Davison *et al.,* 1977). Thus, in this model there are no explicit damage-specific kinematic variables and consequently, no damage-specific conjugate stress terms. See appendix for discussion of the thermodynamics for this model. A constitutive assumption is made for a polyconvex form of the true COL fibril Helmholtz free energy function without damage per unit reference volume (Stender *et al.*, 2012)

$$\breve{\psi}^{COL} = H(E_N)\frac{1}{2}E^f(E_N)^2 \tag{8}$$

where E^f is the COL fibril elastic modulus and $H(E_N)$ is the Heaviside step function. H is a piecewise continuous function used in this work as defined below

$$H\big(f(x)\big) = \begin{Bmatrix} 1, f(x) > 0 \\ 0, f(x) \leq 0 \end{Bmatrix} \tag{9}$$

(*i.e.*, COL fibrils are only active in tension). Note that the assumed form of Ψ^{COL} results in a linear stress-strain response for COL fibrils which has been shown to be appropriate for immature bovine tissue (Stender *et al.*, 2012). However, this assumption may not be appropriate for more mature tissues, or other species and/or locations (see Discussion for additional details).

COL fibrils are assumed to exhibit an elastic brittle damage response wherein COL fibrils exhibit a linear elastic response until Lagrangian fibril strain exceeds the Lagrangian failure strain of a COL fibril, E_N^D (*i.e.,* the maximum elastic strain of a COL fibril) as shown in Figure 4.

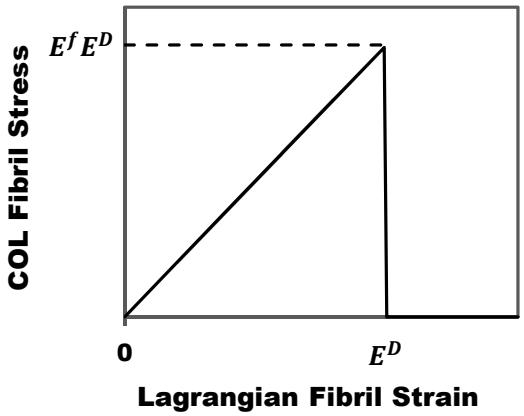

Figure 4. The collagen (COL) fibril constituent stress strain response with damage for a single COL fibril. All COL fibrils are hypothesized to initially respond with a linear elastic response and then fail completely if the COL fibril Lagrangian damage strain in direction N, E_N^D, value is exceeded. Thus, the maximum COL fibril yield stress in direction N is the product of the COL fibril modulus, E^f and the COL fibril Lagrangian failure strain, E_N^D in that direction.

The COL fibril damage parameter, d_N^f is introduced as shown below

$$d_N^f = \begin{Bmatrix} 1, E_N > E_N^D \\ 0, E_N \leq E_N^D \end{Bmatrix} \tag{10}$$

where $d_N^f = 0$ for undamaged, intact fibrils (*i.e.* COL fibril strain, $E_N \leq E_N^D$), and $d_N^f = 1$ for damaged fibrils (*i.e.,* COL fibril strain, $E_N > E_N^D$). The COL fibril damage parameter, d_N^f, is defined and exists for any N number of discrete pyramidal volume elements at a material point each with a unique direction, N. Initially, all fibrils are assumed to be undamaged. The loading history is tracked such that once damaged, COL fibril healing and/or repair is disallowed. For a complete description of the COL fibril damage evolution formulation used in this model including a discussion of the capability to implement alternative forms of d_N^f and the tracking of COL fibril damage history, refer to the appendix.

Previous soft tissue models have used continuous, (*i.e.*, non-discrete) continuum fibril models to study soft fibrous tissues (Lanir, 1983; Lei & Szeri, 2006; Ateshian 2007; Ateshian *et al.*, 2009). Specifically, the continuous fibril model of the anisotropic COL fibril network in AC used here was developed by (Shirazi *et al.*, 2011) and is implemented by discretizing a unit sphere at each material point into N number of pyramidal volume elements. Each pyramidal volume element is then assigned a variable volume fraction of COL fibrils, φ_N^f, in direction N capturing the directional dependence of the COL network at the material point level. Note that when φ_N^f is integrated over the unit sphere, the result is equivalent to the

experimentally measured COL fibril tissue volume fraction, φ^f, which is combined with COL fibril spatial distribution imaging studies to define a realistic and anisotropic COL fibril constituent. For a complete summary of the determination of and implementation of the anisotropic COL fibril distributions used here, refer to Stender *et al.* (2012). In summary, based on experimental results that Poisson's ratios and tensile modulus do not depend on direction in the plane parallel to the articular surface for newborn bovine AC from the patellofemoral groove, (Williamson, *et al.*, 2003; Williams *et al.*, 2010) COL fibril distributions were assumed to not vary in the plane parallel to the articular surface. Planar quantitative polarized light microscopy images were used to estimate COL fibril distribution in a plane perpendicular to the articular surface. COL fibril area fraction distributions in the plane perpendicular to the articular surface were determined from quantitative polarized light microscopy measurements (Stender *et al.*, 2012) and adjusted based on experimental COL fibril tissue volume fraction (Williams *et al.* 2010). A background isotropy and a normalized Gaussian distribution were assumed with the result as shown in Figure 5.

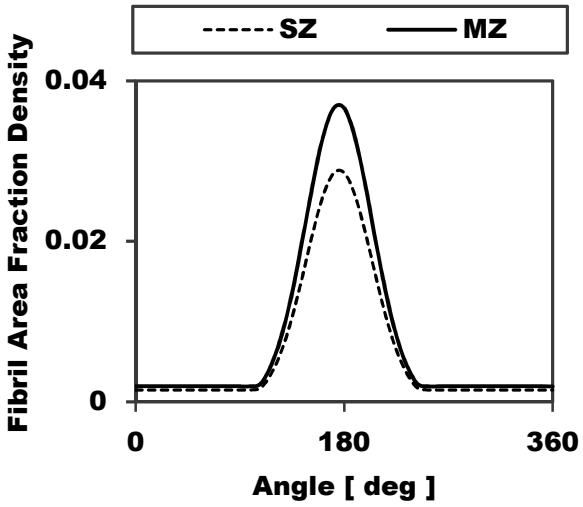

Figure 5. Initial highly anisotropic collagen fibril area density in the superficial zone (SZ) and middle zone (MZ) of newborn bovine articular cartilage from the patellofemoral groove in a plane perpendicular to the articular surface. Initial collagen fibril area fraction distributions are determined via quantitative polarized light microscopy measurements from (Stender et al., 2012) and adjusted for the biochemical collagen fibril volume fraction from (Williams et al., 2010). Note that Angle = 90° corresponds to the direction perpendicular to the articular surface.

Using equations (7, 8, and 10) the COL constituent free energy function per unit reference volume, ψ^{COL}, is extended from Stender *et al.* (2012) to include COL constituent damage as

$$\psi^{COL} = \frac{1}{4\pi}\int_{\phi=0}^{2\pi}\int_{\theta=0}^{\pi} H(E_N)\varphi_N^f \frac{1}{2}E^f(E_N)^2\left[1-d_N^f\right]\sin\theta d\theta d\phi \qquad (11)$$

where θ and ϕ are angles within a spherical coordinate system to determine the unit direction vector $\mathbf{N} = cos(\theta)sin(\phi)\hat{\boldsymbol{\imath}} + sin(\theta)sin(\phi)\hat{\boldsymbol{\jmath}} + cos(\phi)\hat{\boldsymbol{k}}$, with associated Lagrangian strain E_N in equation (3). With the assumptions of a unit sphere at each material point and a local spherical coordinate system, $V = \frac{4\pi}{3}$ and $dV = \frac{1}{3}\sin\theta d\theta d\phi$. Note that this formulation is developed from Shirazi *et al.* (2011) and involves an

integration within the unit sphere rather than on the unit sphere as other studies have proposed (Lei & Szeri, 2006; Ateshian, 2007). For a discussion of the equivalence of the integration approach presented here, and other models where integration is performed on the unit sphere refer to Stender *et al.* (2012). Using the relationship in equation (5), the COL fibril second Piola-Kirchhoff stress tensor, $\mathbf{S}^{\mathrm{COL}}$, is obtained as

$$\mathbf{S}^{\mathrm{COL}} = \frac{1}{4\pi}\int_{\phi=0}^{2\pi}\int_{\theta=0}^{\pi} H(E_N)\varphi_N^f E^f E_N\left[1-d_N^f\right][\mathbf{N}\otimes\mathbf{N}]\sin\theta d\theta d\phi \tag{12}$$

where $\otimes$ denotes the dyadic product. The COL fibril constituent material elasticity tensor can be similarly obtained using equation (6) and represented in indicial notation as

$$\mathbb{C}_{ABCD}^{COL} = \frac{1}{4\pi}\int_{\phi=0}^{2\pi}\int_{\theta=0}^{\pi} H(E_N)\varphi_N^f E^f\left[1-d_N^f\right]N_A N_B N_C N_D\sin\theta d\theta d\phi \tag{13}$$

For a more complete derivation of $\mathbf{S}^{\mathrm{COL}}$ and $\mathbb{C}_{ABCD}^{COL}$ refer to the appendix. The extent of COL fibril damage, D_{col} (%) is calculated in the user-defined material subroutine (UMAT) for each material point as the ratio between number of pyramidal elements at each material point for which $\gamma_N^f \geq 0$ (*i.e.,* pyramidal elements where COL fibril damage has occurred at any point in the loading history) N_f^D, and the total number of pyramid elements, N_{total} , as shown in the following relationship.

$$D_{COL}(\%) = \frac{N_f^D}{N_{total}} * 100 \tag{14}$$

Note that D_{COL} does not specifically quantify the anisotropic nature of COL fibril damage, but is implemented as a parameter to quickly quantify the extent of COL fibril damage at a material point.

Glycosaminoglycan Damage Model

In addition to anisotropic COL fibril damage, an isotropic damage model of the GAG constituent of AC is also proposed. Here, GAG damage is assumed to be isotropic at each material point and to only occur during decreases in tissue volume. Thus, it is assumed that decreases in tissue volume result in leeching and/or cleaving of GAG molecules resulting in an effective decrease in GAG molecular density which is considered to be analogous to GAG damage. For a more complete examination of GAG damage assumptions, refer to the Discussion. The total GAG Helmholtz free energy function per unit reference volume, ψ^{GAG}, is defined as

$$\psi^{GAG} = \breve{\psi}^{GAG}[1 - d^{GAG}] \tag{15}$$

where $\breve{\psi}^{GAG}$ is the undamaged GAG constituent free energy function per unit reference volume and d^{GAG} is a GAG specific damage parameter. The polyconvex GAG constituent Helmholtz free energy function per unit reference volume without damage was derived based on a curve fit to numerical results (Stender *et al.*, 2012) from the Poisson-Boltzmann continuum electromechanical model as applied to GAG molecules (Buschmann & Grodzinsky 1995) and is presented by as

$$\psi^{GAG} = -\alpha_1 \frac{\left(\rho_0^{GAG}\right)^{\alpha_2} J^{(1-\alpha_2)}}{(1-\alpha_2)} \tag{16}$$

where $\alpha_1, \left(\frac{\text{MPa}*\text{ml}^{2.5}}{\text{mg}^{2.5}}\right)$ and α_2(unitless) are GAG material constants, and $\rho_0^{GAG}, \left(\frac{\text{mg}}{\text{ml}}\right)$ is the mass density of GAG molecules in the tissue in the reference configuration. The evolution of GAG damage parameter, d^{GAG}, is proposed based on hypothesized GAG damage behavior as a novel function of the dimensionless GAG damage related

internal state variable (ISV) β, the dimensionless GAG damage scaling parameter η, and the maximum attainable GAG damage scaling parameter d_{max}^{GAG}, with $0 \leq d_{max}^{GAG} \leq 1$:

$$d^{GAG} = d_{max}^{GAG}\left[e^{\left(\frac{-\beta}{\eta}\right)} - e^{\left(\frac{-1}{\eta}\right)}\right] \tag{17}$$

Several plots of d^{GAG} with $d_{max}^{GAG} = 0.5$ are shown in Figure 6A. In all simulations, $\eta = 0.25$ and $d_{max}^{GAG} = 0.5$ are used to demonstrate appreciable GAG damage with volumetric decreases for the simulations in this study as shown in Figure 6B.

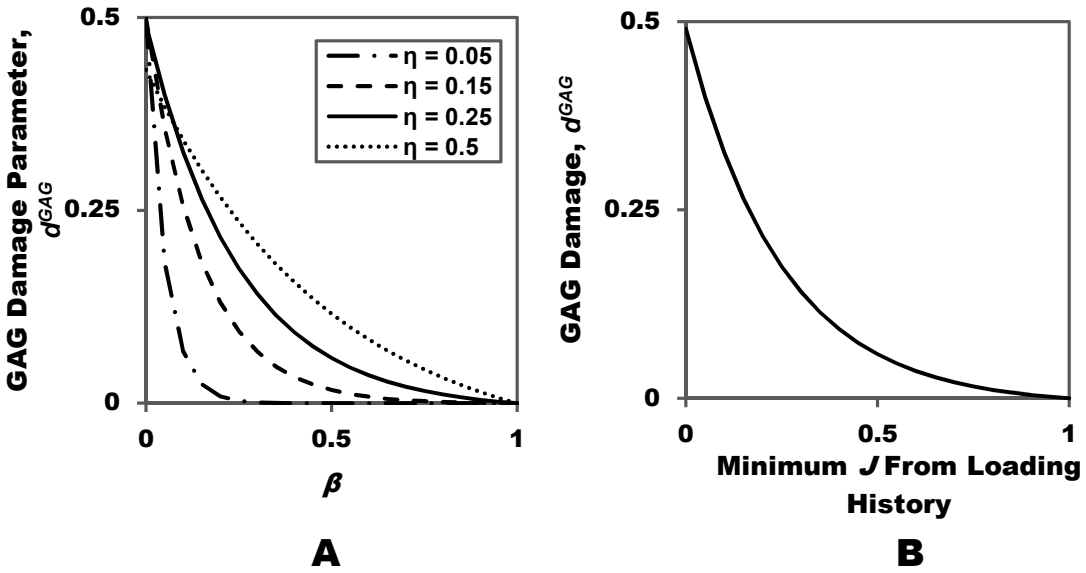

Figure 6. Glycosaminoglycan (GAG) damage parameter, d^{GAG}, plots showing (A) d^{GAG} as a function of GAG damage internal state variable, β, for several values of the GAG damage scaling variable, η , with $d_{max}^{GAG} = 0.5$. (B) GAG damage, d^{GAG}, plotted for values of $d_{max}^{GAG} = 0.5$ and $\eta = 0.25$ as used in this study as a function of the minimum $J = det\mathbf{F}$ value in the material loading history.

The GAG specific damage function, f^{GAG} , that tracks the occurrence and accumulation of GAG constituent damage is defined as

$$f^{GAG} = (\beta - J)\big(H(\beta - J)\big) \tag{18}$$

where $J = det\mathbf{F}$, the determinant of the deformation gradient tensor, $\mathbf{F}$. If $J \geq \beta$ (volumetric expansion greater than ISV β), then $f^{GAG} = 0$ and no damage has occurred. If $J < \beta$, (volumetric contraction) then $f^{GAG} = (\beta - J)$ and additional GAG damage has occurred. For this study, GAG molecules are assumed to be initially undamaged and thus, the initial value of the ISV β is set to $\beta_0 = 1$ such that $d_0^{GAG} = 0$. Similarly to the COL fibril damage model, a relationship is assumed in order to solve for the incremental change of the GAG damage state variable, $\delta\beta$ as shown below.

$$\delta\beta = -f^{GAG} \tag{19}$$

When $f^{GAG} = (\beta - J)$, equation (19) gives $\delta\beta = -(\beta - J)$, and the damage like internal state variable β evolves (decreases). For the case of $f^{GAG} = 0$ equation (19) gives $\delta\beta = 0$ and thus, additional GAG damage has not occurred and there is no evolution of the damage like internal state variable, β. Note that for the GAG constituent, healing and/or repair of GAG molecules is effectively disallowed as the value of β can never increase.

The complete GAG constituent damage free energy density function per unit reference volume, ψ^{GAG} , is obtained by substituting equations (16) and (17) into equation (15) as

$$\psi^{GAG} = -\alpha_1 \frac{(\rho_0^{GAG})^{\alpha_2} \mathrm{J}^{(1-\alpha_2)}}{(1-\alpha_2)} \left\{1 - d_{max}^{GAG}\left[e^{\left(\frac{-\beta}{\eta}\right)} - e^{\left(\frac{-1}{\eta}\right)}\right]\right\} \quad (20)$$

The damage enabled GAG constituent Second Piola-Kirchhoff stress can then be derived using equation (5) as

$$\mathbf{S}^{GAG} = J\mathbf{F}^{-1}\left(-\alpha_1\left(\frac{\rho_0^{GAG}}{\mathrm{J}}\right)^{\alpha_2}\left\{1 - d_{max}^{GAG}\left[e^{\left(\frac{-\beta}{\eta}\right)} - e^{\left(\frac{-1}{\eta}\right)}\right]\right\}\right)\mathbf{F}^{-\mathbf{T}} \quad (21)$$

The damage enabled GAG material stiffness tensor is derived using equation (6) with the result shown below in indicial notation.

$$\mathbb{C}_{ABCD}^{GAG} = \{\alpha_1(\rho_0^{GAG})^{\alpha_2}(C_{AC}C_{BD} + C_{AD}C_{BC}) + \alpha_1\alpha_2(\rho_0^{GAG})^{\alpha_2}C_{DC}^{-1}C_{AB}^{-1}\}\left\{(det\ C)^{-\frac{\alpha_2}{2}}\right\}\left\{1 - d_{max}^{GAG}\left[e^{\left(\frac{-\beta}{\eta}\right)} - e^{\left(\frac{-1}{\eta}\right)}\right]\right\} \quad (22)$$

The extent of GAG damage is easily quantified by the value of the GAG damage parameter, d^{GAG}, which corresponds to the percent decrease in effective GAG molecule concentration.

Matrix Model

The MAT free energy function per unit reference volume was assumed to be a compressible Neo-Hookean strain energy function as proposed in Stender *et al.*, (2012) as

$$\psi^{MAT} = \frac{1}{2}\mu\left[(tr(\mathbf{C}) - 3) - \ln\left(\det(\mathbf{C})\right)\right] \quad (23)$$

where $\mu\ (MPa)$ is a MAT constituent shear modulus parameter. Because the results of Stender *et al.* (2012) indicated that the MAT constituent did not have a significant contribution to the mechanical response of AC tissue from the newborn bovine patellofemoral groove (*i.e.,* $\mu \approx 0$) ,damage to the MAT constituent is not considered

in this work. Using equations (5) and equation (23), the MAT constituent Second Piola-Kirchhoff stress is derived as

$$\mathbf{S}^{MAT} = \mu(\mathbf{I} - \mathbf{C}^{-1}) \tag{24}$$

and the MAT constituent elasticity tensor in the reference configuration is derived in indicial notation using equation 6 as

$$\mathbb{C}^{MAT}_{ABCD} = \mu(C^{-1}_{AC}C^{-1}_{BD} + C^{-1}_{AD}C^{-1}_{BC}) \tag{25}$$

Previous Experimental and Computational Data

Experimental biomechanical and biochemical data from previous studies were used in the implementation of the CDAC model. The AC tissue was taken from the native newborn bovine patellofemoral groove from either the superficial zone (SZ) or the middle zone (MZ). A summary of tissue biochemical parameters that are required model inputs, and the original data sources can be found in Table 1. Biochemical values for GAG content and COL fibril volume fraction were available from Williams *et al.*, (2010). Initial anisotropic COL fibril spatial distributions were determined *via* quantitative polarized light microscopy measurements (Stender *et al.*, 2012) adjusted for the biochemical COL fibril volume fraction from (Williams *et al.*, 2010).

Table 1. Experimental biochemical properties for bovine articular cartilage in the superficial and middle zones established in a previous study (Williams *et al.,* 2010) and used herein.

	Water Content (% Tissue Mass)	Glycosaminoglycan Molecule Density, ρ_0^{GAG} (mg/ml)	COL Fibril Volume Fraction, φ^f (% Tissue Volume)
Superficial Zone	89.3 ±2.6	32.8 ± 7.5	3.9 ± 1.0
Middle Zone	86.6±2.8	47.6 ± 12.1	5.0 ± 1.4

AC material constants not associated with COL fibril or GAG molecule damage parameters are used in this work as presented in Stender *et al.* (2012) for the same tissue source and are listed in Table 2. GAG material constants α_1 and α_2 were obtained from a fit to a Poisson-Boltzmann continuum electromechanical model (Buschmann & Grodzinsky 1995), and are used as constant values. However, because the reference GAG densities differ between the SZ and MZ, the resulting GAG stress-strain equations are regionally dependent. Note that these AC model parameters are derived from fits to tensile and compressive biomechanical test data, and represent the best possible fit to the initially undamaged response of AC from the newborn bovine patellofemoral groove.

Table 2. Predicted articular cartilage constituent glycosaminoglycan (GAG), ground substance matrix (MAT), and collagen fibril (COL) mechanical properties for the superficial zone (SZ) and middle zone (MZ) not related to damage used in this study established previously by Stender *et al.* (2012). Note that GAG constants are identical in the SZ and the MZ.

GAG Constants	$\alpha_1 \left(\frac{MPa*ml^{2.5}}{mg^{2.5}}\right)$	2.87
	α_2	2.5
MAT Constants	μ (SZ, MPa)	0.001
	μ (MZ, MPa)	0.001
COL Constants	E^f (SZ, MPa)	175
	E^f (MZ, MPa)	422

Finite Element Implementation and Simulations

Damage enabled GAG and COL constitutive models were implemented in Abaqus v6.13 using the UMAT capability. The COL fibril, GAG molecule, and MAT constituent material stiffness tensors (equations 13, 22 and 25, respectively) were transformed to the Jacobian, or the tangent stiffness matrix, $\mathbb{C}_{ijkl}^{jac}$ where jac stands for Jacobian, as required by Abaqus (for full derivation see Stender *et al.,* 2012) using the following relationship shown in indicial notation

$$\mathbb{C}_{ijkl}^{jac} = \frac{1}{\mathrm{J}}\left\{\frac{1}{2}\left(\delta_{il}\tau_{jk} + \delta_{jk}\tau_{il} + \delta_{ik}\tau_{jl} + \delta_{jl}\tau_{ik} + \mathbb{C}_{ABCD}F_{iA}F_{jB}F_{kC}F_{lD}\right)\right\} \tag{26}$$

where is τ_{ij} the Kirchhoff stress, and δ_{ij} is the Kronecker delta. To enforce the loading history dependence of the CDAC model, additional state variables were required. The COL fibril ISV as discussed in the appendix, is defined as γ_N^f. GAG and COL fibril constituent ISV damage equations were coded directly in the UMAT. If the state variable values evolved as determined by the constituent state variable relationships, the evolution of state variables was calculated as shown below for COL and GAG damage like internal state variables, respectively as

$$\gamma_{N\,(n+1)}^{f} = \gamma_{N\,(n)}^{f} + \delta\gamma_{N\,(n+1)}^{f}, \qquad \beta_{n+1} = \beta_n + \delta\beta_{n+1} \tag{27}$$

where $\gamma_{N\,(n+1)}^{f}$ and β_{n+1} are the state variable values at the end of the current solution step, $\gamma_{N\,(n)}^{f}$ and β_n are the state variable values from the previous solution step. The evolution of COL and GAG damage like internal state variables, $\delta\gamma_{N\,(n+1)}^{f}$and $\delta\beta_{n+1}$are

determined from the evolution of the state variables in the current step defined in equations (30) and (19) for COL and GAG constituents, respectively.

To study the results of this proposed constitutive damage model of AC, two different finite element models were developed in Abaqus 6.13. First, a uniaxial stress in tension model consisting of a single linear hexahedral element (C3D8) with full integration was developed and used to model AC damage and failure in uniaxial stress in tension loading (Figure 7A). Due to the initial stress of the GAG constituent, to reach an initial equilibrium configuration, all simulations initially solve for an equilibrium stress state in an unloaded solution step (Stender *et al.*, 2012). For uniaxial tension simulations, tissue failure was defined to occur when the uniaxial tensile stress decreased to ≤ 1% of the maximum uniaxial tensile stress. Second, a 3-D finite element model of a spherical indentation test was constructed consisting of 10625 linear hexahedral elements with full integration and a rigid half sphere indenter. The cartilage sample was assumed to have dimensions of 1.0 mm x 1.0 mm x 0.7 mm with a SZ 0.2 mm thick adjacent to the indenter and a 0.5 mm thick MZ directly beneath the SZ (Figure 7B). The adjacent SZ and MZ zones were connected *via* a tied contact constraint. The rigid spherical indenter had a radius of 0.25 mm. Similarly to the uniaxial stress in tension model, all indentation simulations initially solve for an equilibrium stress state in an unloaded solution step. Following equilibrium, the indenter was displaced into the tissue to a depth of 0.06 mm for two cycles using a surface-to-surface contact algorithm for finite sliding and assuming frictionless contact. For uniaxial stress in tension simulations, the COL fibril damage

strain parameter, E_N^D, was simulated as 0.15, 0.30, and 0.45 while spherical indentation simulations used $E_N^D = 0.15$. GAG damage parameters were assumed as $d_{max}^{GAG} = 0.5$ and $\eta = 0.25$ for all simulations. Initial ISVs for COL and GAG constituents were set as $\gamma_{N\,(0)}^{f} = 0$ and $\beta_0 = 1$, respectively, for all simulations. To improve the solution computation time, the number of COL constituent pyramidal elements at material points was decreased to 200 for the spherical indentation simulation compared to 3200 for uniaxial stress in tension simulations. Mesh convergence studies for uniaxial stress in tension and spherical indentation simulations were performed. Because of the equilibrium nature of this model, time dependent effects such as viscoelasticity and poroelasticity were neglected, and thus all results represent the equilibrium response after all time dependent effects have dissipated.

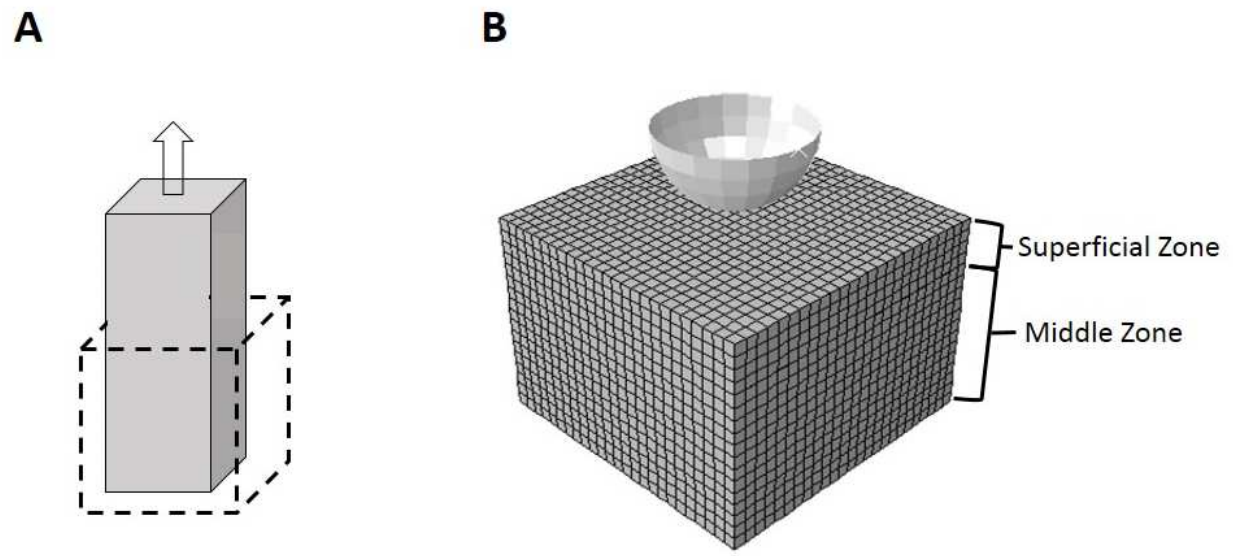

Figure 7. Finite element models showing (A) uniaxial stress in tension finite element model with dashed lines denoting the initial configuration. (B) Spherical indentation model with superficial and middle zones of articular cartilage. For spherical indentation simulations, the spherical indenter was modeled as an analytical rigid surface while the cartilage block was modeled using 10625, 8 node linear hexahedral C3D8 elements with displacements at the bottom surface constrained in all directions. The adjacent SZ and MZ of regions were constrained at the shared surface using a tied contact formulation

2.4 Results

Articular Cartilage Damage Model

An initial unloaded equilibrium step resulted in slight volumetric swelling as a consequence of the intrinsic swelling of GAG molecules. No GAG or COL fibril constituent damage was incurred during the initial equilibrium swelling. During tensile loading, predicted macroscopic tissue failure strains from the CDAC model were highly dependent on the COL fibril failure strain, E_N^D (Figure 8). For all uniaxial tensile failure simulations, COL fibril damage was the primary cause of macroscopic tissue failure.

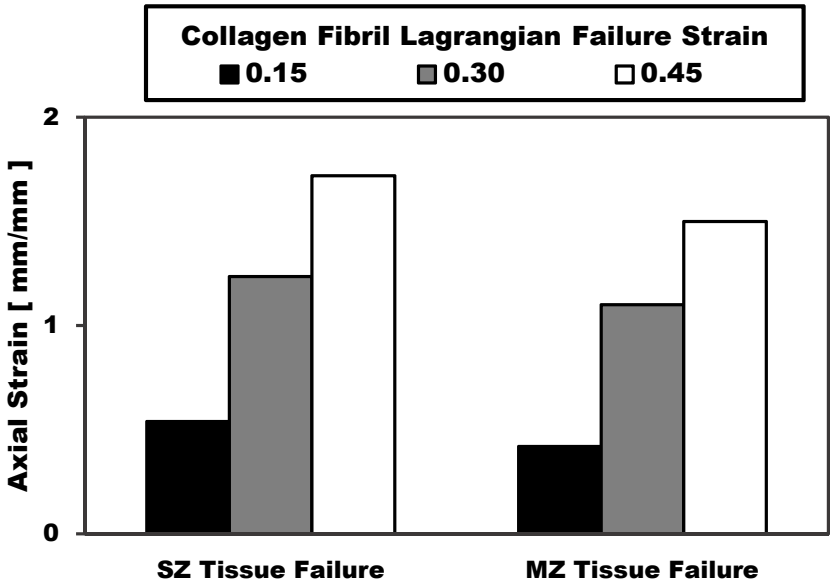

Figure 8. Predicted equilibrium values of articular cartilage ultimate tensile failure strain for collagen fibril Lagrangian failure strain values $E_N^D = 0.15, 0.30, 0.45$ in the superficial zone (SZ) and middle zone (MZ) of bovine articular cartilage. Macroscopic articular cartilage tissue failure strain values were determined as when the tissue axial tensile stress reached 1% of the max stress.

In general, the tensile stress-strain response up to ultimate tissue failure behavior was found to be similar in the SZ and the MZ. Due to the strain-based COL fibril failure criterion, higher ultimate tensile stresses were observed in the MZ which has a higher theoretical COL fibril modulus compared with the SZ (Figure 9).

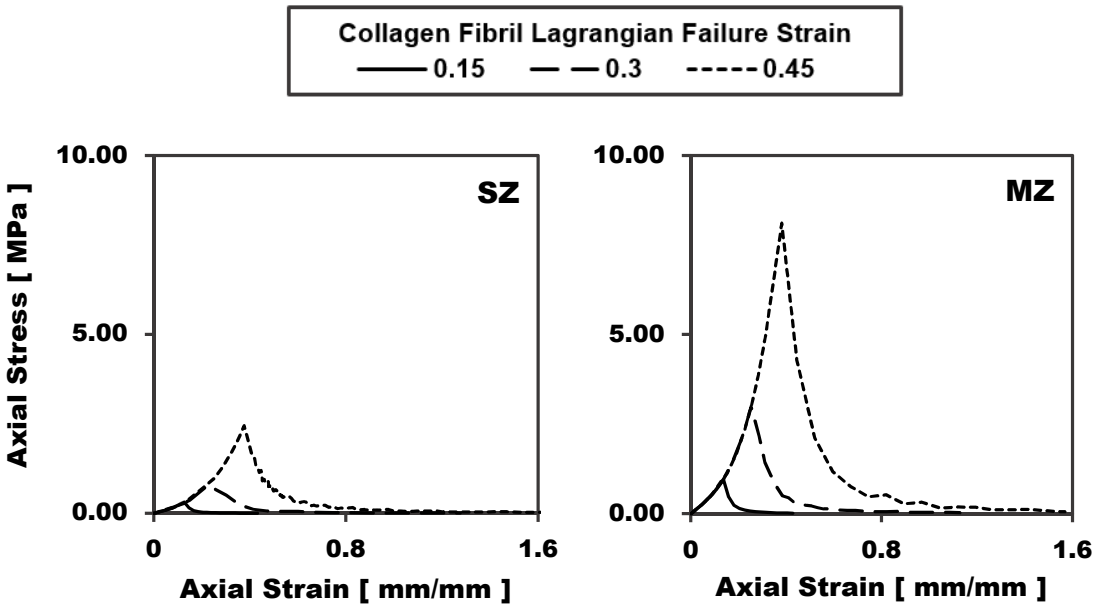

Figure 9. Predicted equilibrium uniaxial tension axial stress strain response in the superficial zone (SZ) and middle zone (MZ) for collagen fibril Lagrangian failure strain values of $E_N^D = 0.15, 0.30, 0.45$. Vertical axis range is uniform for ease of comparison.

Values of the COL spatial damage parameter, D_{col} , indicate severe extents of COL fibril damage at macroscopic tissue failure. In the SZ, D_{col} was calculated at tissue failure as 40.0, 47.1, and 49.1% for COL fibril damage strain values of 0.15, 0.30, and 0.45, respectively. In the MZ, D_{col} was calculated at tissue failure as 34.4, 45.5, and 46.8% for COL fibril damage strain values of 0.15, 0.30, and 0.45, respectively (Figure 10). Additional dependence was found on E_N^D with higher values of E_N^D leading to higher predicted ultimate stress values, and macroscopic tissue failure strain in all cases.

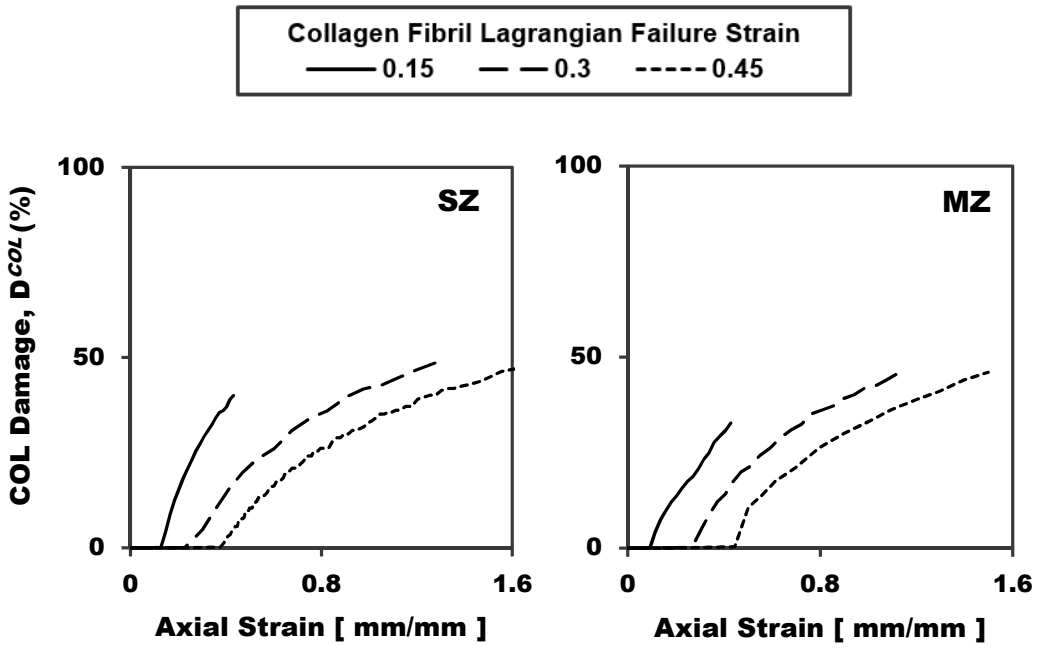

Figure 10. Predicted equilibrium collagen (COL) fibril damage, D_{col} (%), in the superficial zone (SZ) and middle zone (MZ) for collagen fibril Lagrangian failure strain values of $E_N^D = 0.15, 0.30, 0.45$. Vertical axis range is uniform for ease of comparison.

Due to COL damage with uniaxial tensile loading, the effective tissue COL fibril area fraction distributions of intact fibrils were found to vary greatly before and after uniaxial tension loading to failure. In tensile failure simulations, COL fibril damage is primarily aligned in the direction of tensile loading (Figure 11). At macroscopic tissue failure, not all COL fibrils were damaged, with some fibrils (less than 12% by volume fraction in all simulations) oriented perpendicular to the direction of loading left intact.

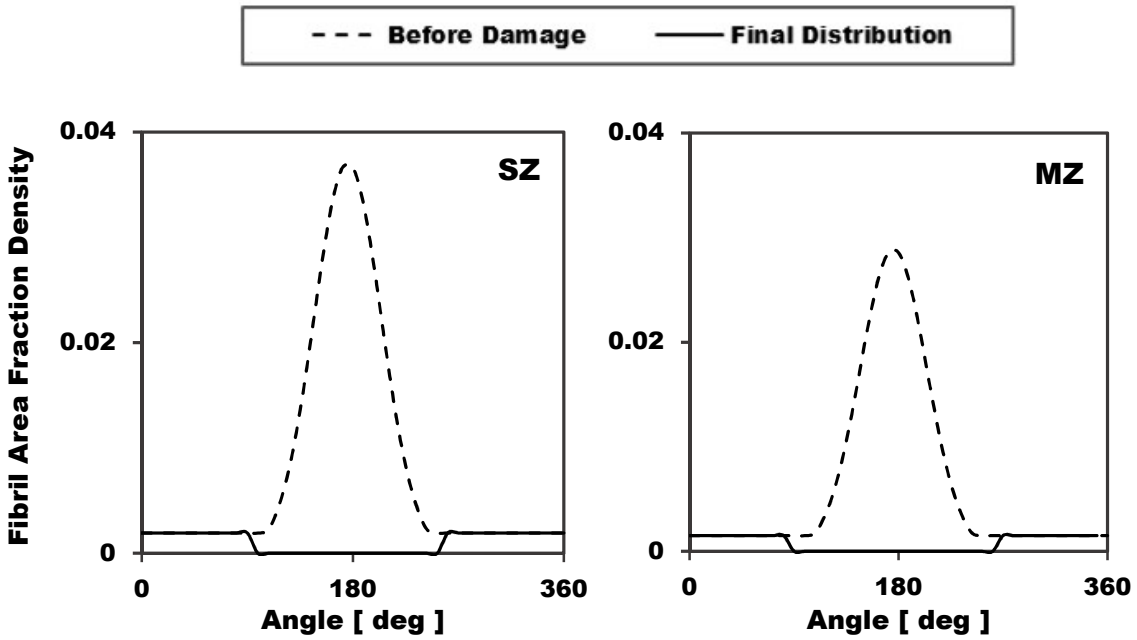

Figure 11. Comparisons of collagen fibril area fraction distribution in the superficial zone (SZ) and middle zone (MZ) in undamaged tissue, and at the point of ultimate macroscopic tensile failure for a Lagrangian failure strain of $E_N^D = 0.30$. Note that uniaxial tensile load was aligned parallel to the articular surface in the 180° direction. Vertical axis range is the same for ease of comparison.

In all uniaxial tension simulations, small amounts of GAG damage (between 0.4% and 6.6%) occurred. In all cases, GAG damage occurred just after the onset of tensile loading due to a slight volumetric decrease in the tissue. During uniaxial tensile loading, all GAG damage values were small and did not propagate with additional uniaxial tensile loading.

Spherical Indentation Simulation

Initial unloaded equilibrium swelling did not result in GAG or COL damage in bi-layered spherical indentation simulations. Locations of both GAG (Figure 12A) and

COL (Figure 12B) damage at peak loading coincided with high strain regions that were concentrated directly beneath the indenter tip.

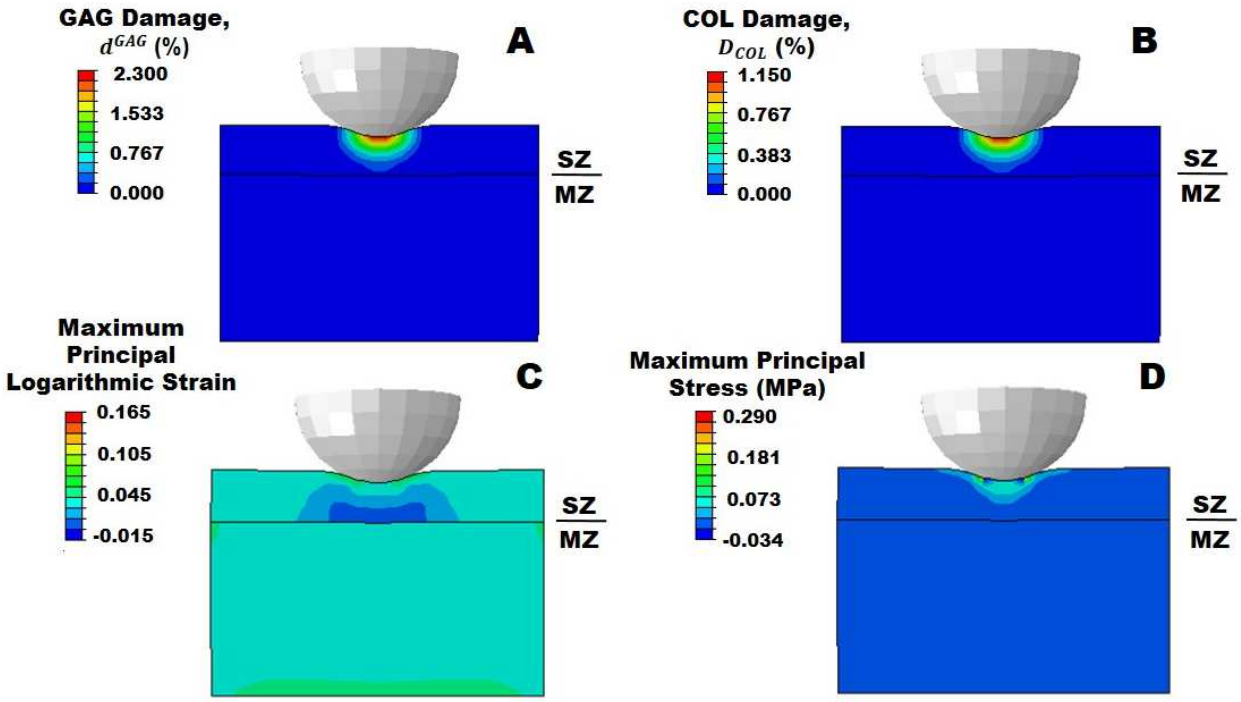

Figure 12. Contour plots of finite element analysis results for (A) glycosaminoglycan (GAG) damage parameter, d^{GAG}, (B) collagen (COL) fibril damage parameter, D_{col}, (C) maximum principal logarithmic (LE) strain, and (D) maximum principal Cauchy stress (MPa) in a bi-layered articular cartilage model with discrete superficial zone (SZ) and middle zone (MZ). A rigid spherical indenter was displaced into the articular surface while displacements in all directions at the bottom of the MZ were held fixed. Damage parameters of $E_N^D = 0.15$, $d_{max}^{GAG} = 0.5$, and $\eta = 0.25$ were used. Mesh lines removed for clarity.

All damage to both COL and GAG constituents was found only in the SZ. During indentation, GAG damage occurred at initial contact, while COL damage required higher indentation depths to occur. With increasing indenter tip displacement into the tissue, GAG damage progressed further from the articular surface and increased in magnitude. COL fibril constituent damage was located almost entirely at, or very

near, the articular surface and increased in magnitude with increasing indenter tip displacement into the tissue. Compared with GAG damage, COL fibril damage did not progress as far from the articular surface. The maximum principal logarithmic strain contour plot (Figure 12C) shows that strain was primarily concentrated in the SZ while the MZ experienced relatively small deformations. Similarly, the maximum principal stress contour plot (Figure 12D) demonstrates that the maximum tensile stresses are concentrated in the SZ near the interaction with the indenter tip, and maximum compressive stresses are again found in the SZ beneath the indenter tip. Increasing indentation depth resulted in a progressive damage response for both COL and GAG constituents (Figure 13).

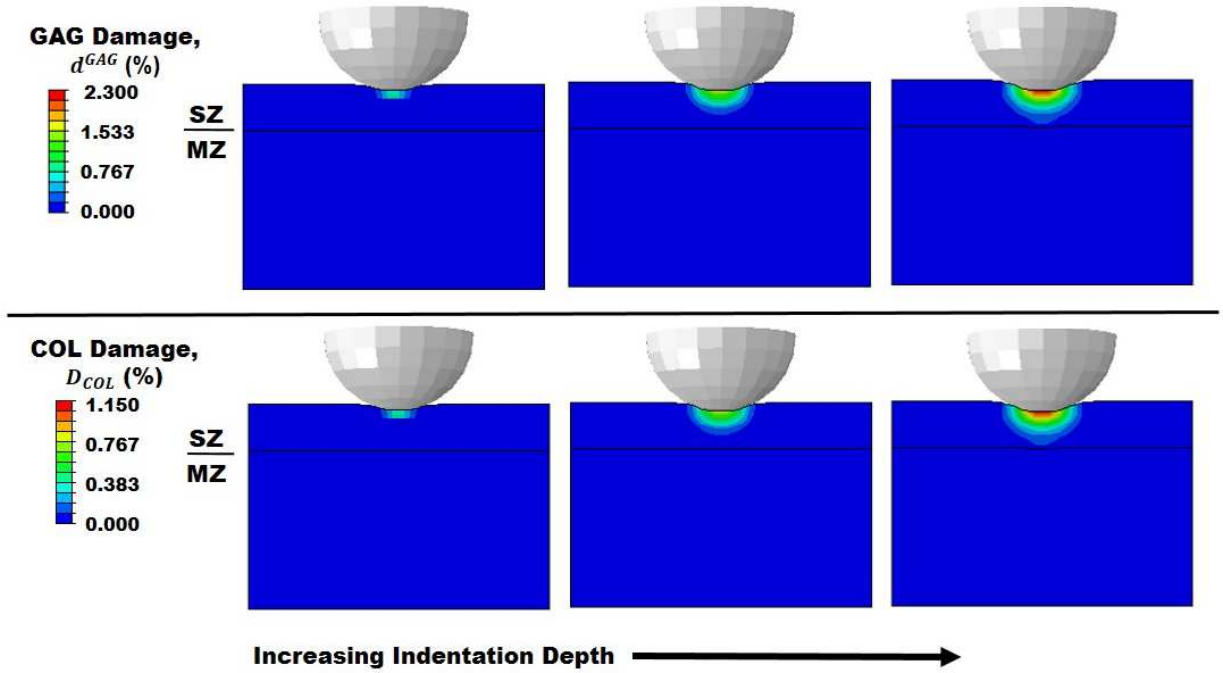

Figure 13. Contour plots of (top) glycosaminoglycan (GAG) damage parameter, d^{GAG}, and (bottom) collagen (COL) fibril damage parameter, D_{col} with progressive spherical indentation loading in a vi-layered articular cartilage model with discrete superficial zone (SZ and middle zone (MZ).). A rigid spherical indenter was displaced into the articular surface while displacements in all directions at the bottom of the MZ were held fixed. Damage parameters of $E_N^D = 0.15$, $d_{max}^{GAG} = 0.5$, and $\eta = 0.25$ were used. Mesh lines removed for clarity.

Following damage inducing loading, a small amount of AC thickening was observed at the articular surface (Figure 11). Additionally, a small amount of hysteresis due to both GAG and COL damage between the initial and second indentation cycles was observed in the reaction force on the indenter tip with reaction force decreasing during the second loading cycle. Indentation force values at maximum indentation depth were similar with a difference of 0.5% between cycles (Figure 14). A mesh convergence study for the spherical indentation simulation indicated that the finite element mesh as presented was sufficiently refined.

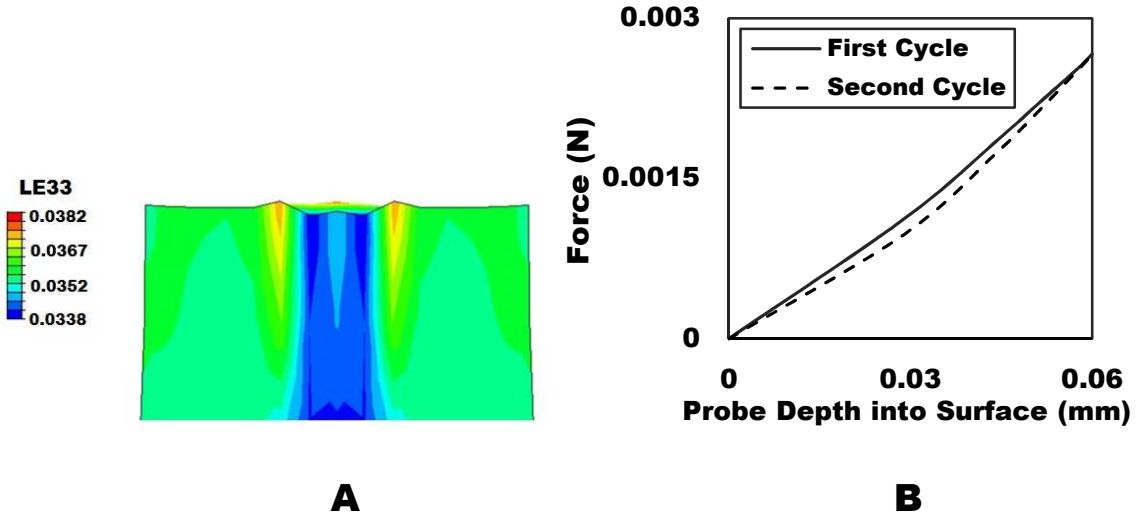

Figure 14. Finite element results. (A) A contour plot of logarithmic strain perpendicular to the articular surface in the superficial zone showing cartilage thickening post damage. Displacements are shown 100x for clarity. (B) Force vs. displacement plots for 2 cycle indentation loading showing hysteresis and a decrease in reaction force in the second cycle compared to the first cycle.

2.5 Discussion

Reduction in the mechanical integrity of AC due to damage, degradation, and disease has been well documented experimentally (McCormack & Mansour, 1997; Bae *et al.*, 2003; Temple *et al.*, 2007; Temple-Wong *et al.*, 2009; Novakofski *et al.*, 2014;). Recently, computational modeling has emerged as a means of studying the mechanical response of AC tissue under various conditions (Wilson *et al.*, 2005a; Wilson *et al.*, 2006; Davol *et al.*, 2007; Ateshian *et al.*, 2009) including the study of AC degeneration and damage (Wilson *et al.*, 2005b; Hosseini *et al.*, 2014). Therefore, in this study, a previously developed equilibrium constitutive model of AC (Stender *et al.*, 2012) was updated to include damage formulations for both COL and GAG constituents creating a highly anisotropic 3-D CDAC model. In the CDAC model,

healing and/or repair of either GAG or COL constituents is disallowed. Previously published experimental biochemical, (Williams *et al.*, 2010) biomechanical, (Williams *et al.*, 2010) and computational (Stender *et al.*, 2012) parameters for newborn bovine AC from the patellofemoral groove were integrated to create a high fidelity anisotropic 3-D constitutive model that could be implemented in a finite element analysis software package. In this study, newborn bovine tissue from the patellofemoral groove is studied because a more comprehensive set of experimental data was currently not available for another tissue source. The MAT constituent of AC is included herein to improve numerical model convergence properties, and to facilitate expansion of this model to additional tissue sources that may have more influential MAT constituent responses. For example, GAG molecule concentration and COL fibril volume fraction vary between immature and adult bovine (Williamson *et al.*, 2005) tissue which may result in a higher MAT shear modulus, μ, for adult AC compared to immature AC tissue. To determine the effects of ultimate COL fibril strain, E_N^D, a single element finite element model of a uniaxial tensile test was created and run to macroscopic tissue failure with a range of E_N^D values. In addition, a spherical indentation of AC with discrete SZ and MZ layers was simulated using finite element analysis. All simulations required an initial unloaded equilibrium step where GAG swelling pressure is balanced by COL and MAT constituents resulting in a small volumetric expansion. With this GAG molecule formulation it is not possible to explicitly reach an unloaded GAG reference configuration. If future experiments show that it is absolute strain of the GAG molecules, rather than the strain relative

to the GAG unloading state (*i.e.* equilibrium) that is influential on GAG damage, a different GAG formulation may be more appropriate. Neither GAG, nor COL fibril damage was calculated in equilibrium solution steps because there was no volumetric compression to cause GAG damage, and the expansion strains were sufficiently small as to not damage to COL fibrils. Although no damage was incurred in the initial equilibrium step, the higher GAG molecule concentration, and consequently, the higher GAG swelling pressure in the MZ caused the MZ to fail at slightly lower ultimate tensile strain values compared to the SZ. In the MZ, higher GAG swelling pressure resulted in greater initial COL fibril strains following the initial equilibrium step. For the same value of E_N^D in the SZ and MZ, the greater initial COL strains in the MZ resulted in lower ultimate tensile strain values. The proposed CDAC model and the developed finite element models were used to simulate AC damage, degradation, and ultimate tissue failure and to compare simulation results with experimental results. Thus, the hypothesis of this study was that a CDAC model utilizing independent anisotropic COL and isotropic GAG constitutive damage models could be used to model AC damage. The computational capability developed here will help researchers to better understand the mechanisms that lead to early stage OA and progress to late stage OA.

The spherical indentation finite element simulation results from this work elucidate the potential damage response, and the constituent specific consequences of overloading on AC. Some extent of validation of these indentation simulation results is possible through comparisons of the locations of COL and GAG damage

between these modeling results and experimental studies. The experimental observation that GAG damage which in this model is considered to be equivalent to reductions in GAG density, was found to occur predominantly in the superficial layers of AC with overloading (Rolauffs *et al.*, 2010) is in good agreement with the location of GAG damage calculated with our CDAC model. Another study observed that in OA, COL denaturation started at the articular surface (Hollander *et al.*, 1995) which is a result that is again in good agreement with our CDAC model results. Although this model predicts that damage initiates in the SZ, propagation of damage into the MZ is not presently simulated and may require additional development such as element deletion and/or fatigue damage criteria. Additionally, through damage to the COL fibrils, and the inherent osmotic swelling pressure of GAG molecules, the CDAC model predicts a post damage increase in cartilage thickness that is consistent with previous observations of AC thickening with OA (Buck *et al.*, 2009; Cotofana *et al.*, 2012). However, it is difficult to directly compare experimental results for AC thickening in OA with our model because the loading history of OA groups is unknown. These CDAC model results indicate that overloading that leads to AC damage may lead to AC thickening. In our CDAC model, swelling is indirectly modeled *via* a GAG molecule induced osmotic pressure rather than an explicit swelling model as proposed by Lai *et al.* (1991) or an intrafibrillar and extrafibrillar compartmental swelling model as proposed by Loret & Simões (2004). For the immature tissue studied here, the intrafibrilliar and extrafibrillar compartmental model of AC is likely unnecessary due to the low GAG concentration (Oungoulian,

2007). In the future, work to include explicit AC swelling models may improve these CDAC model results. The spherical indentation simulation from this work introduces discrete SZ and MZ layers that are attached *via* tied contact constraints. Due to the inherent discrete nature of finite element analysis, our model does not include a smooth transition between SZ and MZ regions. Therefore, the stiffer COL fibril modulus, and higher GAG molecule concentration in the MZ coupled with the strain based damage theory presented here, effectively make the MZ much stiffer focusing deformations as well as damage in the softer SZ. The reduced load carrying capacity with subsequent post damage loading to the same indentation depth (Figure 14) suggests that there is a reduced load carrying capacity of AC following even small amounts of damage that may lead to further damage propagation under otherwise normal loading conditions. The spherical indentation simulations presented here provide insight into the specific constituent responses as well as the overall AC tissue response to loading which induces damage.

The CDAC model presented in this paper is subject to several limitations. For example, the CDAC model is currently calibrated only for newborn bovine AC from the patellofemoral groove because there was not a comprehensive data set in terms of age, depth, anatomical site, and species available for another tissue source. Also, the GAG constituent damage model implies that even for small volumetric compression that may be experienced during normal physiological loading GAG damage will occur. However, the GAG damage function, d^{GAG} is proposed such that small volumetric compressions will not result in significant GAG damage.

Additionally, time-dependent effects such as viscoelasticity and poroelasticity have been neglected. Thus, this CDAC model represents the equilibrium response of AC, and all time dependent effects such as the viscoelasticity of COL fibrils and poroelasticity of the solid matrix of AC are neglected. Therefore, a direct experimental validation of the tensile and/or compressive failure results presented in this work would require extremely slow experimental strain rates (*i.e.* strain rate approaching zero) not currently available in the literature. The CDAC model does represent a first step towards a complete time dependent model of AC damage, and currently, the CDAC model could be used to simulate focal defects and other early injuries to AC both *in vivo* and *in vitro*. Due to the great number of experimental biomechanical and biochemical parameters required for a complete validation of this CDAC model, the present work is presented without complete validation. It should be noted that all of the constituent parameters implemented in this CDAC model including COL fibril and GAG damage parameters are likely subject to large inherent biological variations with respect to factors such as species, anatomical location, age, disease state, and loading history.

Several constitutive assumptions regarding the mechanical behavior of COL fibrils were required for the implementation of the CDAC model. One such assumption is that the mechanical response of a single COL fibril is linearly elastic up to the failure strain. A previous study successfully modeled the experimental behavior of newborn bovine AC from the patellofemoral groove using a constant fibril modulus (Stender *et al.*, 2012). However, this assumption may not be appropriate for

more mature AC tissue, or for AC from a different source. Another assumption is the complete and immediate failure of COL fibrils strained beyond the Lagrangian failure strain parameter, E_N^D which is supported by an imaging study that observed COL fibril rupture and failure (Sasazaki *et al.*, 2006) likely leading to a complete loss of the mechanical integrity of damaged COL fibrils. A different post yield COL fibril behavior (*e.g.* COL fibril softening) and/or the inclusion of time-dependent effects may better capture the macroscopic AC damage response observed experimentally in uniaxial tension (Asanbaeva *et al.*, 2008, 2007b) and tensile fatigue (Weightman, 1976; Weightman *et al.* 1978 Bellucci & Seedhom, 2002). This CDAC model of COL fibril damage is presented in a rigorous and general sense that allows for differential COL fibril failure behaviors to be implemented with additional experimental results. In this CDAC model, finite deformations of the macroscopic tissue lead to progressive COL fibril recruitment, and with sufficient deformations, subsequent COL damage that progresses through fibrils originally oriented in different directions. Due to the progressive loading behavior of the COL fibrils, the damage response of AC tissue is dependent on the initial COL fibril distribution and the direction of loading. The alteration of the effective distribution of COL fibrils in AC due to damage (Figure 11) may have profound effects on the propagation of damage and the evolution of OA. With additional experimental observations, future studies may improve the accuracy of the assumptions made here regarding COL fibril behavior.

The mechanical damage response of AC in our CDAC model has been shown to be highly dependent on the COL fibril Lagrangian failure strain in direction N, E_N^D.

However, precise values of E_N^D have not yet been established. Molecular computational modeling studies have suggested that COL fibrils are capable of attaining large deformations between 15% and 45% which is the range of the COL fibril failure strains studied in this work (Buehler, 2007; Tang *et al.*, 2010). An additional molecular modeling study examined the failure behavior of COL fibrils showing that structural fibril parameters such as fibril length, fibril diameter, and crosslink density had an effect on fibril failure properties in uniaxial stress in tension (Tang *et al.*, 2010). An experimental study using self-assembled uncrosslinked type I COL fibers found fiber failure strains between 24% and 68% strain (Pins & Silver, 1995). To our knowledge, there exists no concise description of the failure behavior or the failure strain of type II COL fibrils. Experimental studies coupled with a fitting of this model to experimental failure data may provide a method of determining an exact value for the COL fibril Lagrangian failure strain, E_N^D.

The GAG constituent damage model presented here hypothesizes that the maximum volumetric contraction in the loading history of AC results in an effective decrease in GAG molecule density as a result of GAG molecule leeching (*I.e.* GAG molecules pushed out of the tissue) and/or cleaving (*i.e.* GAG molecules breaking rendering them ineffective). Note that here there are no conclusions drawn with regards to the precise mechanism(s) of GAG damage. Thus, a potential limitation of the proposed GAG damage formulation is that only maximum volumetric decrease rather than cyclical loading results in GAG damage. Additionally, interactions between COL fibrils and GAG molecules may affect GAG damage evolution wherein

damaged fibrils are no longer able to retain GAG molecules in the solid matrix of AC. Although there is no exact validation of the proposed GAG damage model, several studies suggest that GAG damage may occur in AC during loading and in OA. To our knowledge, there is no consensus regarding the precise mechanisms that cause GAG damage. Thus, this model of GAG damage is presented as an example to propose one way that decreases in GAG concentration as observed experimentally may occur. For example, single impact overloading has been experimentally shown to lead to damage in AC (Jeffrey *et al.*, 1997; Bush *et al.*, 2005) indicating that one time overload scenarios can damage GAG molecules. An experimental study (Lin, 2004) showed in mature bovine cartilage that both cell death and GAG loss which in this work is considered to be equivalent to GAG damage, occurred starting from the articular surface following short term cyclical injury level loading (~6 hours). Another study found GAG molecule and COL fibril fragments in tissue media following loading (Thibault *et al.*, 2002) suggesting that loading can cause GAG molecules to disassociate from the tissue solid matrix. With chemical depletion of GAG molecules experimental studies have shown a diminished compressive response of AC tissue compared with normal AC (Korhonen *et al.*, 2003; Rieppo *et al.*, 2003). Furthermore with severe OA, alterations in GAG concentration have been observed compared with healthy AC tissue (Appleyard, 2003; Temple-Wong *et al.*, 2009) as well as alterations in GAG molecule structure and synthesis (Rizkalla *et al.*, 1992). Although the precise mechanism of GAG damage remains unknown, the GAG damage model proposed in this work establishes an example method for modeling a decrease in effective GAG

concentration, and consequently a decrease in GAG osmotic pressure as observed experimentally during loading and OA scenarios. Future experimental work to develop an understanding of the precise mechanisms of GAG molecule damage can be directly incorporated into this model by implementing alternative functions for d^{GAG}.

Our CDAC model has demonstrated a capability to model constituent specific damage and tensile failure in AC that likely lead to OA *in vivo*. Spherical indentation results demonstrate the experimentally observed locations of AC tissue damage in early term OA as well as cartilage overloading. Although limited simulation results are presented, the goal of this work is to introduce the CDAC model, and to outline constitutive development and implementation thereof. Future studies may use this model to study differential loading conditions and to expand the model to include fatigue damage behavior and/or element deletion criteria to more clearly demonstrate progressive damage behavior. Mesh convergence studies for the uniaxial tension and spherical indentation simulations indicated that both models had sufficiently refined meshes. However, as with other damage models, the CDAC model demonstrated mesh-dependent localization of damage. Further work to expand the CDAC model to include nonlocal effects or enhanced gradient damage methods could be implemented to eliminate mesh-dependent damage localization (Peerlings *et al.* 2001). Further experimental work may enable more precise validation of this model including the exact functional form of GAG molecule damage, and a type II COL fibril post yield behavior and Lagrangian failure strain value. Additional computational work is

proposed to expand this model to include development of constituent based viscoelastic and poroelastic properties to implement a time-dependent capability of this model, and enable more realistic *in vivo* damage simulations and comparisons with experimental data. Future experimental and computational studies that improve the precision of these results could be used to help treat OA patients and at-risk individuals. For example, one potential extension of this model would be to identify exercises or movements that may serve to mitigate the progression of AC damage for patients that are at already at a high risk for osteoarthritis. These results may help to elucidate the mechanisms and consequences of damage and degradation that lead to OA as well as traumatic AC injuries.

2.6 Appendix

The COL fibril damage parameter is specifically proposed as

$$d_N^f = H\left(\gamma_N^f\right) \tag{A1}$$

where γ_N^f is a dimensionless COL fibril damage related ISV in direction N. For this study, all COL fibrils are assumed to be initially undamaged and thus, all initial values of $\gamma_{N\,(0)}^f = 0$ are set such that $d_{N\,(0)}^f = 0$. With the intention of presenting a complete general theory, additional assumptions are required and introduced to define the evolution and history of COL fibril damage. All COL fibril damage history parameters are evaluated in each discrete direction N at each material point. First,

the COL damage function, f_N^{COL}, which tracks COL fibril damage in each direction N at a material point is introduced as

$$f_N^{COL} = -H(E_N - E_N^D) \tag{A2}$$

where H is the Heaviside step function operator, E_N is the current COL fibril directional Lagrangian strain, and E_N^D is the Lagrangian failure strain of a COL fibril (*i.e.* the maximum elastic strain of a COL fibril). If $E_N > E_N^D$ then $f_N^{COL} = -1$ and additional COL fibril damage has occurred in direction N. If $E_N \leq E_N^D$ then $f_N^{COL} = 0$ and no additional COL fibril damage has been incurred. An additional relationship is defined as

$$\delta\gamma_N^f = -f_N^{COL} \tag{A3}$$

where $\delta\gamma_N^f$ is the incremental change of the COL damage ISV, γ_N^f. For the case of $f_N^{COL} = 0$ equation (A3) gives $\delta\gamma_N^f = 0$ meaning that additional damage has not occurred and there is no evolution of the damage like internal state variable, γ_N^f. For $f_N^{COL} = -1$, equation (A3) gives $\delta\gamma_N^f = 1$. Note that because $\delta\gamma_N^f \geq 0$ healing and/or repair of COL fibrils is effectively disallowed as the value of γ_N^f can never decrease. An example of the stress-strain response for a fibril in direction N with E_N^D is shown below in Figure 1. In essence, for all $\delta\gamma_N^f \geq 1$ from equation (A1), $d_N^f = 1$, which represents a fully degraded fibril stress in the direction N. Note that this formulation is presented with the capability to easily implement alternative forms for d_N^f, and thus equations (A1, A2, and A3) are presented independently.

Collagen fibril constituent stress and material stiffness tensors

Using equation (6) and applying the chain rule as shown below

$$\frac{\partial \psi^{COL}}{\partial \mathbf{C}} = \frac{\partial \psi^{COL}}{\partial E_N}\frac{\partial E_N}{\partial \mathbf{C}} \tag{A4}$$

the following result for the COL constituent second Piola-Kirchoff stress tensor, $\mathbf{S}^{\mathrm{COL}}$ is derived.

$$\mathbf{S}^{\mathrm{COL}} = \frac{1}{4\pi}\int_{\phi=0}^{2\pi}\int_{\theta=0}^{\pi}\left[\delta(E_N)\frac{1}{2}\varphi_N^f {E^f}^2 E_N\left[1-H\left(\gamma_N^f\right)\right] + H(E_N)\varphi_N^f E^f E_N\left[1-H\left(\gamma_N^f\right)\right]\right][\mathbf{N}\otimes\mathbf{N}]\sin\theta d\theta d\phi \tag{A5}$$

For the integral, the first term is zero because the Dirac-Delta function $\delta(E_N)$ evaluates the integrand at $E_N = 0$, which leads to multiplication by $E_N = 0$, resulting in a zero term. The second term is the nonzero term, and is reported in equation (12). To derive the COL constituent material stiffness tensor equation (12) is used in equation (6) applying the chain rule as shown below in

$$\frac{\partial \mathbf{S}^{COL}}{\partial \mathbf{C}} = \frac{\partial \mathbf{S}^{COL}}{\partial E_N}\frac{\partial E_N}{\partial \mathbf{C}} \tag{A6}$$

giving the following result *via* a straightforward derivation.

$$\mathbb{C}_{ABCD}^{COL} = \frac{1}{4\pi}\int_{\phi=0}^{2\pi}\int_{\theta=0}^{\pi}\left[\delta(E_N)\varphi_N^f E^f E_N\left[1-H\left(\gamma_N^f\right)\right] + H(E_N)\varphi_N^f E^f\left[1-H\left(\gamma_N^f\right)\right]\right]N_A N_B N_C N_D \sin\theta d\theta d\phi \tag{A7}$$

The same cancellation of the first term in the integral of equation (A7) as used in the derivation of the COL Second Piola-Kirchhoff stress, gives the result reported in equation (13).

Clausius-Duhem Inequality

The Clausius-Duhem inequality ensures that the dissipation and damage related terms introduced in this model are thermodynamically consistent at finite strain. Note that the polyconvexity is satisfied as in Stender *et al.* (2012) yet, the additional damage terms presented must also be thermodynamically correct. The Clausius-Duhem inequality for a single COL fibril in direction N assuming uniaxial stress, isothermal conditions and homogeneous temperature can be written with respect to the reference configuration as

$$S_N^{COL}\dot{E}_N - \dot{\psi} \geq 0 \tag{A8}$$

where S_N^{COL} and $\dot{E_N}$ are the uniaxial COL Second Piola-Kirchhoff stress and Lagrangian strain rate in the direction N, respectively, and ψ is the Helmholtz free energy function per unit reference volume. The true COL fibril Helmholtz free energy function per unit reference volume, ψ^f is assumed to be a combination of elastic and damage terms as written below.

$$\psi^f\left(E_N, E_N^D, \gamma_N^f\right) = H(E_N)\frac{1}{2}E^f(E_N)^2\left[1 - H\left(\gamma_N^f\right)\right] \tag{A9}$$

Taking the material time derivative of ψ^f, neglecting any density changes in a single fibril, and substituting into equation (A8) gives the following result.

$$\left(S_N^{COL} - \frac{\partial(\psi^f)}{\partial E_N}\right)\dot{E}_N - \frac{\partial(\psi^f)}{\partial \gamma_N^f}\dot{\gamma}_N^f \geq 0 \tag{A10}$$

For clarity, the derivative terms are shown to be

$$\frac{\partial(\psi^f)}{\partial E_N} = \delta(E_N)\frac{1}{2}E^f(E_N)^2\left[1 - H\left(\gamma_N^f\right)\right] + H(E_N)E^f E_N\left[1 - H\left(\gamma_N^f\right)\right] \tag{A11}$$

and

$$\frac{\partial(\psi^f)}{\partial\gamma_N^f} = -H(E_N)\frac{1}{2}E^f(E_N)^2\delta\left(\gamma_N^f\right) \tag{A12}$$

Note that the first term of equation (A11) leads to zero integral over the reference configuration because $\delta(E_N)$ when evaluated within an integral over various pyramidal angles returns the integrand at $E_N = 0$ which results in a zero multiplication. In order to satisfy equation (A10) for arbitrary $\dot{E_N}$, the following result is derived for the true COL fibril Second Piola Kirchhoff stress in direction N as

$$S_N^{COL} = H(E_N)E^f E_N\left[1 - H\left(\gamma_N^f\right)\right] \tag{A13}$$

Thus, combining equation (A10) and equation (A12), the remaining inequality must hold

$$H(E_N)\frac{1}{2}E^f(E_N)^2\delta\left(\gamma_N^f\right)\dot{\gamma}_N^f \geq 0 \tag{A14}$$

which is satisfied for $E^f > 0$ noting that $\dot{\gamma}_N^f \geq 0$. In this work, the true COL fibril properties are expanded to the total COL properties by integrating spatially which gives the results presented in the text.

The Clausius-Duhem inequality for the GAG constituent is written with respect to the reference configuration as

$$\frac{1}{2}\mathbf{S}^{GAG}:\dot{\mathbf{C}} - \dot{\psi}^{GAG} \geq 0 \tag{A15}$$

Taking the material time derivative of $\psi^{GAG}(J,\beta)$ gives the following result.

$$\dot{\psi}^{GAG} = \frac{\partial(\psi^{GAG})}{\partial\mathbf{C}}\dot{\mathbf{C}} + \frac{\partial(\psi^{GAG})}{\partial\beta}\dot{\beta} \tag{A16}$$

The chain rule is applied to the $\frac{\partial(\psi^{GAG})}{\partial\mathbf{C}}$ term in equation (A15) as follows.

$$\frac{\partial(\psi^{GAG})}{\partial\mathbf{C}} = \frac{\partial(\psi^{GAG})}{\partial J}\frac{\partial J}{\partial\mathbf{C}} \tag{A17}$$

Noting that $\frac{\partial J}{\partial \mathbf{C}} = \frac{1}{2} J \mathbf{C}^{-1}$ and substituting equations (A17) into equation (A16) gives the result shown below.

$$\dot{\psi}^{GAG} = \left(\frac{1}{2}\frac{\partial(\psi^{GAG})}{\partial J} J \mathbf{C}^{-1}\right) \dot{\mathbf{C}} + \frac{\partial(\psi^{GAG})}{\partial \beta}\dot{\beta} \tag{A18}$$

Substituting equation (A18) into equation (A15) and rearranging terms gives the following result.

$$\left(\frac{1}{2}\mathbf{S}^{GAG} - \frac{1}{2}\frac{\partial(\psi^{GAG})}{\partial J} J \mathbf{C}^{-1}\right) : \dot{\mathbf{C}} - \frac{\partial(\psi^{GAG})}{\partial \beta}\dot{\beta} \geq 0 \tag{A19}$$

For clarity the derivative terms are given below.

$$\frac{\partial(\psi^{GAG})}{\partial J} = -\alpha_1 \left(\frac{\rho_0^{GAG}}{J}\right)^{\alpha_2} \left\{1 - d_{max}^{GAG}\left[e^{\left(\frac{-\beta}{\eta}\right)} - e^{\left(\frac{-1}{\eta}\right)}\right]\right\} \tag{A20}$$

and

$$\frac{\partial(\psi^{GAG})}{\partial \beta} = -\alpha_1 \alpha_2 \frac{(\rho_0^{GAG})^{\alpha_2}}{J^{(\alpha_2 - 1)}} \left\{\frac{d_{max}^{GAG}}{\eta}\left[e^{\left(\frac{-\beta}{\eta}\right)}\right]\right\} \tag{A21}$$

In order to satisfy equation (A19) for any arbitrary $\dot{\mathbf{C}}$, the following result is given for the GAG Second Piola-Kirchoff stress tensor, $\mathbf{S}^{GAG}$.

$$\mathbf{S}^{GAG} = J\mathbf{F}^{-1}\left(-\alpha_1 \left(\frac{\rho_0^{GAG}}{J}\right)^{\alpha_2} \left\{1 - d_{max}^{GAG}\left[e^{\left(\frac{-\beta}{\eta}\right)} - e^{\left(\frac{-1}{\eta}\right)}\right]\right\}\right)\mathbf{F}^{-\mathbf{T}} \tag{A22}$$

Additionally, to fully satisfy equation (A19), the following inequality must also hold.

$$\alpha_1 \frac{(\rho_0^{GAG})^{\alpha_2} J^{(1-\alpha_2)}}{(1-\alpha_2)} \left\{\frac{d_{max}^{GAG}}{\eta}\left[e^{\left(\frac{-\beta}{\eta}\right)}\right]\right\}\dot{\beta} \geq 0 \tag{A23}$$

Equation A23 is satisfied, when $\alpha_1 \geq 0$, $\rho_0^{GAG} \geq 0$, $\alpha_2 > 1$, $d_{max}^{GAG} \geq 0$, $\eta \geq 0$, and $\dot{\beta} \leq 0$ as presented herein. Note that equation (19) ensures that $\delta\beta \leq 0$, and thus, $\dot{\beta} \leq 0$.

2.7 Acknowledgements

This work was supported by NSF *CAREER* award #1055989, and the Innovative Grant Program at The University of Colorado at Boulder.

2.8 References

1. Appleyard, R. (2003). Topographical analysis of the structural, biochemical and dynamic biomechanical properties of cartilage in an ovine model of osteoarthritis. *Osteoarthritis and Cartilage*, *11*(1), 65–77. doi:10.1053/joca.2002.0867
2. Asanbaeva, A., Masuda, K., Thonar, E. J.-M. A., Klisch, S. M., & Sah, R. L. (2007a). Mechanisms of cartilage growth: Modulation of balance between proteoglycan and collagen in vitro using chondroitinase ABC. *Arthritis & Rheumatism*, *56*(1), 188–198. doi:10.1002/art.22298
3. Asanbaeva, A., Masuda, K., Thonar, E. J.-M. A., Klisch, S. M., & Sah, R. L. (2007b). Regulation of immature cartilage growth by IGF-I, TGF-β1, BMP-7, and PDGF-AB: role of metabolic balance between fixed charge and collagen network. *Biomechanics and Modeling in Mechanobiology*, *7*(4), 263–276. doi:10.1007/s10237-007-0096-8
4. Asanbaeva, A., Tam, J., Schumacher, B. L., Klisch, S. M., Masuda, K., & Sah, R. L. (2008). Articular cartilage tensile integrity: modulation by matrix depletion is maturation-dependent. *Archives of Biochemistry and Biophysics*, *474*(1), 175–182.

5. Ateshian, G. A. (2007). Anisotropy of fibrous tissues in relation to the distribution of tensed and buckled fibers. *Journal of biomechanical engineering*,*129*(2), 240-249.

6. Ateshian, G. A., Rajan, V., Chahine, N. O., Canal, C. E., & Hung, C. T. (2009). Modeling the `Many Observed Phenomena. *Journal of Biomechanical Engineering*, *131*(6), 061003. doi:10.1115/1.3118773

7. Bae, W. C., Temple, M. M., Amiel, D., Coutts, R. D., Niederauer, G. G., & Sah, R. L. (2003). Indentation testing of human cartilage: Sensitivity to articular surface degeneration. *Arthritis & Rheumatism*, *48*(12), 3382–3394. doi:10.1002/art.11347

8. Bellucci, G., & Seedhom, B. B. (2002). Tensile fatigue behaviour of articular cartilage. *Biorheology*, *39*(1), 193–199.

9. Botter, S. M., van Osch, G. J. V. M., Waarsing, J. H., van der Linden, J. C., Verhaar, J. A. N., Pols, H. A. P., … Weinans, H. (2008). Cartilage damage pattern in relation to subchondral plate thickness in a collagenase-induced model of osteoarthritis. *Osteoarthritis and Cartilage*, *16*(4), 506–514. doi:10.1016/j.joca.2007.08.005

10. Brocklehurst, R., Bayliss, M. T., Maroudas, A., Coysh, H. L., Freeman, M. A. R., Revell, P. A., & Ali, S. Y. (1984). The composition of normal and osteoarthritic articular cartilage from human knee joints. *J Bone Joint Surg Am*, *66*, 95–106.

11. Buck, R. J., Wyman, B. T., Le Graverand, M. hellio, Hudelmaier, M., Wirth, W., Eckstein, F., & A9001140 Investigators. (2009). Does the use of ordered values of subregional change in cartilage thickness improve the detection of disease

progression in longitudinal studies of osteoarthritis? *Arthritis & Rheumatism*, *61*(7), 917–924. doi:10.1002/art.24613

12. Buckwalter, J. A., & Mankin, H. J. (1998). Articular cartilage repair and transplantation. *Arthritis & Rheumatism*, *41*(8), 1331-1342.
13. Buehler, M. J. (2007). Molecular nanomechanics of nascent bone: fibrillar toughening by mineralization. *Nanotechnology*, *18*(29), 295102. doi:10.1088/0957-4484/18/29/295102
14. Buehler, M. J., & Ackbarow, T. (2008). Nanomechanical strength mechanisms of hierarchical biological materials and tissues. *Computer Methods in Biomechanics and Biomedical Engineering*, *11*(6), 595–607. doi:10.1080/10255840802078030
15. Buschmann M, Grodzinsky A. "A Molecular Model of Proteoglycan-AssociatedForces in Cartilage Mechanics." *Journal of Biomechanical Engineering*, 1995:117: 179-192
16. Bush, P., Hodkinson, P., Hamilton, G., & Hall, A. (2005). Viability and volume of bovine articular chondrocytes?changes following a single impact and effects of medium osmolarity. *Osteoarthritis and Cartilage*, *13*(1), 54–65. doi:10.1016/j.joca.2004.10.007
17. Calvo, B., Peña, E., Martinez, M. A., & Doblaré, M. (2007). An uncoupled directional damage model for fibred biological soft tissues. Formulation and computational aspects. *International Journal for Numerical Methods in Engineering*, *69*(10), 2036–2057. doi:10.1002/nme.1825

18. Cotofana, S., Buck, R., Wirth, W., Roemer, F., Duryea, J., Nevitt, M., … Osteoarthritis Initiative Investigators Group. (2012). Cartilage thickening in early radiographic knee osteoarthritis: A within-person, between-knee comparison. *Arthritis Care & Research*, *64*(11), 1681–1690. doi:10.1002/acr.21719
19. Curl, W. W., Krome, J., Gordon, E. S., Rushing, J., Smith, B. P., & Poehling, G. G. (1997). Cartilage injuries: a review of 31,516 knee arthroscopies. *Arthroscopy: The Journal of Arthroscopic & Related Surgery*, *13*(4), 456–460.
20. Davison, L., Stevens, A. L., & Kipp, M. E. (1977). Theory of spall damage accumulation in ductile metals. *Journal of the Mechanics and Physics of Solids*, *25*(1), 11-28.
21. Davol, A., Bingham, M. S., Sah, R. L., & Klisch, S. M. (2007). A nonlinear finite element model of cartilage growth. *Biomechanics and Modeling in Mechanobiology*, *7*(4), 295–307. doi:10.1007/s10237-007-0098-6
22. Famaey, N., Vander Sloten, J., & Kuhl, E. (2013). A three-constituent damage model for arterial clamping in computer-assisted surgery. *Biomechanics and Modeling in Mechanobiology*, *12*(1), 123–136. doi:10.1007/s10237-012-0386-7
23. Ficklin, T., Thomas, G., Barthel, J. C., Asanbaeva, A., Thonar, E. J., Masuda, K., … Klisch, S. M. (2007). Articular cartilage mechanical and biochemical property relations before and after *in vitro* growth. *Journal of Biomechanics*, *40*(16), 3607–3614.
24. Gajewski, T., Weisbecker, H., Holzapfel, G. A., & \Lodygowski, T. (n.d.). Implementation of a hyperelastic model for arterial layers considering damage

and distributed collagen fiber orientations. Retrieved from http://www.ikb.poznan.pl/tomasz.gajewski/cad.put.poznan.pl/TG/cmm2013_gajewski_weisbecker_holzapfel_logydowski.pdf

25. Gautieri, A., Vesentini, S., Redaelli, A., & Buehler, M. J. (2011). Hierarchical Structure and Nanomechanics of Collagen Microfibrils from the Atomistic Scale Up. *Nano Letters*, *11*(2), 757–766. doi:10.1021/nl103943u
26. Hollander, A. P., Pidoux, I., Reiner, A., Rorabeck, C., Bourne, R., & Poole, A. R. (1995). Damage to type II collagen in aging and osteoarthritis starts at the articular surface, originates around chondrocytes, and extends into the cartilage with progressive degeneration. *Journal of Clinical Investigation*, *96*(6), 2859.
27. Hosseini, S. M., Wilson, W., Ito, K., & van Donkelaar, C. C. (2014). A numerical model to study mechanically induced initiation and progression of damage in articular cartilage. *Osteoarthritis and Cartilage*, *22*(1), 95–103. doi:10.1016/j.joca.2013.10.010
28. Jeffrey, J. E., Thomson, L. A., & Aspden, R. M. (1997). Matrix loss and synthesis following a single impact load on articular cartilage in vitro. *Biochimica et Biophysica Acta (BBA)-General Subjects*, *1334*(2), 223–232.
29. Kiviranta, P., Rieppo, J., Korhonen, R. K., Julkunen, P., Töyräs, J., & Jurvelin, J. S. (2006). Collagen network primarily controls Poisson's ratio of bovine articular cartilage in compression. *Journal of Orthopaedic Research*, *24*(4), 690–699. doi:10.1002/jor.20107

30. Korhonen, R. K., Laasanen, M. S., Töyräs, J., Lappalainen, R., Helminen, H. J., & Jurvelin, J. S. (2003). Fibril reinforced poroelastic model predicts specifically mechanical behavior of normal, proteoglycan depleted and collagen degraded articular cartilage. *Journal of Biomechanics*, *36*(9), 1373–1379. doi:10.1016/S0021-9290(03)00069-1

31. Kuettner, Klaus E. "Biochemistry of articular cartilage in health and disease."*Clinical Biochemistry*, 1992: 25(3): 155-163.

32. Lai, W. M., Hou, J. S., & Mow, V. C. (1991). A triphasic theory for the swelling and deformation behaviors of articular cartilage. *Journal of biomechanical engineering*, *113*(3), 245-258.

33.. Lai, W. M., Mow, V. C., & Roth, V. (1981). Effects of nonlinear strain-dependent permeability and rate of compression on the stress behavior of articular cartilage. *Journal of biomechanical engineering*, *103*(2), 61-66.

34. Lanir, Y. (1983). Constitutive equations for fibrous connective tissues. *Journal of biomechanics*, *16*(1), 1-12.

35. Lei, F., & Szeri, A. Z. (2006). The influence of fibril organization on the mechanical behaviour of articular cartilage. *Proceedings of the Royal Society A: Mathematical, Physical and Engineering Sciences*, *462*(2075), 3301–3322. doi:10.1098/rspa.2006.1732

36. Li, L. P., Buschmann, M. D., & Shirazi-Adl, A. (2003). Strain-rate Dependent Stiffness of Articular Cartilage in Unconfined Compression. *Journal of Biomechanical Engineering*, *125*(2), 161. doi:10.1115/1.1560142

37. Lin, P. (2004). Increased stromelysin-1 (MMP-3), proteoglycan degradation (3B3- and 7D4) and collagen damage in cyclically load-injured articular cartilage. *Osteoarthritis and Cartilage*, *12*(6), 485–496. doi:10.1016/j.joca.2004.02.012

38. Loret, B., & Simões, F. M. (2004). Articular cartilage with intra-and extrafibrillar waters: a chemo-mechanical model. *Mechanics of Materials*, *36*(5), 515-541.

39. Maroudas, A. (1976). Balance between swelling pressure and collagen tension in normal and degenerate cartilage. *Nature*, *260*(5554), 808-809.

40. Maroudas, A., Bannon, C. Measurement of swelling pressure in cartilage and comparison with the osmotic pressure of constituent proteoglycans. Biorheology 1981: 18(3-6): 619-632

41. Maroudas, A., Bayliss, M. T., & Venn, M. F. (1980). Further studies on the composition of human femoral head cartilage. *Annals of the Rheumatic Diseases*, *39*(5), 514–523.

42. Maroudas, A., & Venn, M. (1977). Chemical composition and swelling of normal and osteoarthrotic femoral head cartilage. II. Swelling. *Annals of the rheumatic diseases*, *36*(5), 399-406.

43. McCormack, T., & Mansour, J. M. (1997). Reduction in tensile strength of cartilage precedes surface damage under repeated compressive loading *in vitro*. *Journal of Biomechanics*, *31*(1), 55–61.

44. Novakofski, K. D., Williams, R. M., Fortier, L. A., Mohammed, H. O., Zipfel, W. R., & Bonassar, L. J. (2014). Identification of cartilage injury using quantitative

multiphoton microscopy. *Osteoarthritis and Cartilage*, *22*(2), 355–362. doi:10.1016/j.joca.2013.10.008

45. Noyes, F. R., & Stabler, C. L. (1989). A system for grading articular cartilage lesions at arthroscopy. *The American Journal of Sports Medicine*, *17*(4), 505–513. doi:10.1177/036354658901700410

46. Oungoulian, S. (2007). *Articular Cartilage Constitutive Modeling: A Polyconvex Strain Energy Function for Proteoglycan and Validation of a Growth Mixture Model with Collagen Remodeling: a Thesis* (Master's dissertation, California Polytechnic State University).

47. Pins, G. D., & Silver, F. H. (1995). A self-assembled collagen scaffold suitable for use in soft and hard tissue replacement. *Materials Science and Engineering: C*, *3*(2), 101-107.

48. Peerlings, R. H. J., Geers, M. G. D., De Borst, R., & Brekelmans, W. A. M. (2001). A critical comparison of nonlocal and gradient-enhanced softening continua. *International Journal of solids and Structures*, *38*(44), 7723-7746.

49. Rizkalla, G., Reiner, A., Bogoch, E., & Poole, A. R. (1992). Studies of the articular cartilage proteoglycan aggrecan in health and osteoarthritis. Evidence for molecular heterogeneity and extensive molecular changes in disease. *Journal of Clinical Investigation*, *90*(6), 2268.

50. Rodríguez, J. F., Cacho, F., Bea, J. A., & Doblaré, M. (2006). A stochastic-structurally based three dimensional finite-strain damage model for fibrous soft tissue. *Journal of the Mechanics and Physics of Solids*, *54*(4), 864-886.

51. Rodriguez, J. F., Alastrue, V., & Doblare, M. (2008). Finite element implementation of a stochastic three dimensional finite-strain damage model for fibrous soft tissue. *Computer Methods in Applied Mechanics and Engineering*,*197*(9), 946-958.

52. Rolauffs, B., Muehleman, C., Li, J., Kurz, B., Kuettner, K. E., Frank, E., & Grodzinsky, A. J. (2010). Vulnerability of the superficial zone of immature articular cartilage to compressive injury. *Arthritis & Rheumatism*, *62*(10), 3016–3027. doi:10.1002/art.27610

53. Saarakkala, S., Julkunen, P., Kiviranta, P., Mäkitalo, J., Jurvelin, J. S., & Korhonen, R. K. (2010). Depth-wise progression of osteoarthritis in human articular cartilage: investigation of composition, structure and biomechanics. *Osteoarthritis and Cartilage*, *18*(1), 73–81. doi:10.1016/j.joca.2009.08.003

54. Sasazaki, Y., Shore, R., & Seedhom, B. B. (2006). Deformation and failure of cartilage in the tensile mode. *Journal of Anatomy*, *208*(6), 681–694.

55. Schröder, J., & Neff, P. (2003). Invariant formulation of hyperelastic transverse isotropy based on polyconvex free energy functions. *International journal of solids and structures*, *40*(2), 401-445.

56. Shirazi, R., Vena, P., Sah, R. L., & Klisch, S. M. (2011). Modeling the collagen fibril network of biological tissues as a nonlinearly elastic material using a continuous volume fraction distribution function. *Mathematics and Mechanics of Solids*, *16*(7), 706–715. doi:10.1177/1081286510387866

57. Stender, M. E., Raub, C. B., Yamauchi, K. A., Shirazi, R., Vena, P., Sah, R. L., … Klisch, S. M. (2012). Integrating qPLM and biomechanical test data with an anisotropic fiber distribution model and predictions of TGF- ß1 and IGF-1 regulation of articular cartilage fiber modulus. *Biomechanics and Modeling in Mechanobiology*. doi:10.1007/s10237-012-0463-y

58. Tang, Y., Ballarini, R., Buehler, M. J., & Eppell, S. J. (2010). Deformation micromechanisms of collagen fibrils under uniaxial tension. *Journal of The Royal Society Interface*, *7*(46), 839–850. doi:10.1098/rsif.2009.0390

59. Temple, M. M., Bae, W. C., Chen, M. Q., Lotz, M., Amiel, D., Coutts, R. D., & Sah, R. L. (2007). Age- and site-associated biomechanical weakening of human articular cartilage of the femoral condyle. *Osteoarthritis and Cartilage*, *15*(9), 1042–1052. doi:10.1016/j.joca.2007.03.005

60. Temple-Wong, M. M., Bae, W. C., Chen, M. Q., Bugbee, W. D., Amiel, D., Coutts, R. D., … Sah, R. L. (2009). Biomechanical, structural, and biochemical indices of degenerative and osteoarthritic deterioration of adult human articular cartilage of the femoral condyle. *Osteoarthritis and Cartilage*, *17*(11), 1469–1476. doi:10.1016/j.joca.2009.04.017

61. Thibault, M., Robin Poole, A., & Buschmann, M. D. (2002). Cyclic compression of cartilage/bone explants in vitro leads to physical weakening, mechanical breakdown of collagen and release of matrix fragments. *Journal of Orthopaedic Research*, *20*(6), 1265–1273.

62. Thomas, G. C., Asanbaeva, A., Vena, P., Sah, R. L., & Klisch, S. M. (2009). A Nonlinear Constituent Based Viscoelastic Model for Articular Cartilage and Analysis of Tissue Remodeling Due to Altered Glycosaminoglycan-Collagen Interactions. *Journal of Biomechanical Engineering*, *131*(10), 101002. doi:10.1115/1.3192139

63. Weightman, B. (1976). Tensile fatigue of human articular cartilage. *Journal of Biomechanics*, *9*(4), 193–200.

64. Weisbecker, H., Pierce, D. M., Regitnig, P., & Holzapfel, G. A. (2012). Layer-specific damage experiments and modeling of human thoracic and abdominal aortas with non-atherosclerotic intimal thickening. *Journal of the Mechanical Behavior of Biomedical Materials*, *12*, 93–106. doi:10.1016/j.jmbbm.2012.03.012

65. Williams, G. M., Dills, K. J., Flores, C. R., Stender, M. E., Stewart, K. M., Nelson, L. M., … Klisch, S. M. (2010). Differential regulation of immature articular cartilage compressive moduli and Poisson's ratios by *in vitro* stimulation with IGF-1 and TGF-ß1. *Journal of Biomechanics*, *43*(13), 2501–2507.

66. Williamson, A. K., Chen, A. C., & Sah, R. L. (2001). Compressive properties and function—composition relationships of developing bovine articular cartilage.*Journal of Orthopaedic Research*, *19*(6), 1113-1121.

67. Williamson, A. K., Chen, A. C., Masuda, K., Thonar, E. J.-M. A., & Sah, R. L. (2003). Tensile mechanical properties of bovine articular cartilage: Variations with growth and relationships to collagen network components. *Journal of Orthopaedic Research*, *21*(5), 872–880. doi:10.1016/S0736-0266(03)00030-5

68. Wilson, W., Huyghe, J. M., & Donkelaar, C. C. (2006). Depth-dependent Compressive Equilibrium Properties of Articular Cartilage Explained by its Composition. *Biomechanics and Modeling in Mechanobiology*, *6*(1-2), 43–53. doi:10.1007/s10237-006-0044-z

69. Wilson, W., van Donkelaar, C. C., van Rietbergen, B., & Huiskes, R. (2005a). A fibril-reinforced poroviscoelastic swelling model for articular cartilage. *Journal of Biomechanics*, *38*(6), 1195–1204. doi:10.1016/j.jbiomech.2004.07.003

70. Wilson, W., van Donkelaar, C. C., van Rietbergen, R., & Huiskes, R. (2005b). The role of computational models in the search for the mechanical behavior and damage mechanisms of articular cartilage. *Medical Engineering & Physics*, *27*(10), 810–826. doi:10.1016/j.medengphy.2005.03.004

71. Wong, B. L., Kim, S. H. C., Antonacci, J. M., McIlwraith, C. W., & Sah, R. L. (2010). Cartilage shear dynamics during tibio-femoral articulation: effect of acute joint injury and tribosupplementation on synovial fluid lubrication. *Osteoarthritis and Cartilage*, *18*(3), 464–471. doi:10.1016/j.joca.2009.11.008

CHAPTER 3

A Poroelastic Finite Element Model of the Bone-Cartilage Unit to Determine the Effects of Changes in Permeability with Osteoarthritis

3.1 Abstract

The changes experienced in synovial joints with the onset and progression of osteoarthritis are complex and involve coupled chemical, biological, and mechanical processes. The aim of this study was to investigate the consequences of increasing permeability in articular cartilage (AC), calcified cartilage (CC), subchondral cortical bone (SCB), and subchondral trabecular bone (STB) tissues as observed with osteoarthritis. Two poroelastic finite element models were developed both using a depth-dependent anisotropic model of AC with strain-dependent permeability and poroelastic models of calcified tissues (CC, SCB, and STB). All tissues were combined to create two bone-cartilage unit (BCU) models. The first model simulated a complete BCU in uniaxial unconfined compression, while the second model simulated spherical indentation of the AC surface. Results indicate that the permeability of AC is the primary determinant of the BCU's poromechanical response while the permeability of calcified tissues exerts no appreciable effect on the force-indentation response of

the BCU. In spherical indentation simulations with osteoarthritic tissue permeability properties, fluid velocities were larger in magnitude and distributed over a smaller area compared to normal tissues. *In vivo*, this phenomenon would likely lead to chondrocyte death, tissue remodeling, alterations in joint lubrication, and intensify the progression of osteoarthritis. For both osteoarthritic and normal tissue permeability values, fluid flow was predicted to occur across the osteochondral interface. These results may help elucidate the consequences of increases in the permeability of the BCU that occur with osteoarthritis. Furthermore, this study may help to guide future treatments and strategies designed to counteract osteoarthritis.

3.2 Introduction

Osteochondral tissues such as articular cartilage (AC), calcified cartilage (CC), subchondral cortical bone (SCB), and subchondral trabecular bone (STB) play essential roles in skeletal function and joint health. The bone-cartilage unit (BCU), a term first used by Lories and Luyten (2010) is the functional combination of soft (AC) and calcified tissues (CC, SCB, and STB) in synovial joints. The BCU often afflicted by osteoarthritis leading to severe pain and loss of joint function. With osteoarthritis, mechanically-induced changes in AC, and calcified tissues initiate and propagate to result in progressive worsening of osteoarthritis symptoms (Temple-Wong *et al.*, 2009; Burr & Gallant, 2012). Due to the integrated nature of tissues in the BCU, the loads experienced by any single tissue, are inherently dependent on the other tissues of the BCU. Additionally, *in vivo*, the BCU is saturated with fluids and exhibits a

poromechanical response that is dependent on the permeability of tissues in the BCU (Soltz & Ateshian, 1998; Cowin, 1999; Swan, *et al.*, 2003; Hwang *et al.*, 2008; Taffetani, *et al.*, 2013). Because of the significantly greater stiffness of the calcified tissues within the BCU relative to AC, the inclusion of deformable material models of calcified tissues has little effect on computational results compared with a rigid approximation (Donahue *et al.*, 2002). However, it is presently not clear precisely what role calcified tissues play in the poromechanics of the BCU.

In vivo, all tissues within the BCU are saturated with fluid and thus exhibit a poroelastic response to mechanical loading during healthy tissue function (Cowin, 1999; Wilson, *et al.*, 2004; Hwang *et al.*, 2008). Stress relaxation experiments have shown that in bovine AC, for extended loading periods lasting up to 724 seconds, pore fluid pressure supports more than 90% of the applied stress at a constant 10% confined compression strain with the remaining load supported by the AC solid matrix (Soltz & Ateshian, 1998). The poroelastic properties of the BCU have been shown to vary greatly with the onset and progression of osteoarthritis. Changes with osteoarthritis cause the tissue permeability of all BCU tissues to increase substantially (Setton *et al.*, 1995; Hwang *et al.*, 2008). Recent studies have shown that fluid flow and molecular signaling across the osteochondral interface between AC and CC are likely and are potentially critical to the health of the BCU (Hwang *et al.*, 2008; Pan *et al.*, 2009; Lories & Luyten, 2010; Suri & Walsh, 2012). Moreover, as osteoarthritis progresses, a diminished poromechanical response of the osteochondral tissues may cause additional worsening of osteoarthritis symptoms due to a reduced

load carrying capacity (Hwang *et al.*, 2008; Lories & Luyten, 2010). Due to the importance of the poromechanical response of the BCU and the alterations in permeability that occur with osteoarthritis, this study will explore the specific permeability-dependent response of the BCU for both normal and osteoarthritic permeability values.

There is still much that remains unknown regarding the mechanical behavior of the complete BCU and how osteochondral tissues integrate and interact. Currently, there exists a wide range of computational (Korhonen *et al.*, 2003; Wilson *et al.*, 2004; Wilson, *et al.*, 2005; Julkunen, *et al.*, 2008; Pierce, *et al.*, 2013) and experimental (Lai, *et al.*, 1981; Chen, *et al.*, 2007; Williams *et al.*, 2010) studies that attempt to quantify the poromechanical properties of AC alone. Previous studies have experimentally quantified the mechanical behavior of bone tissue (Li & Aspden, 1997; Nauman, *et al.*,1999; Gupta *et al.*, 2005; Burr & Gallant, 2012). Furthermore, additional work has been completed focusing on modeling the mechanical behavior of subchondral and cortical bone (Niebur, *et al.*, 2000; Hazelwood, *et al.*, 2001; Swan, *et al.*, 2003; Mullins, *et al.*, 2009). However to our knowledge, no previous study has sought to computationally assess the combined poroelastic response of the complete BCU for normal and osteoarthritic permeability values. Thus, to improve upon the current understanding of the function of the BCU in health and with osteoarthritis, this study seeks to combine appropriate constitutive material modeling, finite element modeling, and previously published experimental data with the goal of elucidating consequences of increased permeability in osteochondral tissues within the BCU.

These results will better inform future experimental and computational studies of the BCU and may provide insight into future osteoarthritis prevention and treatment strategies.

3.3 Materials and Methods

To investigate the poromechanics of the BCU, two finite element models were developed using Abaqus (v6.13, Simulia). The first quarter symmetry model simulated uniaxial unconfined compression of an osteochondral block (Figure 15A) while the second simulated spherical indentation of a BCU block (Figure 15B). Although both unconfined compression and spherical indentation simulations could be simulated using 2-D axisymmetric models, the anisotropic constitutive model of AC used herein was developed in 3-D, and consequently the simulations in this work are also developed in 3-D.

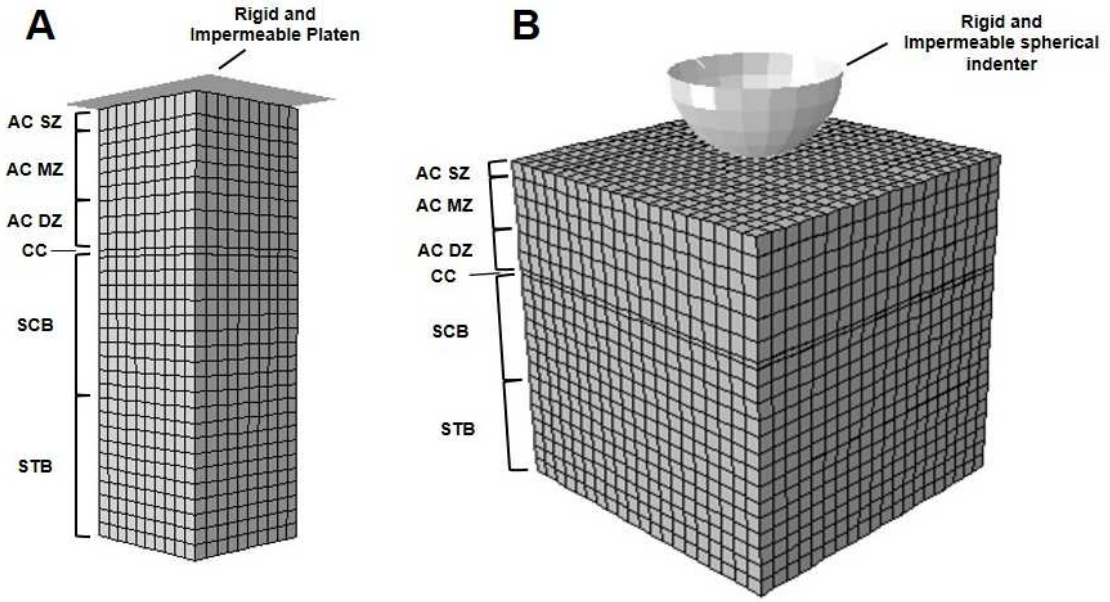

Figure 15. Finite element models for (A) quarter symmetry unconfined compression simulations and (B) spherical indentation simulations. The unconfined compression model consisted of 3000 3-D elements, and the spherical indentation simulations consisted of 8400 3-D elements. Brackets denote differential material regions including articular cartilage superficial zone (AC SZ), articular cartilage middle zone (AC MZ), articular cartilage deep zone (AC DZ), calcified cartilage (CC), subchondral cortical bone (SCB), and subchondral trabecular bone (STB). Each material region was simulated using appropriate constitutive models and permeability values for either normal or osteoarthritic tissues.

Both unconfined compression and spherical indentation models were comprised of six discrete tissue zones including, superficial zone AC, middle zone AC, deep zone AC, CC, SCB, and STB regions. Unconfined compression and spherical indentation simulations assumed tissue thicknesses in each of the six discrete tissue zone as listed in Table 3. Body forces did not significantly affect results at the scales studied and were neglected on both solid and fluid phases in all simulations.

All tissues of the BCU were assumed to be permeable and to exhibit a poroelastic response under applied loading. Due to the finite deformations experienced by AC, a strain-dependent permeability model was implemented for all zones of AC. The following relationship defined in terms of void ratio as required by Abaqus, and used by Ficklin *et al.* (2009), was implemented to define the deformation-dependent permeability in articular cartilage:

$$\hat{k} = \hat{k}_0 \left[\frac{e}{e_0}\right]^2 exp\left(\frac{M}{2}\left(\left(\frac{1+e}{1+e_0}\right)^2 - 1\right)\right) \quad (1)$$

where $\hat{k}$ is the permeability in the current configuration $\left(\frac{mm^2}{Pa \cdot s}\right)$, $\hat{k}_0$ is the permeability at zero strain $\left(\frac{mm^2}{Pa \cdot s}\right)$, e and e_0 are the void ratios of the tissue in the current configuration and at zero strain, respectively, and M is a dimensionless material parameter controlling the nonlinearity of the permeability dependence (Lai *et al.*, 1981; Holmes & Mow, 1990). Abaqus requires permeability to be defined in units of $length \cdot time^{-1}$, thus published values of $\hat{k}$ were transformed according to the following relationship

$$k = \gamma_f \hat{k} \quad (2)$$

where γ_f is the unit weight of the wetting fluid in $\frac{N}{mm^3}$. For a complete description of the strain-dependent permeability model used in this work for AC, refer to Holmes & Mow (1990) and Ateshian *et al.* (1997). For AC, values of $\hat{k}$ were calculated for a range of current configuration void ratio values, and the results were input into Abaqus in a tabular format. All tissues were assumed to be initially fully saturated with fluid.

For all tissues, the wetting fluid was assumed to be water with a unit weight of $\gamma_f = 9.81 \times 10^{-6} \frac{N}{mm^3}$. Due to the relatively small deformations in calcified tissues, compared to the deformations in AC, the permeability values of the calcified tissues were assumed to be constant (*i.e.*, strain-independent). Initial permeability values for normal and osteoarthritic tissues, strain-dependent permeability parameter *M*, and undeformed void ratio values used in this model are listed in Table 3.

Table 3. Permeability parameters and tissue zone thicknesses used in this study for the superficial, middle, and deep zones of articular cartilage, calcified cartilage, subchondral cortical bone, and subchondral trabecular bone. Articular cartilage is assumed to exhibit a strain-dependent permeability, while calcified cartilage, subchondral cortical bone, and subchondral trabecular bone were assumed to exhibit strain-independent permeability. Thicknesses were assumed based on a generalized bone-cartilage unit.

	Tissue	Initial Permeability, Normal $\hat{k}_0 \left(\frac{mm^2}{MPa \cdot s}\right)$	Initial Permeability, Osteoarthritis $\hat{k}_0 \left(\frac{mm^2}{MPa \cdot s}\right)$	Initial Solid Matrix Void Ratio, e_0	M (dimensionless)	Thickness (mm)
Articular Cartilage	Superficial Zone	4.55e-3 [1]	6.81e-3 [6]	4.5 [3]	5.48 [1]	1.5
	Middle Zone	1.46e-3 [1]	2.16e-3 [6]	4.0 [3]	5.49 [1]	5.0
	Deep Zone	0.50e-3 [1]	0.74e-3 [6]	3.2 [3]	7.38 [1]	3.5
Calcified Tissues	Calcified Cartilage	90.0 [2]	140 [2]	1.1	-	0.05
	Subchondral Cortical Bone	90.0 [2]	140 [2]	1.1 [4]	-	10
	Subchondral Trabecular Bone	90.0 [2]	140 [2]	3.7 [5]	-	10

[1] From Chen *et al.,* 2001
[2] From Hwang *et al.,* 2008
[3] From Brocklehurst *et al.*, 1984
[4] From Wei *et al.*, 1998
[5] From Nauman *et al.,* 1998
[6] Adapted based on Setton *et al.*, 1995

Values of $\hat{k}_0$ and M for AC were obtained from an experimental study of human femoral heads (Chen *et al.* 2001), and $\hat{k}_0$ values for calcified tissues were obtained from Hwang *et al.*, (2008) for human knee subchondral bone plate tissue. Initial void ratio values for AC were used from Brocklehurst *et al.*, (1984) from adult human femoral condyles. The void ratio for subchondral cortical bone is from Wei *et al.*, (1998) for rabbit tissue, and the trabecular bone void ratio is from Nauman *et al.*, (1999) for the human proximal femur. The void ratio of CC was assumed to be the same as the void ratio of SCB.

In order to isolate the specific consequences of tissue permeability increases with osteoarthritis, alterations in mechanical properties as a result of AC degradation and bone remodeling were not explicitly considered in these simulations. To develop a baseline response of the BCU, unconfined compression and spherical indentation simulations were initially run while incorporating tissues possessing healthy material permeability values (Case 1, Normal) (Table 3). Additionally, an increase in the AC permeability to osteoarthritic values in the superficial, middle, and deep zones, overlying healthy CC and bone, (Case 2, AC OA) was simulated based on experimental permeability changes with osteoarthritis in mature canine tissues (Setton *et al.* 1995). Next, the effects of increased calcified tissue premeability to osteoarthritic values, with healthy overlying AC, (Case 3, Calcified OA) was simulated based on changes observed with osteoarthritic human femoral condyles (Hwang *et al.* 2008). Finally, spherical indentation and unconfined compression models were run with increased osteoarthritic permeability values for all

osteochondral tissues (Case 4, All OA). All simulations were run in parallel using 8-24 processers. To significantly decrease the computational expense of all simulations, the number of collagen fibril constituent pyramidal elements at each material point was decreased from 3200, as used previously (Stender *et al.*, 2012), to 200. Pilot indentation and uniaxial tension simulations of the reduction of COL fibril pyramidal elements indicated less than 3% differences in the results between 200 and 3200 collagen fibril pyramidal volume element models.

For unconfined compression and spherical indentation finite element simulations, each discrete tissue region was attached directly to the adjacent regions using a tied contact constraint as well as a surface-to-surface contact algorithm. The contact permeability was defined as $1.0\text{x}10^{9}$ $\left(\frac{mm^2 sec}{kg}\right)$ at all dissimilar material interfaces, and was determined, based on test problems to be sufficiently high such that there was no appreciable effect of interface permeability on the results. Contact with the rigid platen in unconfined compression simulations, and the spherical indenter in spherical indentation simulations, was implemented using a frictionless surface-to-surface contact algorithm with finite sliding. In unconfined compression and spherical indentation simulations, the nonlinear geometric effects (NLGEOM) option of Abaqus was activated. Due to the constitutive model chosen for all AC zones, an equilibrium step was run prior to loading for unconfined compression and spherical indentation simulations in order to account for the pre-stress of the AC solid matrix by glycosaminoglycan molecules (Stender, *et al.* 2012). The user material

subroutine (UMAT) capability of Abaqus was used to model the solid matrix response to load of all zones of AC. In Abaqus, total material Cauchy stress, **T**, is calculated as the sum of the solid matrix effective stress, $\mathbf{T}^{\text{eff}}$, as calculated either in the UMAT, or in Abaqus *via* the material library, and the pore fluid pressure, p_f, as

$$\mathbf{T} = \mathbf{T}^{eff} + p_f\mathbf{I} \tag{3}$$

where **T** and $\mathbf{T}^{\text{eff}}$ are positive in tension for their normal components, p_f is positive in compression, and **I** is the identity tensor.

For quarter-symmetry unconfined compression simulations (Figure 15A), BCU samples were compressed, by an impermeable platen, up to a 0.1 mm displacement over 400 seconds at a constant loading rate followed by a hold at constant maximum displacement for an additional 800 seconds to allow for pore fluid diffusion. For unconfined compression simulations, all regions of the BCU were given dimensions of 1.0 cm x 1.0 cm length x width, fluid pore pressure at the radial boundary was set to 0 MPa, and the top and bottom surfaces were impermeable (*i.e.*, fluid flow out of the sample was allowed only at the radial boundary). Following a mesh refinement study, the final unconfined compression model was implemented using 3000 hybrid pore fluid/stress trilinear displacement, trilinear pore pressure hexahedral elements (C3D8P) with full integration.

For the spherical indentation model simulations, size determination studies were conducted to determine the minimum BCU block dimensions such that the free boundary did not affect results. Based on BCU size determination studies, each tissue region in the spherical indentation model was defined with a 3.0 cm length x 3.0 cm

width. The indenter tip was simulated as a 1.50 cm radius rigid spherical indenter. Indentation loading was applied *via* a displacement of the spherical indenter into the articular cartilage surface layer to a depth of 0.1 cm over a 2 second duration, with a subsequent unloading back to the initial indenter location over an additional 2 seconds. The bottom surface of the STB was held fixed. Pore pressure was set to 0 MPa at the articular surface and the bottom of the STB (*i.e.*, fluid flow was only allowed out of the top and bottom free surfaces). A mesh convergence study was conducted and two models containing 8400 and 27000 C3D8P full integration elements were developed with the 8400 element version as shown in Figure 15B.

Due to the variety of tissues in the BCU, and the complex nature of the constitutive AC material model used, many material parameters are required to fully define solid matrix material behavior across each of the six discrete tissue regions. Previously, Stender *et al.*, (2012) established material parameters for the superficial zone and middle zone of native newborn bovine AC as used herein. Deep zone AC parameters were extrapolated linearly from the results for the superficial and middle zones (Stender *et al.*, 2012). Note that the AC material parameters are intended to represent a general mechanical response of AC rather than material properties AC from a specific source. For a full description of the AC model used here, as well as the meaning of specific AC material constants refer to (Stender, *et al.*, 2012). The AC material properties used in this work are listed in Table 4. For calcified tissues a linear elastic material behavior was assumed. Young's modulus for CC and SCB was available from a previous experimental study using tissue from the bovine femur

(Mente & Lewis, 1994). A compressive Young's modulus for STB was used based on an experimental study (Morgan & Keaveny, 2001) for the human proximal tibia. For SCB and STB a Poisson's ratio of 0.3 was used (Borchers & Reichart, 1983), and a Poisson's ratio of 0.3 was assumed for CC. A comprehensive list of material properties of calcified tissues used in the present study is shown in Table 4.

Table 4. Material properties for articular cartilage superficial zone, middle zone, and deep zone, calcified cartilage, subchondral cortical bone, and subchondral trabecular bone used in this study. Superficial zone and middle zone articular cartilage values are from previous computational (Stender *et al.* 2012) and experimental (Williams *et al.* 2010) studies for newborn bovine articular cartilage from the patellofemoral groove. Deep zone articular cartilage properties are a linear extrapolation of SZ and MZ values. Articular cartilage model parameters are for a tri-constituent model composed of collagen fibrils, glycosaminoglycan (GAG) molecules, and a ground substance matrix (MAT). These properties are intended to represent a generalized articular cartilage tissue sample rather than from a specific source.

	Parameter	Description	Value
All Articular Cartilage Layers	μ (MPa)	MAT constituent shear modulus	0.001
	α_1(MPa-ml$^{2.5}$/mg$^{2.5)}$	GAG material constant	2.87
	α_2 (dimensionless)	GAG material constant	2.50
Articular Cartilage Superficial Zone	E^f (MPa)	Collagen fibril elastic modulus	175
	φ^f (%)	Collagen fibril volume fraction	3.9
	ρ_0^{GAG} (mg/ml)	Initial GAG molecule density	3.28
Articular Cartilage Middle Zone	E^f (MPa)	Collagen fibril elastic modulus	422
	φ^f (%)	Collagen fibril volume fraction	5.0
	ρ_0^{GAG} (mg/ml)	Initial GAG molecule density	4.76
Articular Cartilage Deep Zone	E^f (MPa)	Collagen fibril elastic modulus	670
	φ^f (%)	Collagen fibril volume fraction	6.1
	ρ_0^{GAG} (mg/ml)	Initial GAG molecule density	6.24
Calcified Cartilage	E (MPa)	Elastic modulus	320 [1]
	ν	Poisson's Ratio	0.3
Subchondral Cortical Bone	E (MPa)	Elastic modulus	3,900 [2]
	ν	Poisson's Ratio	0.3 [4]
Subchondral Trabecular Bone	E (MPa)	Elastic modulus	1,091 [3]
	ν	Poisson's Ratio	0.3 [4]

[1] From Mente & Lewis (1994)
[2] From Mente & Lewis (1994)
[3] From Morgan & Keaveny, (2001)
[4] From Borchers & Reichart, (1983)

Anisotropic distributions of collagen fibrils in AC were defined in the superficial middle and deep zones of AC based on previously established experimental studies of collagen fibril distributions across a range of species (Benninghoff, 1925; Minns & Steven, 1977; Aspden & Hukins, 1981; Clark 1990; Hyttinen *et al.*, 2009) and

biochemical measurements of collagen fibril volume fraction (Williams *et al.*, 2010) for newborn bovine AC (Figure 16). For all zones of AC, collagen fibrils were assumed to be anisotropic only in a plane perpendicular to the articular surface.

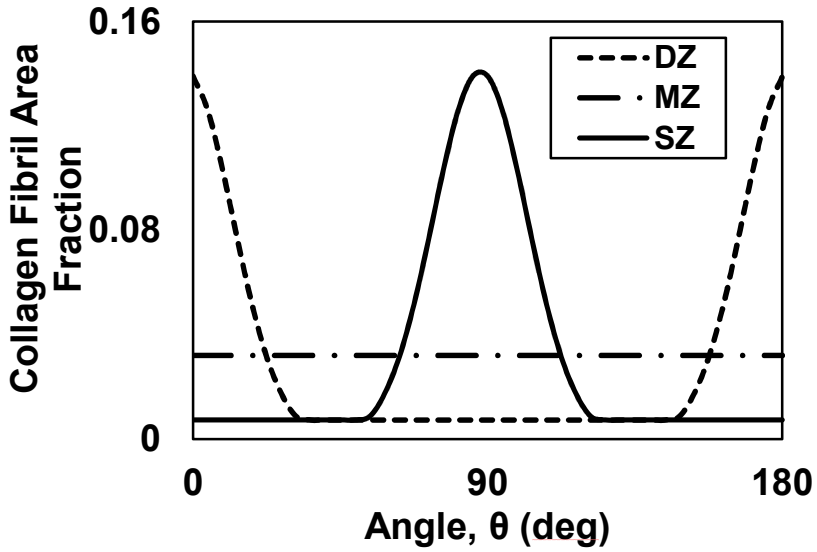

Figure 16. Initial collagen fibril distributions in the superficial zone (SZ), middle zone (MZ), and deep zone (DZ) of articular cartilage where θ = 90° is defined the plane parallel to the articular surface.

3.4 Results

Spherical indentation and unconfined compression simulations were run for each of the four cases including: healthy permeability properties (Case 1, Normal), osteoarthritic permeability properties in AC (Case 2, AC OA), osteoarthritic permeability properties in calcified tissues (Case 3, Calcified OA), and osteoarthritic permeability properties in all tissues (Case 4, All OA). Only negligible differences were found between cases 1 and 3 or cases 2 and 4. Thus, changes in the permeability

of the calcified tissues showed no variation in unconfined compression and spherical indentation simulations. Therefore, the following results will be presented showing only results for normal permeability values (Case 1, Normal) and for all osteoarthritic permeability values (Case 4, All OA). Unconfined compression loading showed a diminished peak load and a shortened relaxation time for the All OA case, compared to the Normal case (Figure 17). As a result of pore fluid diffusion, the solid matrix of the BCU experienced a time-dependent stress response resulting in a stress relaxation behavior of the BCU at constant displacement in both Normal and All OA simulations (Figure 17).

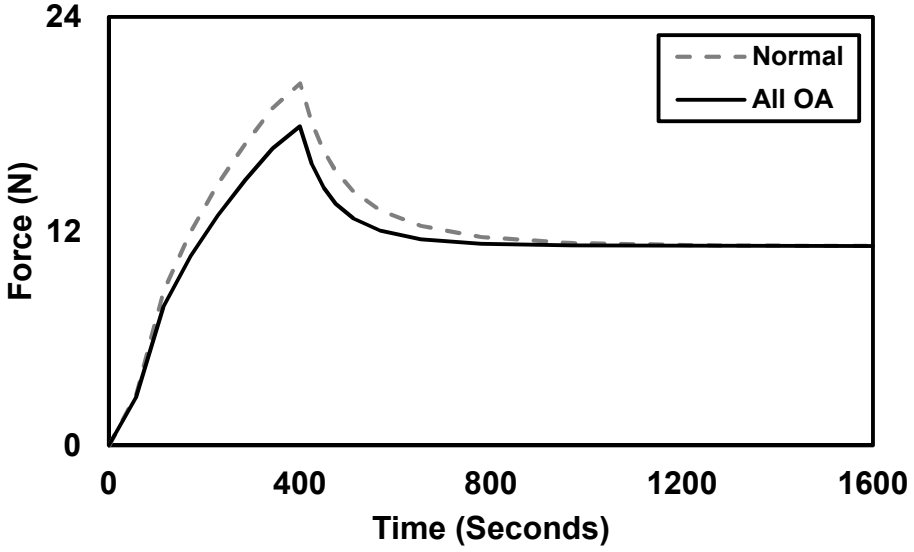

Figure 17. Plot of force (N) vs. time (seconds) for finite element simulation of unconfined compression of osteochondral plugs for healthy permeabilities (Normal) and, osteoarthritic permeabilities (All OA). Force values are converted to full symmetry. Loading was applied *via* an impermeable platen which was ramped to a 0.1 mm displacement over the first 400 seconds, and subsequently held at a constant displacement for an additional 800 seconds.

Pore pressure magnitudes in unconfined compression were higher for Normal permeability values, compared with the All OA case (Figure 18A). Peak pore pressure magnitude was roughly 30% higher in Normal compared to All OA cases. Fluid velocities at peak loading were similar in both Normal and All OA unconfined compression simulations (Figure 18B).

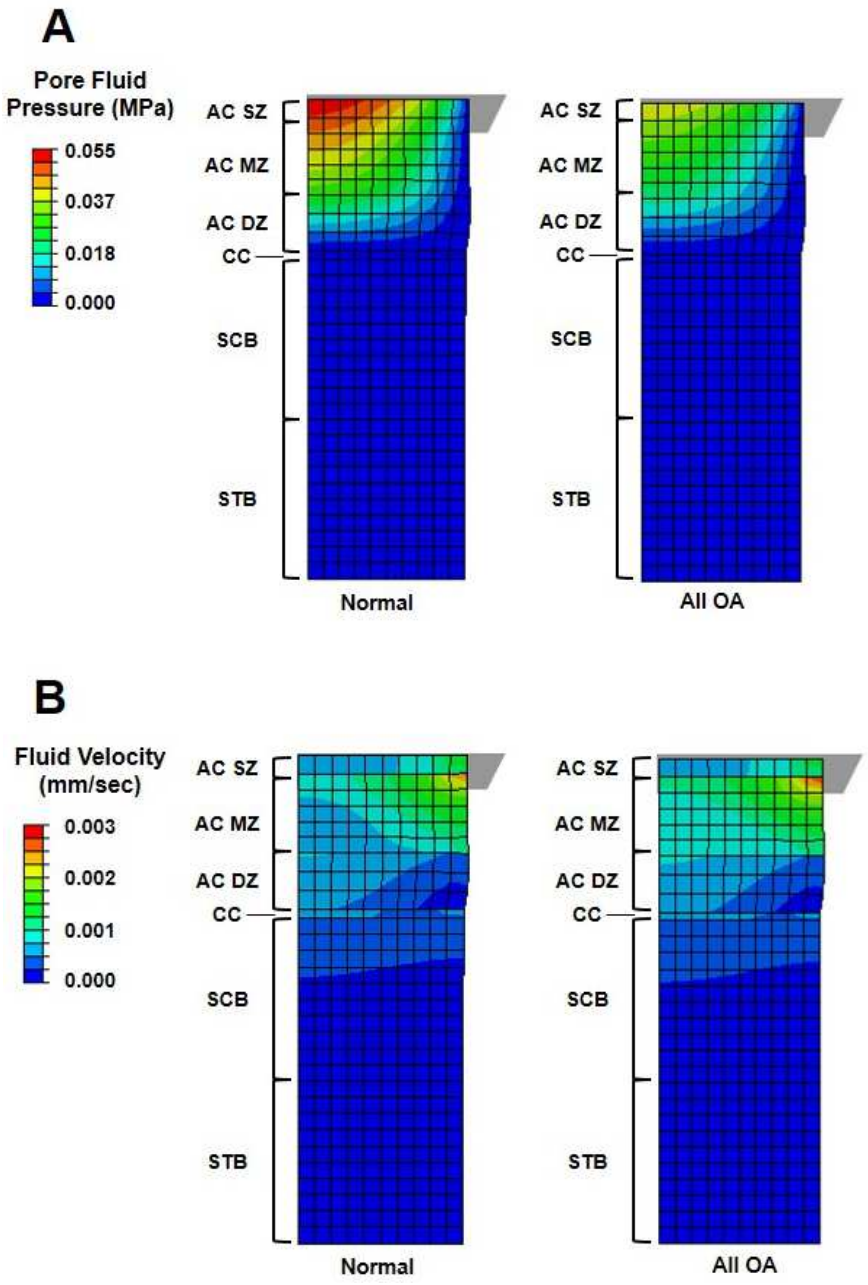

Figure 18. Contour plots showing quarter symmetry finite element simulation results for (A) pore fluid pressure (MPa) and (B) fluid velocity (mm/sec) at peak compressive loading prior to relaxation for full thickness osteochondral plugs with healthy (Normal) and osteoarthritic (All OA) permeability values. Brackets denote differential material regions including articular cartilage superficial zone (AC SZ), articular cartilage middle zone (AC MZ), articular cartilage deep zone (AC DZ), calcified cartilage (CC), subchondral cortical bone (SCB), and subchondral trabecular bone (STB).

Spherical indentation simulation results predict a 6% higher peak indentation force for the All OA case compared to Normal case (Figure 19). Additionally, compared with Normal, the All OA case took longer to achieve relaxation during unloading.

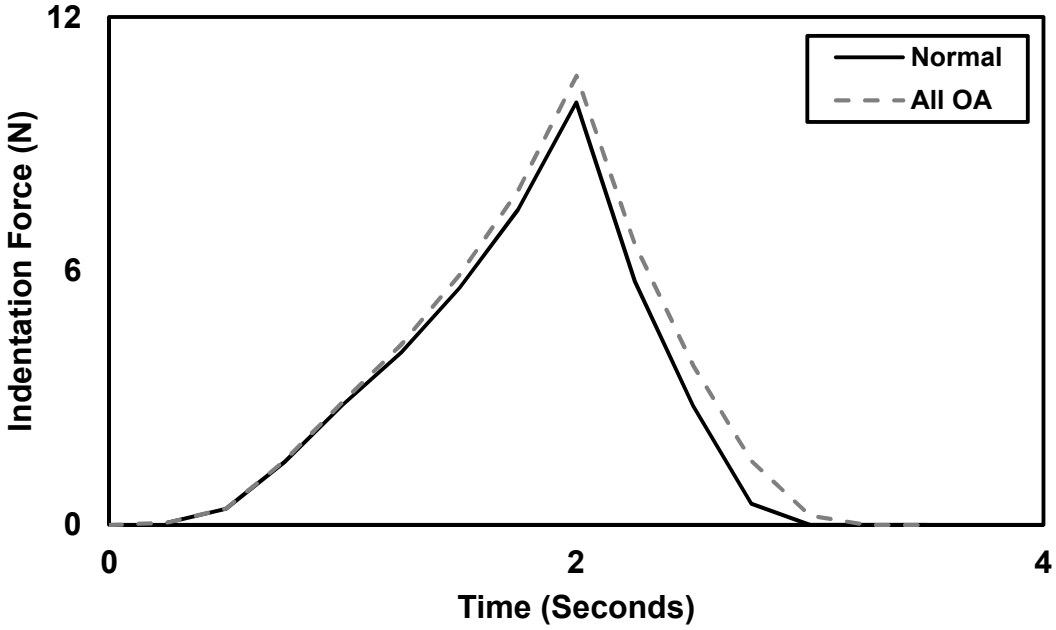

Figure 19. Indentation force (N) vs. Time (seconds) plot from spherical indentation finite element simulations for healthy (Normal) and osteoarthritis (All OA) spherical indentation simulations. BCU blocks were loaded via displacement of a rigid spherical indenter with a 1.5 cm radius following a triangular waveform up to a maximum 0.1 cm indentation depth over 2 seconds and subsequent unloading back to the initial indenter tip location over an additional 2 seconds.

For the Normal case, the largest fluid velocities at peak indentation displacement included the SZ and MZ of AC, while for the All OA case, the highest fluid velocities were present only in the SZ of AC (Figure 20).

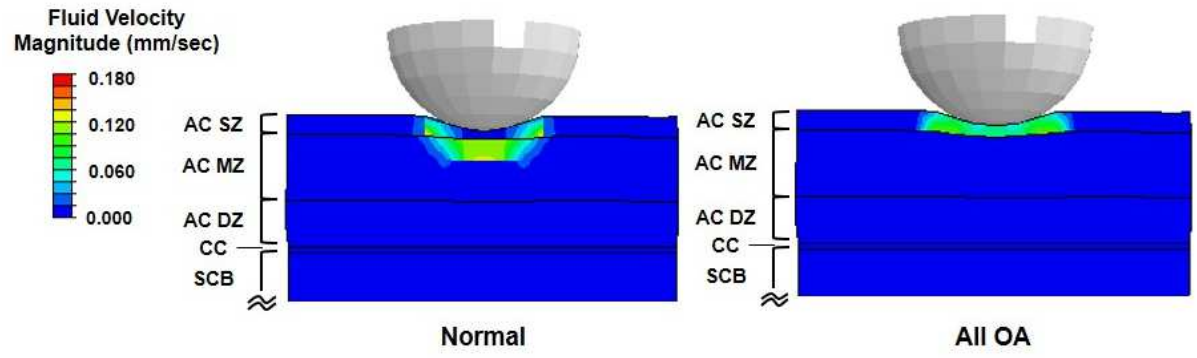

Figure 20. Contour plots of fluid velocity (mm/sec) for spherical indentation finite element simulation results for normal and osteoarthritic (All OA) permeabilities of the bone-cartilage unit. Brackets denote differential material regions including articular cartilage superficial zone (AC SZ), articular cartilage middle zone (AC MZ), articular cartilage deep zone (AC DZ), calcified cartilage (CC), and subchondral cortical bone (SCB). Mesh lines are removed for clarity.

The pore fluid pressure responses also varied in magnitude and distribution of pore pressure throughout loading, peak loading and unloading between Normal and All OA cases (Figure 21). Peak pore pressure was approximately 30% greater in All OA simulations compared to Normal simulations. During unloading in All OA and Normal simulations, a negative pore fluid pressure (*i.e.,* a vacuum) was present in the MZ and DZ of AC.

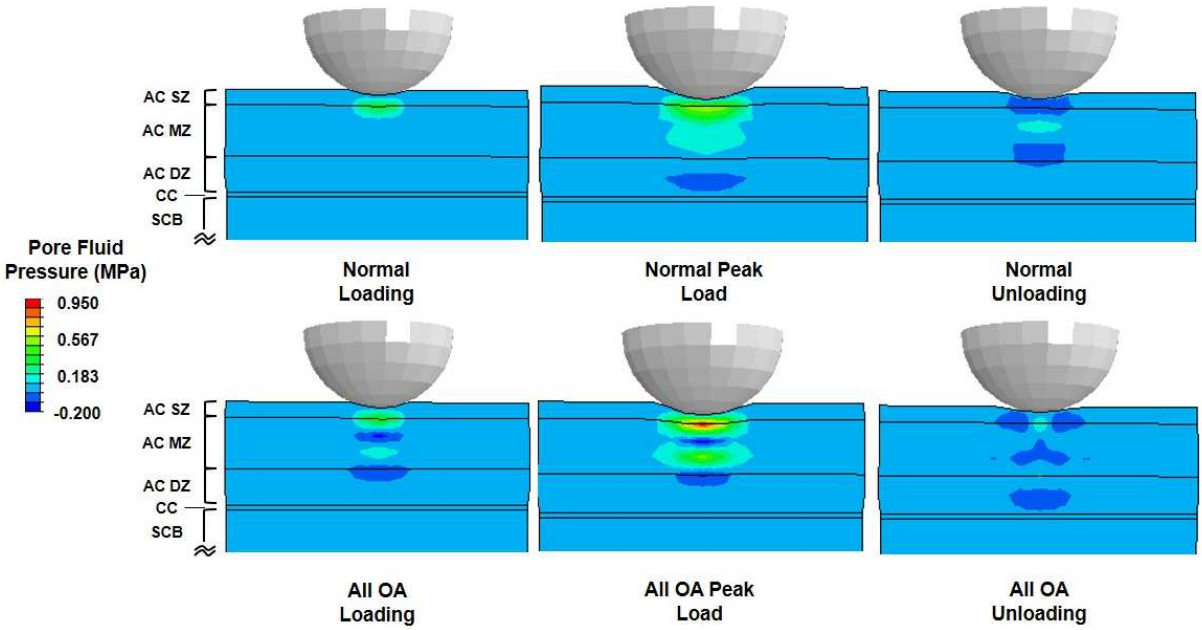

Figure 21. Contour plots showing pore fluid pressure (MPa) values for healthy (Normal) and osteoarthritic (All OA) permeability simulations midway through loading, at peak loading, and half way through unloading. Brackets (far left) denote differential material regions including articular cartilage superficial zone (AC SZ), articular cartilage middle zone (AC MZ), articular cartilage deep zone (AC DZ), calcified cartilage (CC), and subchondral cortical bone (SCB). Mesh lines are removed for clarity.

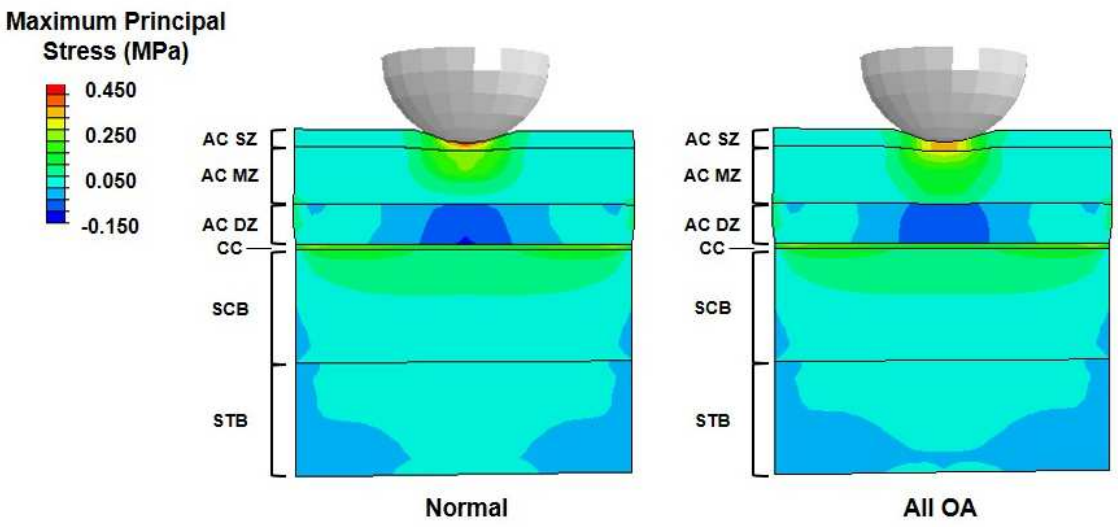

Figure 22. Contour plots showing maximum principal solid matrix effective stress (MPa) as calculated in finite element simulations for healthy (Normal) and osteoarthritic (All OA) permeabilities at peak indentation loading. Brackets denote differential material regions including articular cartilage superficial zone (AC SZ), articular cartilage middle zone (AC MZ), articular cartilage deep zone (AC DZ), calcified cartilage (CC), subchondral cortical bone (SCB), and subchondral trabecular bone (STB). Mesh lines are removed for clarity.

Under spherical indentation, maximum principal effective stress, $\mathbf{T}^{eff}$, contours revealed a sharp transition in stress magnitudes between DZ AC and CC at the osteochondral interface in Normal and All OA simulations at peak loading (Figure 22). Fluid transfer across the interface between cartilage and subchondral cortical bone occurs with loading to peak loads (Figure 23), and subsequently reverses in direction with unloading. During loading, fluid velocity was directed away from the spherical indenter from DZ AC into CC and SCB across the osteochondral interface. During unloading, fluid movement was predicted across the osteochondral interface from CC and SCB into DZ AC. All OA simulations showed a more chaotic flow path,

higher fluid velocity magnitudes, and negligible MZ AC fluid velocities as compared to Normal simulations (Figure 23).

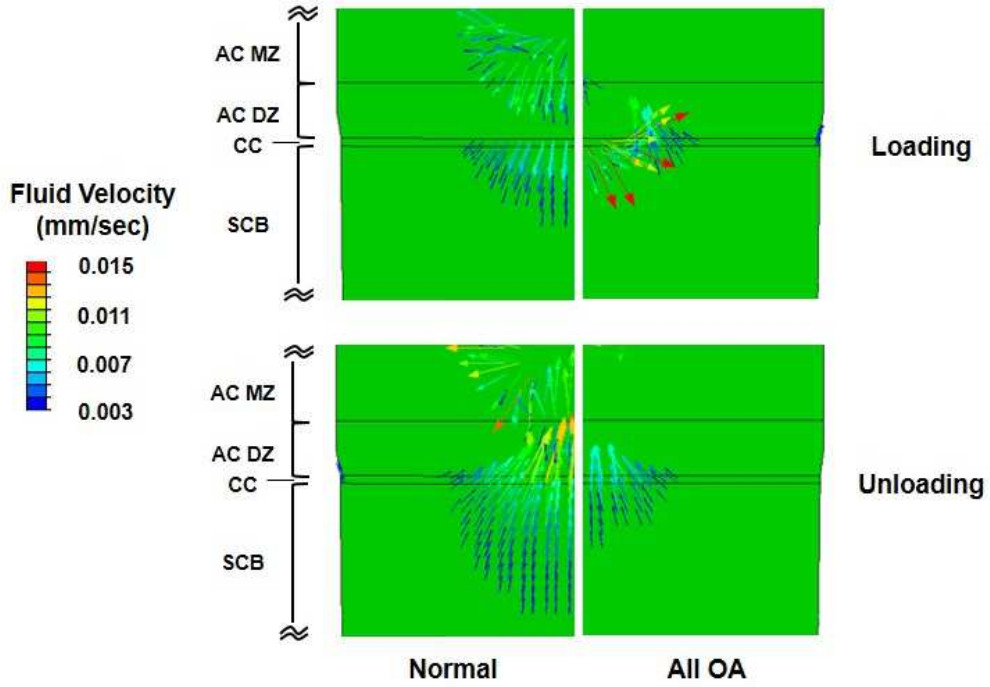

Figure 23. Vector plots showing fluid flow direction and magnitude near the osteochondral interface as calculated in finite element spherical indentation simulations for healthy (Normal) and osteoarthritic (All OA) permeabilities during the final loading step and initial unloading step. Brackets denote differential material regions including articular cartilage superficial zone (AC SZ), articular cartilage middle zone (AC MZ), articular cartilage deep zone (AC DZ), calcified cartilage (CC), and subchondral cortical bone (SCB). Vector orientation corresponds to fluid flow direction while vector color and size correspond to fluid velocity magnitude. Mesh lines are removed for clarity.

3.5 Discussion

The computational BCU model developed in this work incorporates a permeable, depth-dependent, and anisotropic model of AC with deformable and permeable models of the underlying calcified tissues (*i.e.,* CC, SCB, and STB) and a

poroelastic finite element modeling framework. The permeability values used for osteoarthritic tissues are from previous experimental studies (Setton *et al.*, 1995; Hwang *et al.*, 2008) that showed a roughly 50% higher permeability in tissues of the BCU with osteoarthritis. To investigate alterations in permeability with osteoarthritis, unconfined compression and spherical indentation simulations were run for four cases; 1) normal permeability values, 2) increased permeability values in AC, 3) increased permeability values in the calcified tissues, and 4) increased permeability values in all tissues within the BCU. Alterations in the permeability of the calcified tissues did not have an appreciable effect on results for any of the simulations, suggesting that the permeability of AC is the most influential factor in the poromechanics of the intact BCU. However, breakdown and/or loss of AC tissue as observed with late stage osteoarthritis (Hwang *et al.*, 2008; Saarakkala *et al.*, 2010) may make alterations in the permeability of calcified tissues more influential on the poromechanics of the BCU. The combination of modeling techniques, and experimental data as applied herein provides insight into the poromechanical behavior of the BCU.

In spherical indentation simulations, indentation force increased slightly when assigned with osteoarthritic permeability values as compared to Normal permeability values. In contrast, unconfined compression simulations predicted a decreased compressive force for tissues when assigned with osteoarthritic permeability values. Increased indentation force in spherical indentation simulations with higher osteoarthritic permeability values (All OA, case 4) is due to a modification of the fluid

flow path out of the articular surface and within AC. The increased osteoarthritic permeability values resulted in a, 'short circuit' effect wherein lowered fluid resistance in superficial zone AC isolated maximum fluid velocities near the articular surface. Fluid flowing primarily within the superficial zone of AC and out of the articular surface, rather than deeper into AC results in a slightly softer superficial zone, and effectively stiffer middle and deep zones of AC. It is presently unclear if this result is similar to what occurs *in vivo* with osteoarthritis. In all spherical indentation simulations, fluid flow also occurred between the CC and AC across the osteochondral interface; an interface which was once thought to be impermeable, particularly in mature joints (Maroudas *et al.*, 1968). Fluid velocity magnitudes were approximately one order of magnitude smaller, but were not trivial, near the osteochondral interface region as compared to velocities within AC. These results are in agreement with contemporary studies that demonstrate molecular transport across the osteochondral interface (Arkill & Winlove., 2008; Pan *et al.*, 2009). In particular, these simulations imply that altered fluid flow with osteoarthritis may have profound consequences including a reduction in cellular signaling and cellular nutrition in all zones of AC (Lories & Luyten, 2010; Urban, 1994; O'Hara *et al.*, 1990) and may contribute to mechanisms responsible for AC degradation. Furthermore, modified molecular signaling and transport across the osteochondral interface as a result of alterations in fluid flow likely lead to progression and worsening of osteoarthritis symptoms including tidemark advancement and subchondral remodeling (Burr & Gallant, 2012; Suri *et al.*, 2007).

Several assumptions regarding the incorporation of currently available experimental data were required to develop the finite element models used and may be considered limitations of this study. One critical concern lies in the lack of available experimental data in the current literature that necessitated collecting mechanical constants from a wide variety of sources. Ideally, all required experimental model parameters would be obtained from a single species and anatomical location. However, the present use of data allows for a first approximation of the poroelastic BCU with the caveat that the results are not developed from a comprehensive data set. The Poisson's ratio for CC was assumed to be the same as SCB and STB, and the modulus of CC was assumed to be one order magnitude lower than that of the SCB (Mente & Lewis, 1994), whereas others have shown this property to be similar across CC and SCB (Ferguson, *et al.*, 2003; Gupta, *et al.,* 2005; Ferguson, *et al.,* 2007). However, due to the relatively small deformations experienced by calcified tissues and the large modulus difference between these hard tissues and AC, the exact material properties used for calcified tissues have little effect. Additionally, due to the computational expense of a more complex geometry, the often uneven geometry of the osteochondral interface between AC and CC (Ferguson *et al.*, 2003; Paietta *et al.*, 2013) was not considered. Because geometrical features at the osteochondral interface exist at length scales that are much smaller than the osteochondral tissues, such features would likely not significantly alter these simulation results. STB was approximated as a continuum without a precise trabecular structure which is appropriate as the interactions near the SCB and STB

interface do not have a significant impact on these results (Harrigan, *et al.*, 1988). Last, and potentially most important to the simulation of fluid flow, the wetting fluid in all tissues was assumed to have the same viscosity and weight as water. However, interstitial fluid within AC and bone fluid likely have different properties than pure water. Due to the variety of experimental inputs required in the development of this model, the modes and simulations presented herein serve as a general, characteristic model of the BCU that demonstrates fundamental phenomena related to interstitial fluid flow in healthy and osteoarthritic tissues. Thus, the limitations discussed above would minimally influence the development of a general model, whereas considering each of these factors in future studies would certainly enable refinement of these analyses by utilizing tissues from specific species, anatomical sites, and stages of age and disease.

The changes in the BCU with osteoarthritis are complex, involving evolutions in both permeability, tissue structure, and mechanics (Hwang et al., 2008; Lories & Luyten, 2010; Burr & Gallant, 2012). This present study investigated the consequences specifically associated with increasing permeability. However, there are additional changes in the BCU with osteoarthritis that are not captured. For example, alterations in the solid matrix tissues of the BCU consistent with osteoarthritis are not simulated including AC damage and loss (Saarakkala *et al.,* 2010; Hwang *et al.*, 2008) and calcified tissue remodeling (Li *et al.*, 1999; Norrdin, *et al.*, 1999; Burr, 2004; Botter *et al.*, 2008). The permeability of calcified tissues is a consequence of the geometric pore arrangement which changes during remodeling

that occurs in osteoarthritis (Mastbergen & Lafeber, 2011; Norrdin, *et al.*, 1999). Expansions on the present model that incorporate remodeling are needed to consider these factors. The permeability values used herein are assumed to be isotropic in each zone of AC. Permeability values in AC are considered to be a consequence of the hydrophilic nature of glycosaminoglycan molecules in addition to the structure of AC (Maroudas *et al.*, 1969; Federico & Herzog, 2007). Due to the anisotropic distribution of collagen fibrils in AC, there is likely an anisotropy in the permeability of AC as described by Nabovati et al. (2009) for general fibrous porous media. Integration of results from additional experimental work aimed at characterizing the anisotropic permeability of AC into this model may improve the accuracy of these results. However, due to the relatively low volume fraction of collagen fibrils simulated here the permeability response in AC is likely close to isotropic. Decreases in GAG molecule density with osteoarthritis may also have profound consequences on permeability of AC (Rolauffs *et al.*, 2010; Temple-Wong *et al.*, 2009). Future modeling and experimental studies may provide additional insight into the specific consequences of osteoarthritis, including depth-dependent permeability changes in AC, AC damage and degeneration, and calcified tissue remodeling.

This work presents an approximation of the behavior of the BCU as a complete poromechanical unit, and the corresponding consequences of alterations in permeability in tissues of the BCU with osteoarthritis. Due to the limited extent of currently available experimental data, only healthy and late-stage osteoarthritic permeability conditions are considered. Future experimental measurements of

permeability may be used to extend this model to include early-term and post-traumatic osteoarthritis. Furthermore, it is not currently understood if there are depth-dependent permeability increases in AC with osteoarthritis. Therefore, future studies that measure the depth-dependent changes in the permeability of AC with osteoarthritis may improve the accuracy of these results. Additionally, the incorporation of the effects of degradations of AC and the remodeling of calcified tissues into this model may improve the accuracy of this study. Presently, these results help to elucidate the role that permeability plays in the poromechanics of the BCU as well as to guide future experimental and computational studies aimed at preventing and/or alleviating the symptoms of osteoarthritis.

3.6 Acknowledgements

This work was supported by NSF *CAREER* award #1055989, and the Innovative Grant Program at the University of Colorado Boulder.

3.7 References

1. Arkill, K. P., & Winlove, C. P. (2008). Solute transport in the deep and calcified zones of articular cartilage. *Osteoarthritis and Cartilage*, *16*(6), 708-714.
2. Aspden, R. M., & Hukins, D. W. L. (1981). Collagen organization in articular cartilage, determined by X-ray diffraction, and its relationship to tissue

function. *Proceedings of the Royal Society of London. Series B, Biological Sciences*, 299-304.

3. Ateshian, G., Warden, W., Kim, J., Grelsamer, R., Mow, V. (1997) Finite Deformation Biphasic Material Properties of Bovine Articular Cartilage from Confined Compression Experiments. *Journal of Biomechanics*. 30 (11), 1157-1164.
4. Benninghoff, A. (1925). Form und Bau der Gelenkknorpel in ihren Beziehungen zur Funktion. II.Der Aufbau des Gelenkknorpels in seinen Beziehungen zur Funktion.Zeitschrift fur Zellforschung und mikroskopische Anatomie 2, 783-862.
5. Borchers, L., and P. Reichart. "Three-dimensional stress distribution around a dental implant at different stages of interface development." *Journal of Dental Research* 62.2 (1983): 155-159.
6. Botter, S. M., van Osch, G. J. V. M., Waarsing, J. H., van der Linden, J. C., Verhaar, J. A. N., Pols, H. A. P., … Weinans, H. (2008). Cartilage damage pattern in relation to subchondral plate thickness in a collagenase-induced model of osteoarthritis. *Osteoarthritis and Cartilage*, *16*(4), 506–514. doi:10.1016/j.joca.2007.08.005
7. Brocklehurst, R., Bayliss, M. T., Maroudas, A., Coysh, H. L., Freeman, M. A. R., Revell, P. A., & Ali, S. Y. (1984). The composition of normal and osteoarthritic articular cartilage from human knee joints. *J Bone Joint Surg Am*, *66*, 95–106.

8. Burr, D. B., & Gallant, M. A. (2012). Bone remodelling in osteoarthritis. *Nature Reviews Rheumatology*, *8*(11), 665–673. doi:10.1038/nrrheum.2012.130
9. Chen, S. (2007). Depth-dependent compressive properties of normal aged human femoral head articular cartilage: relationship to fixed charge density. *Osteoarthritis and Cartilage*, *9*(6), 561–569. doi:10.1053/joca.2001.0424
10. Chen, S. S., Falcovitz, Y. H., Schneiderman, R., Maroudas, A., & Sah, R. L. (2001). Depth-dependent compressive properties of normal aged human femoral head articular cartilage: relationship to fixed charge density. *Osteoarthritis and Cartilage*, *9*(6), 561-569.
11. Clark, John M. "The organisation of collagen fibrils in the superficial zones of articular cartilage." *Journal of anatomy* 171 (1990): 117.
12. Cowin, S. C. (1999). Bone poroelasticity. *Journal of Biomechanics*, *32*(3), 217–238.
13. Federico, S., & Herzog, W. (2007). The Effect of Collagen Fibres on Permeability of Articular Cartilage. In *Proceedings of the 31st Annual Meeting of the American Society of Biomechanics*. Retrieved from http://www.asbweb.org/conferences/2007/149.pdf
14. Ferguson, V. L., Bushby, A. J., & Boyde, A. (2003). Nanomechanical properties and mineral concentration in articular calcified cartilage and subchondral bone. *Journal of Anatomy*, *203*(2), 191–202.
15. Ferguson, V. L., Bushby, A. J., Firth, E. C., Howell, P. G., & Boyde, A. (2007). Exercise does not affect stiffness and mineralisation of third metacarpal

condylar subarticular calcified tissues in 2 year old thoroughbred racehorses.*European cells & materials*, *16*, 40-6.

16. Ficklin, T. P., Davol, A., & Klisch, S. M. (2009). Simulating the Growth of Articular Cartilage Explants in a Permeation Bioreactor to Aid in Experimental Protocol Design. *Journal of Biomechanical Engineering*, *131*(4), 041008. doi:10.1115/1.3049856
17. Gupta, H. S., Schratter, S., Tesch, W., Roschger, P., Berzlanovich, A., Schoeberl, T., … Fratzl, P. (2005). Two different correlations between nanoindentation modulus and mineral content in the bone–cartilage interface. *Journal of Structural Biology*, *149*(2), 138–148. doi:10.1016/j.jsb.2004.10.010
18. Harrigan, T. P., Jasty, M., Mann, R. W., & Harris, W. H. (1988). Limitations of the continuum assumption in cancellous bone. *Journal of Biomechanics*, *21*(4), 269–275.
19. Hazelwood, S. J., Bruce Martin, R., Rashid, M. M., & Rodrigo, J. J. (2001). A mechanistic model for internal bone remodeling exhibits different dynamic responses in disuse and overload. *Journal of Biomechanics*, *34*(3), 299–308.
20. Holmes, M. H., & Mow, V. C. (1990). The nonlinear characteristics of soft gels and hydrated connective tissues in ultrafiltration. *Journal of Biomechanics*, *23*(11), 1145–1156.
21. Hull, M. L. (2002). A Finite Element Model of the Human Knee Joint for the Study of Tibio-Femoral Contact. *Journal of Biomechanical Engineering*, *124*(3), 273. doi:10.1115/1.1470171

22. Hwang, J., Bae, W. C., Shieu, W., Lewis, C. W., Bugbee, W. D., & Sah, R. L. (2008). Increased hydraulic conductance of human articular cartilage and subchondral bone plate with progression of osteoarthritis. *Arthritis & Rheumatism*, *58*(12), 3831–3842. doi:10.1002/art.24069

23. Hyttinen, M. M., Holopainen, J., Rene van Weeren, P., Firth, E. C., Helminen, H. J., & Brama, P. A. (2009). Changes in collagen fibril network organization and proteoglycan distribution in equine articular cartilage during maturation and growth. *Journal of anatomy*, *215*(5), 584-591.

24. Julkunen, P., Korhonen, R. K., Herzog, W., & Jurvelin, J. S. (2008). Uncertainties in indentation testing of articular cartilage: A fibril-reinforced poroviscoelastic study. *Medical Engineering & Physics*, *30*(4), 506–515. doi:10.1016/j.medengphy.2007.05.012

25. Korhonen, R. K., Laasanen, M. S., Töyräs, J., Lappalainen, R., Helminen, H. J., & Jurvelin, J. S. (2003). Fibril reinforced poroelastic model predicts specifically mechanical behavior of normal, proteoglycan depleted and collagen degraded articular cartilage. *Journal of Biomechanics*, *36*(9), 1373–1379. doi:10.1016/S0021-9290(03)00069-1

26. Lai, W. ., Mow, V. C., & Roth, V. (1981). Effects of Nonlinear Strain-Dependent Permeability and Rate of Compression on the Stress Behavior of Articular Cartilage. *Journal of Biomechanical Engineering*, *103*, 60.

27. Li, B., & Aspden, R. M. (1997). Mechanical and material properties of the subchondral bone plate from the femoral head of patients with osteoarthritis or osteoporosis. *Annals of the Rheumatic Diseases*, *56*(4), 247–254.

28. LI, B., MARSHALL, D., ROE, M., & ASPDEN, R. M. (1999). The electron microscope appearance of the subchondral bone plate in the human femoral head in osteoarthritis and osteoporosis. *Journal of Anatomy*, *195*(1), 101–110.

29. Lories, R. J., & Luyten, F. P. (2010). The bone–cartilage unit in osteoarthritis. *Nature Reviews Rheumatology*, *7*(1), 43–49. doi:10.1038/nrrheum.2010.197

30. Maroudas A, Bullough P, Swanson SA, Freeman MA. The permeability of articular cartilage. J Bone Joint Surg Br 1968;50:166–77

31. Maroudas, A., Muir, H., & Wingham, J. (1969). The correlation of fixed negative charge with glycosaminoglycan content of human articular cartilage. *Biochimica et Biophysica Acta (BBA)-General Subjects*, *177*(3), 492-500.

32. Mastbergen, S. C., & Lafeber, F. P. J. G. (2011). Changes in subchondral bone early in the development of osteoarthritis. *Arthritis & Rheumatism*, *63*(9), 2561–2563. doi:10.1002/art.30306

33. Mente, P. L., & Lewis, J. L. (1994). Elastic modulus of calcified cartilage is an order of magnitude less than that of subchondral bone. *Journal of Orthopaedic Research*, *12*(5), 637–647.

34. Minns, R. J., & Steven, F. S. (1977). The collagen fibril organization in human articular cartilage. *Journal of anatomy*, *123*(Pt 2), 437.

35. Morgan, E. F., & Keaveny, T. M. (2001). Dependence of yield strain of human trabecular bone on anatomic site. *Journal of Biomechanics*, *34*(5), 569–577.

36. Mullins, L. P., Bruzzi, M. S., & McHugh, P. E. (2009). Calibration of a constitutive model for the post-yield behaviour of cortical bone. *Journal of the Mechanical Behavior of Biomedical Materials*, *2*(5), 460–470. doi:10.1016/j.jmbbm.2008.11.003

37. Nabovati, A., Llewellin, E. W., & Sousa, A. C. (2009). A general model for the permeability of fibrous porous media based on fluid flow simulations using the lattice Boltzmann method. *Composites Part A: Applied Science and Manufacturing*, *40*(6), 860-869.

38. Nauman, E. A., Fong, K. E., & Keaveny, T. M. (1999). Dependence of intertrabecular permeability on flow direction and anatomic site. *Annals of Biomedical Engineering*, *27*(4), 517–524.

39. Niebur, G. L., Feldstein, M. J., Yuen, J. C., Chen, T. J., & Keaveny, T. M. (2000). High-resolution finite element models with tissue strength asymmetry accurately predict failure of trabecular bone. *Journal of Biomechanics*, *33*(12), 1575–1583.

40. Norrdin, R. W., Kawcak, C. E., Capwell, B. A., & McIlwraith, C. W. (1999). Calcified cartilage morphometry and its relation to subchondral bone remodeling in equine arthrosis. *Bone*, *24*(2), 109–114.

41. O'Hara, B. P., Urban, J. P., & Maroudas, A. (1990). Influence of cyclic loading on the nutrition of articular cartilage. *Annals of the Rheumatic Diseases*, *49*(7), 536–539.

42. Paietta, R. C., Burger, E. L., & Ferguson, V. L. (2013). Mineralization and collagen orientation throughout aging at the vertebral endplate in the human lumbar spine. *Journal of Structural Biology*. doi:10.1016/j.jsb.2013.08.011

43. Pan, J., Zhou, X., Li, W., Novotny, J. E., Doty, S. B., & Wang, L. (2009). In situ measurement of transport between subchondral bone and articular cartilage. *Journal of Orthopaedic Research*, *27*(10), 1347–1352. doi:10.1002/jor.20883

44. Pierce, D. M., Ricken, T., & Holzapfel, G. A. (2013). A hyperelastic biphasic fibre-reinforced model of articular cartilage considering distributed collagen fibre orientations: continuum basis, computational aspects and applications. *Computer methods in biomechanics and biomedical engineering*, *16*(12), 1344-1361.

45. Rolauffs, B., Muehleman, C., Li, J., Kurz, B., Kuettner, K. E., Frank, E., & Grodzinsky, A. J. (2010). Vulnerability of the superficial zone of immature articular cartilage to compressive injury. *Arthritis & Rheumatism*, *62*(10), 3016–3027. doi:10.1002/art.27610

46. Saarakkala, S., Julkunen, P., Kiviranta, P., Mäkitalo, J., Jurvelin, J. S., & Korhonen, R. K. (2010). Depth-wise progression of osteoarthritis in human articular cartilage: investigation of composition, structure and biomechanics. *Osteoarthritis and Cartilage*, *18*(1), 73–81. doi:10.1016/j.joca.2009.08.003

47. Setton, L. A., Mow, V. C., & Howell, D. (1995). Mechanical behavior of articular cartilage in shear is altered by transection of the anterior cruciate ligament.*Journal of Orthopaedic Research*, *13*(4), 473-482.

48. Soltz, M. A., & Ateshian, G. A. (1998). Experimental verification and theoretical prediction of cartilage interstitial fluid pressurization at an impermeable contact interface in confined compression. *Journal of Biomechanics*, *31*(10), 927–934.

49. Stender, M. E., Raub, C. B., Yamauchi, K. A., Shirazi, R., Vena, P., Sah, R. L., … Klisch, S. M. (2012). Integrating qPLM and biomechanical test data with an anisotropic fiber distribution model and predictions of TGF- ß1 and IGF-1 regulation of articular cartilage fiber modulus. *Biomechanics and Modeling in Mechanobiology*. doi:10.1007/s10237-012-0463-y

50. Suri, S., Gill, S. E., de Camin, S. M., McWilliams, D. F., Wilson, D., & Walsh, D. A. (2007). Neurovascular invasion at the osteochondral junction and in osteophytes in osteoarthritis. *Annals of the rheumatic diseases*, *66*(11), 1423-1428.

51. Suri, S., & Walsh, D. A. (2012). Osteochondral alterations in Osteoarthritis. *Bone*, *51*(2), 204-211.

52. Swan, C. C., Lakes, R. S., Brand, R. A., & Stewart, K. J. (2003). Micromechanically Based Poroelastic Modeling of Fluid Flow in Haversian Bone. *Journal of Biomechanical Engineering*, *125*(1), 25. doi:10.1115/1.1535191

53. Temple-Wong, M. M., Bae, W. C., Chen, M. Q., Bugbee, W. D., Amiel, D., Coutts, R. D., … Sah, R. L. (2009). Biomechanical, structural, and biochemical indices of degenerative and osteoarthritic deterioration of adult human articular cartilage of the femoral condyle. *Osteoarthritis and Cartilage*, *17*(11), 1469–1476. doi:10.1016/j.joca.2009.04.017

54. Urban, J. P. G. (1994). The chondrocyte: a cell under pressure. *Rheumatology*,*33*(10), 901-908.

55. Wei, X., Räsänen, T., & Messner, K. (1998). Maturation-related compressive properties of rabbit knee articular cartilage and volume fraction of subchondral tissue. *Osteoarthritis and Cartilage*, *6*(6), 400–409.

56. Williams, G. M., Dills, K. J., Flores, C. R., Stender, M. E., Stewart, K. M., Nelson, L. M., … Klisch, S. M. (2010). Differential regulation of immature articular cartilage compressive moduli and Poisson's ratios by *in vitro* stimulation with IGF-1 and TGF-β1. *Journal of Biomechanics*, *43*(13), 2501–2507.

57. Wilson, W., van Donkelaar, C. C., van Rietbergen, B., & Huiskes, R. (2005). A fibril-reinforced poroviscoelastic swelling model for articular cartilage. *Journal of Biomechanics*, *38*(6), 1195–1204. doi:10.1016/j.jbiomech.2004.07.003

58. Wilson, W., van Donkelaar, C. C., van Rietbergen, B., Ito, K., & Huiskes, R. (2004). Stresses in the local collagen network of articular cartilage: a poroviscoelastic fibril-reinforced finite element study. *Journal of Biomechanics*, *37*(3), 357–366. doi:10.1016/S0021-9290(03)00267-7

CHAPTER 4

An Evolutionary Model of Osteoarthritis Including Articular Cartilage Damage, and Bone Remodeling in a Computational Study

4.1 Abstract

With osteoarthritis a complex set of coupled chemical, biological, and mechanical progressive changes have been observed to occur. The aim of this study was to examine using a high-fidelity computational model, the evolution of the bone-cartilage unit that incorporates articular cartilage (AC) damage, subchondral cortical bone (SCB) remodeling, and subchondral trabecular bone (STB) remodeling as observed to occur in osteoarthritis. A finite element model of spherical indentation was developed with a depth-dependent anisotropic model of articular cartilage, a calcified cartilage (CC) zone, and SCB and STB bone remodeling regions. Calcified tissue (CC, SCB, and STB) and damage AC, material regions were integrated to create an example finite element model of an evolutionary bone-cartilage unit. A spherical indenter was displaced into the tissue up to a 0.1 cm indentation depth in ten equal increments. At each increment an additional 1000 load cycles were simulated at each step for bone remodeling. Results indicate that with indentation loading, articular cartilage damage occurs starting at the articular surface.

Furthermore, regions of bone remodeling were predicted to occur with a net stiffening effect on the subchondral bone plate. Changes in indentation force were minimal (<2%) with evolutions in AC damage and bone remodeling. However, additional degradation and wear of AC and/or alterations in loading structure may have more pronounced effects on the mechanical response of the bone-cartilage unit. Bone remodeling and articular cartilage predictions are consistent with experimental observations that articular cartilage damage begins at the articular surface and that subchondral bone experiences a thickening (i.e. stiffening) response with OA. These results provide an initial insight into the early-term initiation behavior of OA, and the potential consequences of evolutions in AC, SCB, and STB, and may guide future experimental and computational studies aimed at alleviation and/or preventing osteoarthritis.

4.2 Introduction

Recent studies have proposed the importance of considering the complete bone-cartilage unit (BCU), a term used by Lories & Luyten (2010), as opposed to any single tissue, when studying the initiation and progression of osteoarthritis (OA) (Goldring & Goldring, 2010; Burr & Gallant, 2012). For example, remodeling leading to softening or stiffening in calcified cartilage (CC) subchondral cortical bone (SCB) and subchondral trabecular bone (STB) have been proposed to play integral roles in the pathogenesis of OA (Grynpas, *et al.*, 1991; Bobinac, *et al.*, 2003; Burr, 2004; Burr & Gallant, 2012). Additionally, researchers have proposed that molecular communication

channels and fluid flow between AC and calcified tissues (CC, SCB, and STB) exist that may contribute to the evolution of osteoarthritis (Hwang *et al.*, 2008; Pan *et al.*, 2009; Lories & Luyten, 2010; Suri & Walsh, 2012), emphasizing the cohesiveness of the BCU. One study proposed that the evolution of OA symptoms occurs simultaneously in calcified tissues and AC (Lories & Luyten, 2010). Another study hypothesized that for non-traumatic OA, changes in bone may antedate AC damage and degradation (Goldring & Goldring, 2010). Indeed, the contemporary consensus is that OA is a disease of the complete BCU as a complete functional unit rather than a disease of any single tissue (Brandt *et al.*, 2006; Burr & Gallant, 2012). However, there is no current consensus on how OA progresses within the complete BCU for any given loading condition. Thus, this study sought to integrate an evolutionary computational model of the BCU with experimental data to elucidate the changes in the mechanical response, and the propensity to incur additional degradations of the BCU with OA.

In the calcified tissues of the BCU, many experimental studies have examined the effects that occur with OA in synovial joints. For example, an evaluation of the short term effects of OA induction on mice knees, observed that SCB initially thins relative to healthy joints and then increases in thickness (Botter *et al.*, 2008). Another study observed an increased rate of SCB turnover such that the SCB is thicker and stiffer in joints with OA (Burr, 2004). In a canine model of induced OA, initial SCB thinning and increased bone plate porosity were observed at 10 and 20 weeks post OA induction (Sniekers *et al.,* 2008). Additionally, increased bone porosity, a more textured surface, and increased osteoclast resorption pits indicating increased

remodeling activity were observed in human femoral heads from patients with OA (Li *et al.*, 1999). The experimentally observed thickening of the calcified tissues in the BCU causes an effective stiffening that may modify the strain distributions of the healthy BCU thus resulting in progression of OA symptoms. To integrate the evolutionary changes in SCB and STB with OA observed experimentally, this study will use an established bone remodeling theory (Beaupré *et al.*, 1990a; Beaupré *et al.*, 1990b) for SCB and STB tissues within a complete BCU model to investigate the effects of bone remodeling with OA.

AC provides a load bearing, low friction surface where relative motion occurs in synovial joints. With OA, AC experiences chemical, mechanical, and structural changes (Brocklehurst *et al.,* 1984; Grushko *et al.*, 1989; Temple-Wong *et al.,* 2009), and in extreme cases, complete AC erosion can occur (Pritzker, *et al.*, 2006). Typically in AC with OA, degeneration starts at the superficial zone (SZ) of AC and progresses away from the articular surface into the middle zone (MZ) and the deep zone (DZ) (Thambyah & Broom, 2007; Saarakkala *et al.*, 2010). A weakening in the tensile strength, likely as a result of collagen degradation and loss as well as an increase in water contact, has been observed in AC with OA compared with healthy AC (Temple *et al.*, 2007; Temple-Wong *et al.*, 2009). Furthermore, with OA, compressive and shear moduli of AC decrease compared to healthy AC (Setton *et al.*, 1999). Additionally, the density of glycosaminoglycan molecules that act to resist compressive loading in AC has been shown to decrease (Maroudas & Venn, 1977; Venn & Maroudas, 1977; Brocklehurst et al., 1984; Temple-Wong et al., 2009) resulting in a weakened

compressive response in AC with OA. To incorporate the effects of AC degeneration, the present analysis will use a constituent-based anisotropic AC model (Stender et al., 2015 *In Review*; Stender et al., 2012) with specific glycosaminoglycan and collagen fibril damage to model AC damage with OA. The overreaching aim of this investigation is to integrate experimental data with appropriate high-fidelity computational modeling techniques (*i.e.* constitutive AC damage and bone remodeling) to elucidate the changes that take place with OA. Thus, the hypothesis of this study is that evolutionary computational models and finite element modeling can be used to model experimentally observed initiation and progression behavior of OA within the complete BCU. These results may guide future work aimed at alleviating and preventing the symptoms of OA by providing insight into how osteoarthritis begins and progresses over time.

4.3 Materials and Methods

A finite element model of the complete BCU was implemented in the commercial finite element analysis software Abaqus (v6.13). The user material subroutine, or UMAT was used to model the material behaviors of AC, SCT, and STB. In order to capture the evolution of the BCU, a previously established bone remodeling algorithm (Beaupré, *et al.*, 1990a, 1990b) was used to model SCB and STB. An anisotropic constituent based damage model of AC was used to model the superficial zone, middle zone, and deep zone of AC based on previously established

constitutive AC models (Stender *et al.*, 2012, 2015). Brief descriptions of the material models used are provided below.

Bone Remodeling Model

A previously established framework (Beaupré *et al.*, 1990a, 1990b) for computational modeling of SCB, and STB remodeling was chosen to simulate bone remodeling in the BCU. The daily Stress stimulus at the continuum level of SCB and STB, ψ_b is calculated as follows

$$\psi_b = (\sum n_i \sigma_i^m)^{\frac{1}{m}} \tag{1}$$

where n_i is the number of load cycles of load type i, $m = 4$ is the stress exponent that weights the importance of stress magnitude and load cycles, and σ_i is a continuum level stress of load type i defined as

$$\sigma_i = (2EU)^{\frac{1}{2}} \tag{2}$$

where E is continuum elastic modulus and U is the continuum strain energy density. The calculated value of ψ_b for a given load type i and number of cycles is used to determine the remodeling rate, $\dot{r}$ used here as by Carpenter and Carter (2008) and shown graphically in figure 24.

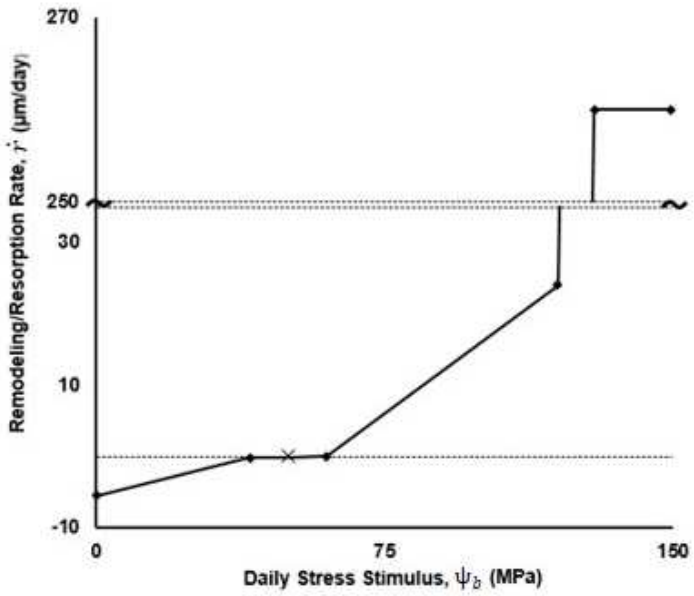

Figure 24. The Bone remodeling rate, $\dot{r}$, as a function of daily stress stimulus, ψ_b, based on experimental results as used in Carpenter and Carter (2008).

The remodeling rate, $\dot{r}$, is the apposition-resorption rate (um/day), ψ_b, is the daily tissue level stress stimulus as determined by cycles and loading, $\psi_{as} = 50\ MPa$, is the attractor state stress where no net remodeling or resorption occurs. The bone remodeling rate, $\dot{r}$, is converted to a density evolution *via* the following relationship

$$\rho = \dot{r} S_v \rho_t \Delta t + \rho_0 \tag{3}$$

where S_v is the bone surface area per unit tissue volume ($4\ \mu m^{-1}$), ρ_t is the true density of bone (*i.e.* the density of fully mineralized tissue), and ρ_0 is the initial density of bone from the previous step that is initially set to $1.5818\ \frac{g}{cm^3}$ for SCB, and $0.6414\ \frac{g}{cm^3}$ for STB (Beaupré, *et al.*, 1990b). The elastic modulus of SCB and STB can be calculated using the following relationship as used by Eser *et al.*, (2013).

$$E = 3790\rho^3 \tag{4}$$

Articular Cartilage Damage Model

A previously established model (Stender *et al.,* 2015) of constituent specific anisotropic AC damage was implemented in this study. In this model, strain based damage is assumed to occur either to collagen fibrils or glycosaminoglycan molecule constituents of AC. Collagen fibrils are assumed to behave with an elastic-brittle damage behavior wherein collagen fibrils exhibit a linear elastic behavior in tension until an elastic damage strain parameter E_N^D is exceeded, at which point collagen fibrils are assumed to fail completely. Collagen fibrils are also assumed to not provide any resistance in compression. The second Piola-Kirchoff stress tensor for the collagen fibril constituent with damage, $\mathbf{S}^{\mathrm{COL}}$ is implemented as the form shown below

$$\mathbf{S}^{\mathrm{COL}} = \frac{1}{4\pi}\int_{\phi=0}^{2\pi}\int_{\theta=0}^{\pi} H(E_N)\varphi_N^f E^f E_N\left[1 - d_N^f\right][\mathbf{N}\otimes\mathbf{N}]\sin\theta d\theta d\phi \tag{5}$$

where E_N is the Lagrangian fibril strain in direction N, H is the Heaviside step function operator, φ_N^f is the collagen fibril tissue volume fraction in direction N, E^f is the collagen fibril elastic modulus (MPa), d_N^f is the collagen fibril damage parameter which is zero for undamaged fibrils and 1 for damaged fibrils, and θ and ϕ are angles within a spherical coordinate system to determine the unit direction vector $\mathbf{N} = cos(\theta)sin(\phi)\hat{\boldsymbol{\imath}} + sin(\theta)sin(\phi)\hat{\boldsymbol{\jmath}} + cos(\phi)\hat{\boldsymbol{k}}$.

Glycosaminoglycan molecules are assumed to incur damage as a result of volumetric compression. Glycosaminoglycan damage is enforced as a reduction in

glycosaminoglycan molecule density as a smooth function of volumetric compression that is hypothesized to result from a leeching and/or cleaving of glycosaminoglycan molecules from AC (Rolauffs *et al.*, 2010; Stender *et al.* 2015). The Second Piola-Kirchoff stress tensor for the glycosaminoglycan constituent with damage, $\mathbf{S}^{\mathrm{GAG}}$ is implemented as

$$\mathbf{S}^{\mathrm{GAG}} = J\mathbf{F}^{-1}\left(-\alpha_1\left(\frac{\rho_0^{GAG}}{\mathrm{J}}\right)^{\alpha_2}\left\{1 - d_{max}^{GAG}\left[e^{\left(\frac{-\beta}{\eta}\right)} - e^{\left(\frac{-1}{\eta}\right)}\right]\right\}\right)\mathbf{F}^{-\mathbf{T}} \tag{6}$$

where $J = \det\mathbf{F}$ is the determinant of the deformation gradient tensor, $\mathbf{F}$ is the deformation gradient tensor, α_1 and α_2 are glycosaminoglycan constituent material constants from Stender et al. (2012), ρ_0^{GAG} is the glycosaminoglycan molecule density in the reference configuration (mg/ml), d_{max}^{GAG} is a glycosaminoglycan damage parameter for the maximum attainable glycosaminoglycan damage, and β and η are glycosaminoglycan damage scaling parameters from Stender et al. (2015). The ground substance matrix constituent is assumed to not incur damage and is implemented as a compressible Neo-Hookean material with the following Second Piola-Kirchoff stress tensor, $\mathbf{S}^{\mathrm{MAT}}$

$$\mathbf{S}^{\mathrm{MAT}} = \mu(\mathbf{I} - \mathbf{C}^{-1}) \tag{7}$$

where μ is the ground substance matrix shear modulus (MPa), $\mathbf{I}$ is the identity tensor, and $\mathbf{C}$ is the right Cauchy-Green deformation tensor. The total articular cartilage second Piola-Kirchoff solid matrix stress is calculated *via* the stress balance hypothesis as shown below.

$$\mathbf{S}^{\mathrm{AC}} = \mathbf{S}^{\mathrm{COL}} + \mathbf{S}^{\mathrm{GAG}} + \mathbf{S}^{\mathrm{MAT}}$$

For a complete explanation of the development and implementation of the AC damage used here refer to Stender *et al.* (2012, 2015). Anisotropic and depth-dependent distributions of collagen fibrils were defined in AC based on previously established experimental studies of collagen fibril distributions across a range of species (Benninghoff, 1925; Minns & Steven, 1977; Aspden & Hukins, 1981; Clark 1990; Hyttinen *et al.*, 2009) and biochemical measurements of collagen fibril volume fraction (Williams *et al.*, 2010) for newborn bovine AC. The primary direction of collagen fibril alignment is listed in table 5.

Finite Element Model

A finite element model of the BCU including discrete tissue zones of superficial zone, middle, and deep zone AC, calcified cartilage, SCB, and STB was developed and implemented in Abaqus (v 6.13) (Figure 25). For all finite element simulations, each discrete tissue region was attached directly to the adjacent regions using a tied contact constraint as well as a surface-to-surface contact algorithm. Contact between the spherical indenter and the articular surface was implemented using a frictionless surface-to-surface contact algorithm with finite sliding. In all simulations, the nonlinear geometric effects (NLGEOM) option in Abaqus was activated. Due to the constitutive model chosen for all AC zones, an equilibrium step was run prior to loading for unconfined compression and spherical indentation simulations in order to account for the pre-stress of the AC solid matrix by glycosaminoglycan molecules (Stender *et al.* 2012). During the initial equilibrium loading step, remodeling in SCB

and STB was disallowed. Indentation loading was simulated *via* a displacement control boundary condition on the spherical indentation that was ramped in 0.01 cm indentation depth increments (*i.e.* 10 steps) up to a 0.10 cm maximum indentation depth. For bone remodeling, the number of loading cycles at each progressive indentation depth was defined as $n_i = 1000$. Thus, cycle 1 as presented in the results represents 10,000 loading cycles with 1,000 cycles at each progressive indentation depth. Cycle 2 as presented in the results, represents a total of 30,000 progressive cycles (10,000 load, 10,000 unload, and 10,000 load) up to maximum indentation depth.

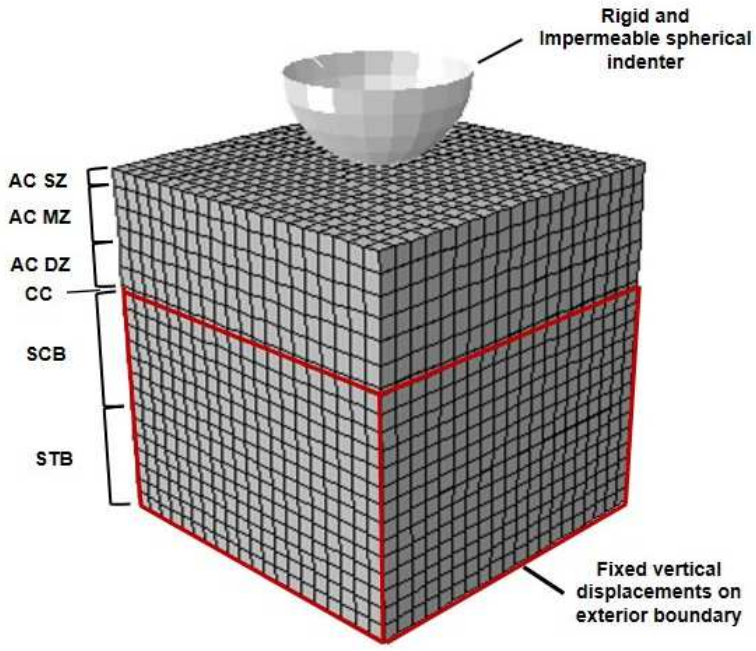

Figure 25. Finite element model of spherical indentation of the bone cartilage unit. Brackets denote differential material regions including articular cartilage superficial zone (AC SZ), articular cartilage middle zone (AC MZ), articular cartilage deep zone (AC DZ), calcified cartilage (CC), subchondral cortical bone (SCB), and subchondral trabecular bone (STB).

Material properties and parameters used in this model are listed in table 5. Note that SCB and STB elastic moduli are determined by the bone remodeling algorithm (Figure 24).

Table 5. Material properties for articular cartilage superficial zone, middle zone, and deep zone, calcified cartilage, subchondral cortical bone, and subchondral trabecular bone used in this study. Superficial zone and middle zone articular cartilage values are from previous computational (Stender *et al.*, 2012) and experimental (Williams *et al.*, 2010) studies for newborn bovine articular cartilage from the patellofemoral groove. Deep zone articular cartilage properties are a linear extrapolation of SZ and MZ values. Articular cartilage model parameters are for a tri-constituent model composed of collagen fibrils, glycosaminoglycan (GAG) molecules, and a ground substance matrix (MAT). In general, these properties are intended to represent a generalized articular cartilage tissue sample rather than from a specific source.

	Parameter	Description	Value
All Articular Cartilage Layers	μ (MPa)	MAT constituent shear modulus	0.001
	α_1(MPa-ml$^{2.5}$/mg$^{2.5)}$	GAG material constant	2.87
	α_2 (dimensionless)	GAG material constant	2.50
	E_N^D (length/length)	Collagen fibril maximum Lagrangian fibril strain	0.15
	d_{max}^{GAG} (dimensionless)	Maximum GAG damage	0.50
	η (dimensionless)	GAG damage scaling parameter	0.25
Articular Cartilage Superficial Zone	E^f (MPa)	Collagen fibril elastic modulus	175
	φ^f (%)	Collagen fibril volume fraction	3.9
	Collagen alignment	Primarily oriented parallel to the articular surface	N/A
	ρ_0^{GAG} (mg/ml)	Initial GAG molecule density	3.28
Articular Cartilage Middle Zone	E^f (MPa)	Collagen fibril elastic modulus	422
	φ^f (%)	Collagen fibril volume fraction	5.0
	Collagen alignment	Isotropic	N/A
	ρ_0^{GAG} (mg/ml)	Initial GAG molecule density	4.76
Articular Cartilage Deep Zone	E^f (MPa)	Collagen fibril elastic modulus	670
	φ^f (%)	Collagen fibril volume fraction	6.1
	Collagen alignment	Primarily oriented perpendicular to the articular surface	N/A
	ρ_0^{GAG} (mg/ml)	Initial GAG molecule density	6.24
Calcified Cartilage	E (MPa)	Elastic modulus	320 [1]
	ν	Poisson's Ratio	0.3
Subchondral Cortical Bone	ν	Poisson's Ratio	0.3[2]
Subchondral Trabecular Bone	ν	Poisson's Ratio	0.3[2]

[1] From Mente & Lewis, (1994)

[2] From Borchers and Reichart (1983)

4.4 Results

A simulation of the bone-cartilage unit was run using a high fidelity constitutive model of AC including damage to the glycosaminoglycan and collagen fibril constituents and an established bone remodeling algorithm. A spherical indentation simulation was developed to approximate *in vivo* loading in synovial joints, and to minimize computational expense. Bone remodeling was disallowed during the initial step, and deformations in articular cartilage as a result of glycosaminoglycan molecule swelling pressure were not sufficient to cause damage. During indentation loading, damage to articular cartilage collagen fibril and glycosaminoglycan constituents was concentrated beneath the indenter and in the superficial zone of articular cartilage (Figure 26). Indentation force at peak displacement was calculated as 1.47 N and 1.46 N for cycles 1 and 2, respectively. As a result of bone remodeling and AC damage, indentation force at peak indentation depth decreased 0.4% and 0.8% following cycles 1 and 2, respectively compared with a model without bone remodeling and AC damage.

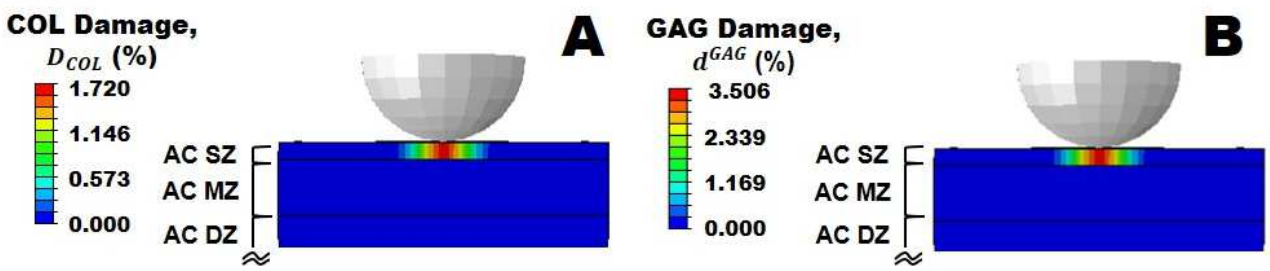

Figure 26. Contour plots of articular cartilage constituent damage results following spherical indentation loading for collagen fibril (COL) and glycosaminoglycan (GAG) molecule damage. The parameters D_{COL} and d^{GAG} correspond to the percentage of damaged (*i.e.,* completely failed) collagen fibrils, and the percentage decrease in GAG molecule concentration, respectively. Brackets correspond to differential tissue zones including articular cartilage superficial zone (AC SZ), articular cartilage middle zone (AC MZ), and articular cartilage deep zone (AC DZ). Mesh lines are removed for clarity.

During loading steps, evolutions of bone density, and consequently, modulus were predicted in subchondral cortical bone, and subchondral trabecular bone (Figure 27). A bone remodeling (*i.e.* stiffening) response was predicted in subchondral bone near the interface between subchondral cortical bone and calcified cartilage where subchondral cortical bone was 5.9% and 11.7% stiffer compared to initial stiffness following cycles 1 and 2, respectively. At the interface between subchondral cortical bone and subchondral trabecular bone, subchondral cortical bone was 25.8% and 64.7% stiffer compared to the initial stiffness following cycles 1 and 2, respectively. A bone resorption (*i.e.* softening) response was predicted towards the center of the subchondral cortical bone region with maximum stiffness decreasing 2.8% and 6.2% compared to the initial stiffness following cycles 1 and 2, respectively. Similarly, a 2.5% increase in stiffness was predicted in subchondral trabecular bone following cycle 1 with no change as a result of cycle 2.

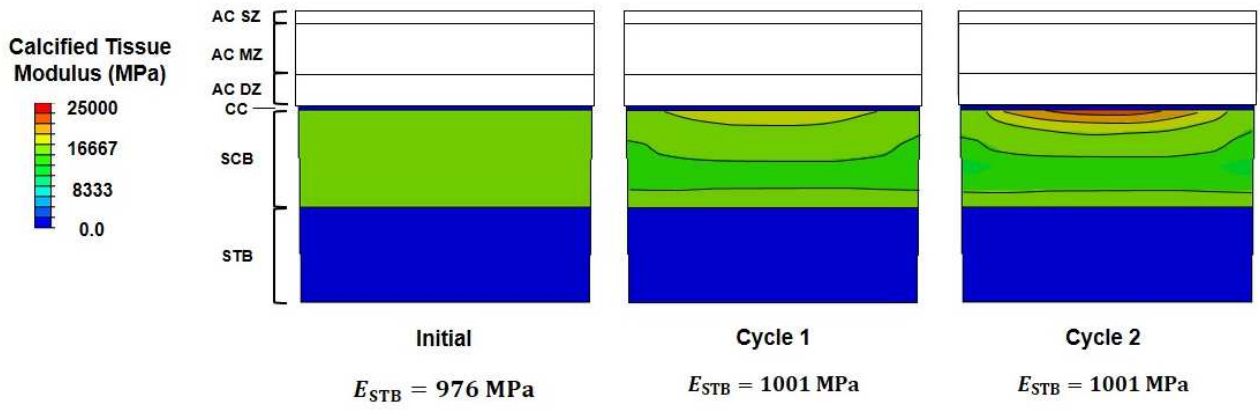

Figure 27. Contour plot showing evolution of calcified tissue modulus as a result of spherical indentation loading at the articular surface in subchondral cortical bone (SCB) and subchondral trabecular bone (STB) in a plane directly beneath the indenter. An initially uniform modulus evolved following 10,000 loading repetitions for two cycles. E_{STB} is the modulus of STB. Brackets denote differential material regions including articular cartilage superficial zone (AC SZ), articular cartilage middle zone (AC MZ), articular cartilage deep zone (AC DZ), calcified cartilage (CC), subchondral cortical bone (SCB), and subchondral trabecular bone (STB). Note that each cycle as presented corresponds to a cumulative response as a result of 10,000 varied indentation depth loading cycles.

With additional cycles of loading, the remodeling response maintained a similar pattern through the depths of bone tissue with increased magnitudes (Figure 28).

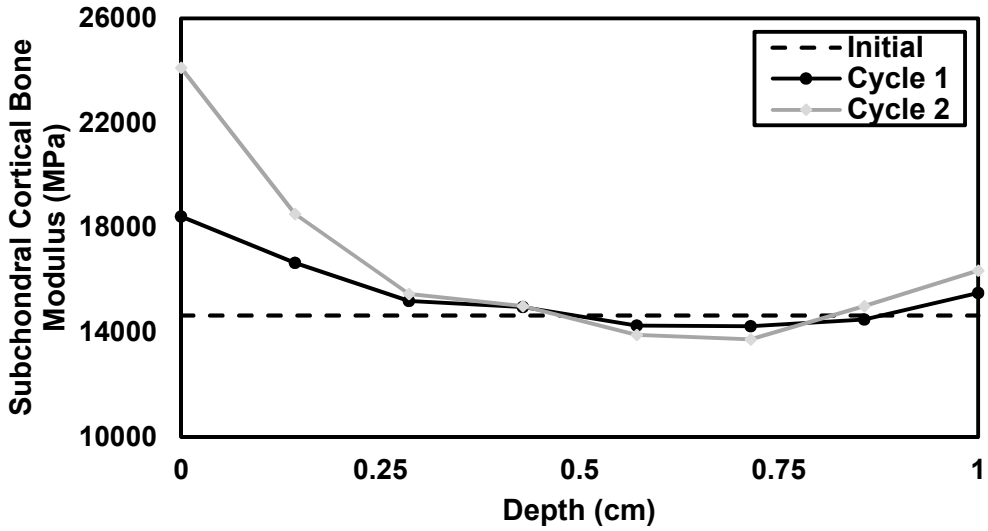

Figure 28. Plot showing evolution of subchondral bone modulus as a function of depth directly beneath the spherical indenter due to remodeling from indentation loading. A depth of 0 cm corresponds to the interface of subchondral bone and calcified cartilage, and depth of 1 cm corresponds to the interface of subchondral cortical bone and subchondral trabecular bone. Cycles 1 and 2 correspond to long term cyclic loading of 10,000 high strain load repetitions of varied indentation depth.

4.5 Discussion

A model was developed with the capacity to simulate both damage to AC, SCB remodeling, and STB remodeling in a single simulation of the BCU. This capability enables simulation of the paramount mechanical evolutions in synovial joints with OA. Recently, a previously established anisotropic constitutive model of AC (Stender *et al.,* 2012) was updated to include a strain-based elastic brittle collagen fibril damage and volumetric compression based glycosaminoglycan molecule damage (Stender *et al.,* 2015) as used here to model AC. An established model of bone remodeling was used to model time-dependent subchondral cortical and trabecular bone remodeling (Beaupré *et al.*, 1990a; 1990b) with a remodeling curve as used by Carpenter and

Carter (2008). Overloading indentation simulations predicted both AC damage, SCB changes, and STB remodeling. These results indicate that there are mechanical effects of damage and remodeling in the BCU, and that initial changes may lead to long term negative effects following long term loading and/or overloading scenarios.

This modeling enables previously unforeseen predictions of the BCU that may be the initial changes that eventually lead to OA. The combination of bone remodeling and AC damage models enables coupling of effects between evolutionary models not previously possible, but believed to occur with OA (Radin & Rose, 1986; Burr, 2004; Burr & Gallant, 2012). For example, AC softening as a result of damage may lead to additional bone remodeling, and bone remodeling that leads to subchondral stiffening may induce additional AC damage leading to a progression of OA symptoms. Predicted changes in the overall force response as a result of AC damage and bone remodeling were subtle, but may have progressive negative consequences *in vivo*. As a result of bone remodeling and AC damage, indentation force at peak indentation depth decreased 0.4% and 0.8% following cycles 1 and 2, respectively versus with a model without bone remodeling and AC damage. Although bone remodeling and AC damage did not have significant impacts on the force response of the BCU in these results, as articular cartilage is eroded with the progression of OA it is likely that bone remodeling plays a more significant role in the overall stiffness of the BCU. In these simulations, bone remodeling and articular cartilage damage processes appear to be roughly independent in the as simulated initial phases of OA. Bone remodeling

activity is primarily present in subchondral cortical bone, and articular cartilage damage is present only in the superficial zone (Figure 29).

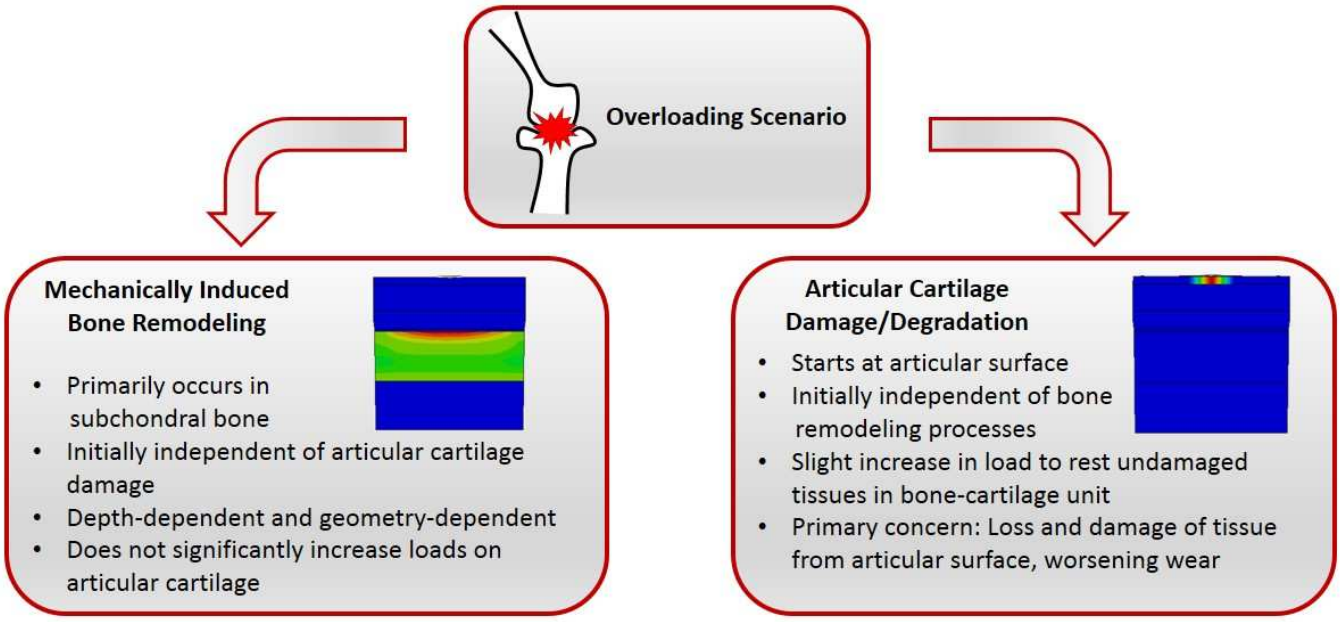

Figure 29. Tissue specific evolution as a result of overloading in the bone-cartilage unit.

Comprehensive validation of these model results would require quantification of an extensive list of experimental parameters in normal and osteoarthritic tissues that lies far outside the scope of this study. However, a comparison of these results to general experimental results of OA is possible to provide a limited verification of results of this work. For example, with OA decreases in GAG concentration have been observed to occur in AC (Appleyard, 2003; Temple-Wong *et al.*, 2009) and are consistent with the results of this model. Additionally, a significant decrease in the tensile modulus of AC has been observed with experimentally induced OA (Elliott *et al.*, 1999), suggesting that damage occurs to collagen fibrils which is again consistent

with our observed model results. Experimental studies of osteoarthritis show that collagen fibril damage (Hollander *et al.*, 1995) and GAG depletion (Rolauffs *et al.*, 2010) initiate at or near the articular surface, which is in agreement with the predictions of AC damage presented herein. Additionally, several studies have observed thickening of SCB with OA (Milz, *et al.*, 1995; Li & Aspden, 1997; Goldring & Goldring, 2010) which is consistent with the result of SCB stiffening calculated in this work. Future experimental results including a complete characterization of necessary biomechanical and biochemical parameters for a single tissue source, and corresponding evaluation of the changes with osteoarthritis would help to improve the validation of these results.

There are undoubtedly limitations associated with this current modeling approach. For example, the AC damage model used here is a strain-based formulation. Therefore, bone remodeling which may result in a general stiffening of the joint, but does not drastically change the strain response of the BCU is not likely to elicit damage to AC. Due to the long term time scales (*i.e.* days to years) of the bone remodeling simulated here, short term effects (*i.e.* seconds to hours) attributed to viscoelasticity, and poroelasticity of tissues of the BCU are neglected. Additional loading cycles resulted in bone stiffness values as a result of remodeling, that were beyond reasonable limits, and so were excluded from the analysis in this manuscript. Also, this model incorporates a wide variety of input parameters from differential sources, and thus does not represent a specific site and/or source of data but rather a generalized BCU model. Additionally, precise joint geometry and structure may play

a role in the response of this model, particularly with regards to the bone remodeling response, which is likely influenced by joint geometry. Further experimental work to establish a more comprehensive set of biochemical, mechanical, and geometric parameters for a single site and source would likely improve the accuracy of these results. Despite the limitations of this model, these results provide insight into the specific long-term mechanical response of the BCU that ultimately may contribute to OA initiation and progression.

4.6 Acknowledgements

This work was supported by NSF *CAREER* award #1055989, and the Innovative Grant Program at the University of Colorado at Boulder.

4.7 References

1. Appleyard, R. (2003). Topographical analysis of the structural, biochemical and dynamic biomechanical properties of cartilage in an ovine model of osteoarthritis. *Osteoarthritis and Cartilage*, *11*(1), 65–77. http://doi.org/10.1053/joca.2002.0867
2. Aspden, R. M., & Hukins, D. W. L. (1981). Collagen organization in articular cartilage, determined by X-ray diffraction, and its relationship to tissue function. *Proceedings of the Royal Society of London. Series B, Biological Sciences*, 299-304.

3. Beaupré, G. S., Orr, T. E., & Carter, D. R. (1990). An approach for time-dependent bone modeling and remodeling—theoretical development. *Journal of Orthopaedic Research*, *8*(5), 651-661.
4. Beaupré, G. S., Orr, T. E., & Carter, D. R. (1990). An approach for time-dependent bone modeling and remodeling—application: A preliminary remodeling simulation. *Journal of Orthopaedic Research*, *8*(5), 662-670.
5. Benninghoff, A. (1925). Form und Bau der Gelenkknorpel in ihren Beziehungen zur Funktion. II.Der Aufbau des Gelenkknorpels in seinen Beziehungen zur Funktion.Zeitschrift fur Zellforschung und mikroskopische Anatomie 2, 783-862.
6. Bobinac, D., Spanjol, J., Zoricic, S., & Maric, I. (2003). Changes in articular cartilage and subchondral bone histomorphometry in osteoarthritic knee joints in humans. *Bone*, *32*(3), 284–290. http://doi.org/10.1016/S8756-3282(02)00982-1
7. Borchers, L., and P. Reichart. "Three-dimensional stress distribution around a dental implant at different stages of interface development." *Journal of Dental Research* 62.2 (1983): 155-159
8. Botter, S. M., van Osch, G. J. V. M., Waarsing, J. H., van der Linden, J. C., Verhaar, J. A. N., Pols, H. A. P., … Weinans, H. (2008). Cartilage damage pattern in relation to subchondral plate thickness in a collagenase-induced model of osteoarthritis. *Osteoarthritis and Cartilage*, *16*(4), 506–514. http://doi.org/10.1016/j.joca.2007.08.005

9. Brandt, K. D., Radin, E. L., Dieppe, P. A., & Van De Putte, L. (2006). Yet more evidence that osteoarthritis is not a cartilage disease. *Annals of the Rheumatic Diseases*, *65*(10), 1261–1264.
10. Brocklehurst, R., Bayliss, M. T., Maroudas, A., Coysh, H. L., Freeman, M. A. R., Revell, P. A., & Ali, S. Y. (1984). The composition of normal and osteoarthritic articular cartilage from human knee joints. *J Bone Joint Surg Am*, *66*, 95–106.
11. Burr, D. (2004). Anatomy and physiology of the mineralized tissues: Role in the pathogenesis of osteoarthrosis. *Osteoarthritis and Cartilage*, *12*, 20–30. http://doi.org/10.1016/j.joca.2003.09.016
12. Burr, D. B., & Gallant, M. A. (2012). Bone remodeling in osteoarthritis. *Nature Reviews Rheumatology*, *8*(11), 665–673. http://doi.org/10.1038/nrrheum.2012.130
13. Carpenter, R. D., & Carter, D. R. (2008). The mechanobiological effects of periosteal surface loads. *Biomechanics and modeling in mechanobiology*, *7*(3), 227-242.
14. Clark, John M. "The organisation of collagen fibrils in the superficial zones of articular cartilage." *Journal of anatomy* 171 (1990): 117.
15. Elliott, D. M., Guilak, F., Parker Vail, T., Wang, J. Y., & Setton, L. A. (1999). Tensile properties of articular cartilage are altered by meniscectomy in a canine model of osteoarthritis. *Journal of orthopaedic research*, *17*(4), 503-508.

16. Eser, A., Tonuk, E., Akca, K., Dard, M. M., & Cehreli, M. C. (2013). Predicting bone remodeling around tissue- and bone-level dental implants used in reduced bone width. *Journal of Biomechanics*, *46*(13), 2250–2257. http://doi.org/10.1016/j.jbiomech.2013.06.025
17. Goldring, M. B., & Goldring, S. R. (2010). Articular cartilage and subchondral bone in the pathogenesis of osteoarthritis: Articular cartilage and subchondral bone. *Annals of the New York Academy of Sciences*, *1192*(1), 230–237. http://doi.org/10.1111/j.1749-6632.2009.05240.x
18. Grushko, G., Schneiderman, R., & Maroudas, A. (1989). Some biochemical and biophysical parameters for the study of the pathogenesis of osteoarthritis: a comparison between the processes of ageing and degeneration in human hip cartilage. *Connective tissue research*, *19*(2-4), 149-176.
19. Grynpas, M. D., Alpert, B., Katz, I., Lieberman, I., & Pritzker, K. P. H. (1991). Subchondral bone in osteoarthritis. *Calcified Tissue International*, *49*(1), 20–26.
20. Hollander, A. P., Pidoux, I., Reiner, A., Rorabeck, C., Bourne, R., & Poole, A. R. (1995). Damage to type II collagen in aging and osteoarthritis starts at the articular surface, originates around chondrocytes, and extends into the cartilage with progressive degeneration. *Journal of Clinical Investigation*, *96*(6), 2859.
21. Hyttinen, M. M., Holopainen, J., Rene van Weeren, P., Firth, E. C., Helminen, H. J., & Brama, P. A. (2009). Changes in collagen fibril network organization

and proteoglycan distribution in equine articular cartilage during maturation and growth. *Journal of anatomy*, *215*(5), 584-591.

22. Hwang, J., Bae, W. C., Shieu, W., Lewis, C. W., Bugbee, W. D., & Sah, R. L. (2008). Increased hydraulic conductance of human articular cartilage and subchondral bone plate with progression of osteoarthritis. *Arthritis & Rheumatism*, *58*(12), 3831–3842. http://doi.org/10.1002/art.24069
23. Li, B., & Aspden, R. M. (1997). Mechanical and material properties of the subchondral bone plate from the femoral head of patients with osteoarthritis or osteoporosis. *Annals of the Rheumatic Diseases*, *56*(4), 247–254.
24. LI, B., MARSHALL, D., ROE, M., & ASPDEN, R. M. (1999). The electron microscope appearance of the subchondral bone plate in the human femoral head in osteoarthritis and osteoporosis. *Journal of Anatomy*, *195*(1), 101–110.
25. Lories, R. J., & Luyten, F. P. (2010). The bone–cartilage unit in osteoarthritis. *Nature Reviews Rheumatology*, *7*(1), 43–49. http://doi.org/10.1038/nrrheum.2010.197
26. Maroudas, A., & Venn, M. (1977). Chemical composition and swelling of normal and osteoarthritic femoral head cartilage. II. Swelling. *Annals of the rheumatic diseases*, *36*(5), 399-406.
27. Mente, P. L., & Lewis, J. L. (1994). Elastic modulus of calcified cartilage is an order of magnitude less than that of subchondral bone. *Journal of Orthopaedic Research*, *12*(5), 637–647.

28. Milz, S., Eckstein, F., & Putz, R. (1995). The thickness of the subchondral plate and its correlation with the thickness of the uncalcified articular cartilage in the human patella. *Anatomy and Embryology*, *192*(5), 437–444.

29. Minns, R. J., & Steven, F. S. (1977). The collagen fibril organization in human articular cartilage. *Journal of anatomy*, *123*(Pt 2), 437.

30. Pan, J., Zhou, X., Li, W., Novotny, J. E., Doty, S. B., & Wang, L. (2009). In situ measurement of transport between subchondral bone and articular cartilage. *Journal of Orthopaedic Research*, *27*(10), 1347–1352. http://doi.org/10.1002/jor.20883

31. Pritzker, K. P. H., Gay, S., Jimenez, S. A., Ostergaard, K., Pelletier, J. P., Revell, P. A., ... & Van den Berg, W. B. (2006). Osteoarthritis cartilage histopathology: grading and staging. *Osteoarthritis and cartilage*, *14*(1), 13-29.

32. Radin, E. L., & Rose, R. M. (1986). Role of subchondral bone in the initiation and progression of cartilage damage. *Clinical orthopaedics and related research*, *213*, 34-40.

33. Rolauffs, B., Muehleman, C., Li, J., Kurz, B., Kuettner, K. E., Frank, E., & Grodzinsky, A. J. (2010). Vulnerability of the superficial zone of immature articular cartilage to compressive injury. *Arthritis & Rheumatism*, *62*(10), 3016–3027. http://doi.org/10.1002/art.27610

34. Saarakkala, S., Julkunen, P., Kiviranta, P., Mäkitalo, J., Jurvelin, J. S., & Korhonen, R. K. (2010). Depth-wise progression of osteoarthritis in human articular cartilage: investigation of composition, structure and biomechanics.

Osteoarthritis and Cartilage, *18*(1), 73–81. http://doi.org/10.1016/j.joca.2009.08.003

35. Setton, L. A., Elliott, D. M., & Mow, V. C. (1999). Altered mechanics of cartilage with osteoarthritis: human osteoarthritis and an experimental model of joint degeneration. *Osteoarthritis and Cartilage*, *7*(1), 2-14.

36. Sniekers, Y. H., Intema, F., Lafeber, F. P., van Osch, G. J., van Leeuwen, J. P., Weinans, H., & Mastbergen, S. C. (2008). A role for subchondral bone changes in the process of osteoarthritis; a micro-CT study of two canine models. *BMC Musculoskeletal Disorders*, *9*(1), 20. http://doi.org/10.1186/1471-2474-9-20

37. Stender, M. E., Regueiro, R. A., Klisch, S. M., & Ferguson, V. L. (2015). An Equilibrium Constitutive Model of Anisotropic Cartilage Damage to Elucidate Mechanisms of Damage Initiation and Progression. *Journal of biomechanical engineering*, *137*(8), 081010.

38. Stender, M. E., Raub, C. B., Yamauchi, K. A., Shirazi, R., Vena, P., Sah, R. L., … Klisch, S. M. (2012). Integrating qPLM and biomechanical test data with an anisotropic fiber distribution model and predictions of TGF- ß1 and IGF-1 regulation of articular cartilage fiber modulus. *Biomechanics and Modeling in Mechanobiology*. http://doi.org/10.1007/s10237-012-0463-y

39. Temple, M. M., Bae, W. C., Chen, M. Q., Lotz, M., Amiel, D., Coutts, R. D., & Sah, R. L. (2007). Age- and site-associated biomechanical weakening of human articular cartilage of the femoral condyle. *Osteoarthritis and Cartilage*, *15*(9), 1042–1052. http://doi.org/10.1016/j.joca.2007.03.005

40. Temple-Wong, M. M., Bae, W. C., Chen, M. Q., Bugbee, W. D., Amiel, D., Coutts, R. D., … Sah, R. L. (2009). Biomechanical, structural, and biochemical indices of degenerative and osteoarthritic deterioration of adult human articular cartilage of the femoral condyle. *Osteoarthritis and Cartilage*, *17*(11), 1469–1476. http://doi.org/10.1016/j.joca.2009.04.017

41. Thambyah, A., & Broom, N. (2007). On how degeneration influences load-bearing in the cartilage–bone system: a microstructural and micromechanical study. *Osteoarthritis and Cartilage*, *15*(12), 1410–1423. http://doi.org/10.1016/j.joca.2007.05.006

42. Venn, M., & Maroudas, A. (1977). Chemical composition and swelling of normal and osteoarthrotic femoral head cartilage. I. Chemical composition. *Annals of the Rheumatic Diseases*, *36*(2), 121-129.

43. Williams, G. M., Dills, K. J., Flores, C. R., Stender, M. E., Stewart, K. M., Nelson, L. M., … Klisch, S. M. (2010). Differential regulation of immature articular cartilage compressive moduli and Poisson's ratios by *in vitro* stimulation with IGF-1 and TGF-β1. *Journal of Biomechanics*, *43*(13), 2501–2507.

CHAPTER 5

Conclusions

The studies described in the preceding chapters were conducted 1) to develop and implement a constitutive damage model in order to simulate the degradation behavior of articular cartilage consistent with osteoarthritis, 2) to establish a poroelastic finite element model of the bone-cartilage unit to demonstrate the *in vivo* effects of increases in permeability as observed experimentally with osteoarthritis, and 3) to model the initiation and progression behavior of osteoarthritis by combining the articular cartilage damage model from 1, with an established bone remodeling algorithm. The principal findings of these studies are summarized below and suggestions for further related research directions are discussed.

5.1 Summary of Results

Articular cartilage damage behavior, including incremental damage and complete tissue failure was simulated using a constitutive damage model with strain-based damage criteria for collagen fibrils and glycosaminoglycan molecules (**Chapter 2**). Collagen fibril Lagrangian failure strain, E_N^D, was the primary factor in the progressive damage and failure behavior of articular cartilage in uniaxial stress in tension loading. Although the value of E_N^D is currently unknown for healthy articular cartilage, Chapter 2 includes a parameter study using $E_N^D = 0.15, 0.30, 0.45$ to

demonstrate that the articular cartilage response varied greatly with differential values of E_N^D. Glycosaminoglycan damage was assumed to result from a leaching and/or cleaving of glycosaminoglycan molecules as a result of volumetric compression. Decreases in glycosaminoglycan molecule concentration are observed to occur with overloading (Rolauffs *et al.* 2010) and with osteoarthritis (Maroudas & Venn, 1977; Temple-Wong *et al.* 2009). The constituent articular cartilage damage model from Chapter 2 developed a capability to model fully anisotropic collagen fibril damage and glycosaminoglycan molecule concentration decreases in 3-D analyses. Indentation damage simulations indicated that both collagen fibril and glycosaminoglycan damage initiate in the superficial zone of articular cartilage; a result that is consistent with experimental observations of early-term osteoarthritis (Hollander *et al.,* 1995). All damage model results from Chapter 2 are subject to an inherent mesh dependent localization of damage wherein damage can only occur within model element length scales. Therefore, the location of damage is dependent on the mesh size. The capability to model articular cartilage damage will enable future studies of the mechanical response of articular cartilage and degradations and failures with osteoarthritis and traumatic injuries.

Considering the simultaneous permeable behavior of all tissues of the bone-cartilage unit including articular cartilage, calcified cartilage, subchondral cortical bone, and subchondral trabecular bone in a fully poroelastic model showed that the permeability of articular cartilage is the controlling parameter in the poroelastic response of the bone-cartilage unit (**Chapter 3**). In contrast, the permeabilities of

calcified cartilage, subchondral cortical bone, and subchondral trabecular bone had a negligible effect on the poromechanics of the bone-cartilage unit. The poroelastic behavior of the bone-cartilage unit was shown to be dependent on loading and boundary conditions. For example, unconfined compression loading expelled fluid out of the free radial boundary, and spherical indentation expelled fluid from the articular surface. While articular cartilage permeability and boundary conditions play an important role, there are additional biomechanical factors that are also influential on the poromechanical response of the bone-cartilage unit including osteoarthritis.

Osteoarthritis has been shown to lead to an increase in permeability in all tissues of the bone-cartilage unit (Setton *et al.,* 1995; Hwang *et al.,* 2008). Increases in permeability as measured with osteoarthritis were shown to decrease the peak compressive force magnitude in unconfined compression, and to slightly increase the maximum indentation force in spherical indentation simulations. For spherical indentation simulations with healthy permeability properties, appreciable fluid velocities were present in all articular cartilage zones. However, appreciable fluid velocities were present only in the superficial zone with osteoarthritic bone-cartilage unit permeability properties. The osteochondral interface, or the transition from articular cartilage to calcified cartilage which was previously considered to be impermeable to fluid flow (Maroudas *et al.,* 1968) has been recently experimentally shown to be permeable (Hwang *et al.,* 2008). In spherical indentation simulations, fluid flow across the osteochondral interface that is consistent with contemporary

experiments was predicted (Akrill & Winlove, 2008; Pan *et al.,* 2009). Overall, these results demonstrate the importance of considering the poromechanics of the complete bone-cartilage unit when studying the *in vivo* poromechanical response of osteochondral tissues subject to healthy and osteoarthritic conditions.

Subchondral bone remodeling and articular cartilage damage/degradation may simultaneously occur, but they progress as independent processes during early-stage osteoarthritis (**Chapter 4**). Although experimentalists have quantified that both articular cartilage damage/degradation and subchondral bone remodeling occur with osteoarthritis there was not a clear understanding of which came first, or if there are coupling effects between bone remodeling and cartilage damage (Burr, 2004; Burr & Gallant, 2012). Simulation results indicate that damage to articular cartilage occurs in the superficial zone and remodeling with occurs primarily in subchondral cortical bone. Due to the already vast stiffness mismatch between articular cartilage and bone, remodeling in subchondral cortical and trabecular bone does not drastically alter the response of the bone-cartilage unit, or the loads seen in articular cartilage. Displacement controlled simulations showed a diminished peak load response (~2% decrease in peak load) with AC damage and bone remodeling that may lead to progression of damage and increased displacements in articular cartilage under normal loading conditions. Based on these simulation results, the initial response to overloading in the bone-cartilage unit is independent articular cartilage damage and subchondral bone remodeling. However, it is possible that progression towards late-

stage osteoarthritis involves further coupling between the effects of bone remodeling and articular cartilage damage.

5.2 Discussion of Future Research Directions

5.2.1 Experiments to Refine Modeling Results

The models developed and implemented in this dissertation require a wide variety of input parameters that must be obtained through experimental measurements. Thus, the modeling results as presented are inherently dependent on experimental measurements, and the availability and quality of experimental data. Additionally, there is a considerably large variability in data obtained from biological specimens making the analysis of a wide variety of biochemical, and biomechanical parameters difficult. One set of studies combined biochemical, biomechanical, and imaging data with a computational model to examine articular cartilage tissue from a specific location, age, and species (Williams *et al.,* 2010; Stender *et al.,* 2012). However, due to the ambitious modeling goals developed in this dissertation, it was not practical to develop a completely comprehensive data set as required for all simulations. Additional experimental studies with results that could be directly implemented to improve the accuracy of the models developed in this dissertation are described briefly below.

Experimental data could be easily and directly input into the models developed herein to improve the accuracy of modeling predictions. For example, uniaxial stress

in tension to failure data for articular cartilage can be used to establish a value for collagen fibril failure strain, E_N^D in Chapter 2. Using newborn bovine articular cartilage from the patellofemorral groove would enable expansion of previous results (Williams *et al.,* 2010; Stender *et al.,* 2012). Experimental measurements of permeability at different depths in osteoarthritic articular cartilage would eliminate the need to assume a uniform increase in permeability with osteoarthritis across all cartilage depths as done in Chapter 3. Currently, the bone remodeling response used in chapter 4 is as determined for the diaphysis of long bones, yet is applied to remodeling of subchondral cortical and trabecular bone. More precise measurements of subchondral bone remodeling could improve the accuracy of the bone remodeling simulated in chapter 4. Certainly, additional experimental results including the studies outlined above, would improve the confidence and accuracy of the computational results presented throughout this dissertation.

5.2.2 Modeling Based Extensions

In addition to the incorporation of higher quality and more specific experimental inputs, there are a number of improvements that could be made in future studies to improve the modeling-centric results developed here. The mesh-dependent localization of damage as discussed in detail in section 2.6 could be eliminated through the implementation of nonlocal effects and/or gradient enhanced damage methods (Peerlings *et al.,* 2001). The results in Chapter 2 could be extended to include the long-term cyclical fatigue damage behavior of articular cartilage

observed experimentally in tension (Weightman, 1976). Although not practical for this work due to the extreme computational expense, the incorporation of a physically realistic joint geometry would improve the relevance and applicability of the results from chapters 3 and 4. Furthermore, the development of a model of articular cartilage that is capable of simulating complete articular loss and/or wear, perhaps through element deletion criteria, would enable the simulation of late-stage osteoarthritis rather than only the early-stage osteoarthritis results in chapter 4. Additional development of the computational work in presented in these chapters would further the understanding of the mechanics of synovial joints and the initiation and progression behavior of osteoarthritis.

5.2.3 Translational Considerations

In addition to the relevance of this work to researchers considering the mechanics of the bone-cartilage unit and osteoarthritis, there are additional areas of research that may glean inspiration from these results. Through an improved understanding of the *in vivo* mechanics of the bone-cartilage unit, tissue engineering researchers may find value in the results of this dissertation while developing biomimetic engineering solutions to treat osteoarthritis and other biomechanical ailments. Additionally, the results from chapter 3 show perhaps counterintuitive results regarding the behavior of complex materials composed of tissues possessing differential permeabilities that may be of interest to researchers studying related problems in soil mechanics. This work also demonstrates the mechanics of interfaces

between mechanically mismatched materials, primarily articular cartilage, calcified cartilage, and subchondral bone. Such mechanical mismatches can occur in other engineering situations such as in fuel cells composed of differential material elements, or aircraft parts composed of composites materials and aluminum that must be interfaced. In the osteoarthritis research community, future experimental and computational studies seeking both an improved understanding of the mechanics of the bone-cartilage unit in healthy and osteoarthritic conditions may lead to vastly improved treatment techniques and quality of life for patients suffering from osteoarthritis.

5.3 References

1. Arkill, K. P., & Winlove, C. P. (2008). Solute transport in the deep and calcified zones of articular cartilage. *Osteoarthritis and Cartilage*, *16*(6), 708-714.
2. Burr, D. (2004). Anatomy and physiology of the mineralized tissues: Role in the pathogenesis of osteoarthrosis. *Osteoarthritis and Cartilage*, *12*, 20–30. http://doi.org/10.1016/j.joca.2003.09.016
3. Burr, D. B., & Gallant, M. A. (2012). Bone remodeling in osteoarthritis. *Nature Reviews Rheumatology*, *8*(11), 665–673. http://doi.org/10.1038/nrrheum.2012.130.
4. Hollander, A. P., Pidoux, I., Reiner, A., Rorabeck, C., Bourne, R., & Poole, A. R. (1995). Damage to type II collagen in aging and osteoarthritis starts at the articular surface, originates around chondrocytes, and extends into the

cartilage with progressive degeneration. *Journal of Clinical Investigation*, *96*(6), 2859.

5. Hwang, Jennifer, Won C. Bae, Wendy Shieu, *et al.* 2008 Increased Hydraulic Conductance of Human Articular Cartilage and Subchondral Bone Plate with Progression of Osteoarthritis. Arthritis & Rheumatism 58(12): 3831–3842.
6. Maroudas A, Bullough P, Swanson SA, Freeman MA. The permeability of articular cartilage. J Bone Joint Surg Br 1968;50:166–77.
7. Maroudas, A., & Venn, M. (1977). Chemical composition and swelling of normal and osteoarthritic femoral head cartilage. II. Swelling. *Annals of the rheumatic diseases*, *36*(5), 399-406.
8. Pan, J., Zhou, X., Li, W., Novotny, J. E., Doty, S. B., & Wang, L. (2009). In situ measurement of transport between subchondral bone and articular cartilage. *Journal of Orthopaedic Research*, *27*(10), 1347–1352. doi:10.1002/jor.20883
9. Peerlings, R. H. J., Geers, M. G. D., De Borst, R., & Brekelmans, W. A. M. (2001). A critical comparison of nonlocal and gradient-enhanced softening continua. *International Journal of solids and Structures*, *38*(44), 7723-7746.
10. Rolauffs, B., Muehleman, C., Li, J., Kurz, B., Kuettner, K. E., Frank, E., & Grodzinsky, A. J. 11 (2010). Vulnerability of the superficial zone of immature articular cartilage to compressive injury. *Arthritis & Rheumatism*, *62*(10), 3016–3027. doi:10.1002/art.27610

11. Setton LA, Mow VC, Muller FJ, Pita JC, Howell DS. Mechanical properties of canine articular cartilage are significantly altered following transection of the anterior cruciate ligament. J Orthop Res 1994;12:451–63.
12. Stender, M. E., Raub, C. B., Yamauchi, K. A., Shirazi, R., Vena, P., Sah, R. L., … Klisch, S. M. (2012). Integrating qPLM and biomechanical test data with an anisotropic fiber distribution model and predictions of TGF- ß1 and IGF-1 regulation of articular cartilage fiber modulus. *Biomechanics and Modeling in Mechanobiology*. doi:10.1007/s10237-012-0463-y
13. Temple-Wong, M. M., Bae, W. C., Chen, M. Q., Bugbee, W. D., Amiel, D., Coutts, R. D., … Sah, R. L. (2009). Biomechanical, structural, and biochemical indices of degenerative and osteoarthritic deterioration of adult human articular cartilage of the femoral condyle. *Osteoarthritis and Cartilage*, *17*(11), 1469–1476. doi:10.1016/j.joca.2009.04.017
14. Weightman, B. (1976). Tensile fatigue of human articular cartilage. *Journal of biomechanics*, *9*(4), 193-200.
15. Williams, G. M., Dills, K. J., Flores, C. R., Stender, M. E., Stewart, K. M., Nelson, L. M., … Klisch, S. M. (2010). Differential regulation of immature articular cartilage compressive moduli and Poisson's ratios by *in vitro* stimulation with IGF-1 and TGF-ß1. *Journal of Biomechanics*, *43*(13), 2501–2507.

Bibliography

1. Adouni, M., A. Shirazi-Adl, and R. Shirazi 2012 Computational Biodynamics of Human Knee Joint in Gait: From Muscle Forces to Cartilage Stresses. Journal of Biomechanics 45(12): 2149–2156.
2. Anderson, Andrew E., Benjamin J. Ellis, Steve A. Maas, and Jeffrey A. Weiss

   2010 Effects of Idealized Joint Geometry on Finite Element Predictions of Cartilage Contact Stresses in the Hip. Journal of Biomechanics 43(7): 1351–1357.
3. Appleyard, R. (2003). Topographical analysis of the structural, biochemical and dynamic biomechanical properties of cartilage in an ovine model of osteoarthritis. *Osteoarthritis and Cartilage*, *11*(1), 65–77. doi:10.1053/joca.2002.0867
4. Arkill, K.P., and C.P. Winlove 2008 Solute Transport in the Deep and Calcified Zones of Articular Cartilage. Osteoarthritis and Cartilage 16(6): 708–714.Asanbaeva, Anna, Koichi Masuda, Eugene J.-M. A. Thonar, Stephen M. Klisch, and Robert L. Sah 2007a Mechanisms of Cartilage Growth: Modulation of Balance between Proteoglycan and Collagen *in Vitro* Using Chondroitinase ABC. Arthritis & Rheumatism 56(1): 188–198.
5. Asanbaeva, A., Masuda, K., Thonar, E. J.-M. A., Klisch, S. M., & Sah, R. L. (2007b). Regulation of immature cartilage growth by IGF-I, TGF-ß1, BMP-

7, and PDGF-AB: role of metabolic balance between fixed charge and collagen network. *Biomechanics and Modeling in Mechanobiology*, *7*(4), 263–276. doi:10.1007/s10237-007-0096-8

6. Aspden, R. M., and D. W. L. Hukins 1981a Collagen Organization in Articular Cartilage, Determined by X-Ray Diffraction, and Its Relationship to Tissue Function. Proceedings of the Royal Society B: Biological Sciences 212(1188): 299–304.
7. Aspden, R. M and D.W.L. Hulkins 1981bCollagen Organization in Articular Cartilage, Determined by X-Ray Diffraction, and Its Relationship to Tissue Function. Proceedings of the Royal Society B: Biological Sciences 212(1188): 299–304.
8. Ateshian, G. A. (2007). Anisotropy of fibrous tissues in relation to the distribution of tensed and buckled fibers. *Journal of biomechanical engineering*,*129*(2), 240-249.
9. Ateshian, Gerard A., Steve Maas, and Jeffrey A. Weiss 2010 Finite Element Algorithm for Frictionless Contact of Porous Permeable Media Under Finite Deformation and Sliding. Journal of Biomechanical Engineering 132(6): 061006.
10. Ateshian, G., Warden, W., Kim, J., Grelsamer, R., Mow, V. (1997) Finite Deformation Biphasic Material Properties of Bovine Articular Cartilage from Confined Compression Experiments. *Journal of Biomechanics*. 30 (11), 1157-1164.

11. Ateshian, Gerard A., Vikram Rajan, Nadeen O. Chahine, Clare E. Canal, and Clark T. Hung 2009 Modeling the Matrix of Articular Cartilage Using a Continuous Fiber Angular Distribution Predicts Many Observed Phenomena. Journal of Biomechanical Engineering 131(6): 061003.
12. Bae, W. C., Temple, M. M., Amiel, D., Coutts, R. D., Niederauer, G. G., & Sah, R. L. (2003). Indentation testing of human cartilage: Sensitivity to articular surface degeneration. *Arthritis & Rheumatism*, *48*(12), 3382–3394. doi:10.1002/art.11347
13. Baroud, G., R. Falk, M. Crookshank, S. Sponagel, and T. Steffen 2004 Experimental and Theoretical Investigation of Directional Permeability of Human Vertebral Cancellous Bone for Cement Infiltration. Journal of Biomechanics 37(2): 189–196.
14. Beaupré, G. S., Orr, T. E., & Carter, D. R. (1990). An approach for time-dependent bone modeling and remodeling—theoretical development. *Journal of Orthopaedic Research*, *8*(5), 651-661.
15. Beaupré, G. S., Orr, T. E., & Carter, D. R. (1990). An approach for time-dependent bone modeling and remodeling—application: A preliminary remodeling simulation. *Journal of Orthopaedic Research*, *8*(5), 662-670.
16. Bellucci, G., & Seedhom, B. B. (2002). Tensile fatigue behaviour of articular cartilage. *Biorheology*, *39*(1), 193–199.

17. Bendjaballah, M. Z., A. Shirazi-Adl, and D. J. Zukor 1997 Finite Element Analysis of Human Knee Joint in Varus-Valgus. Clinical Biomechanics 12(3): 139–148.

18. Benninghoff, A. (1925). Form und Bau der Gelenkknorpel in ihren Beziehungen zur Funktion. II.Der Aufbau des Gelenkknorpels in seinen Beziehungen zur Funktion.Zeitschrift fur Zellforschung und mikroskopische Anatomie 2, 783-862.

19. Bobinac, D., Spanjol, J., Zoricic, S., & Maric, I. (2003). Changes in articular cartilage and subchondral bone histomorphometry in osteoarthritic knee joints in humans. *Bone*, *32*(3), 284–290. http://doi.org/10.1016/S8756-3282(02)00982-1

20. Borchers, L., and P. Reichart. "Three-dimensional stress distribution around a dental implant at different stages of interface development." *Journal of Dental Research* 62.2 (1983): 155-159.

21. Botter, S.M., G.J.V.M. van Osch, J.H. Waarsing, *et al.* 2008 Cartilage Damage Pattern in Relation to Subchondral Plate Thickness in a Collagenase-Induced Model of Osteoarthritis. Osteoarthritis and Cartilage 16(4): 506–514.

22. Bowman, Steven M., Tony M. Keaveny, Lorna J. Gibson, Wilson C. Hayes, and Thomas A. McMahon 1994 Compressive Creep Behavior of Bovine Trabecular Bone. Journal of Biomechanics 27(3): 301–310.

23. Brandt, K. D., E. L. Radin, P. A. Dieppe, and L. Van De Putte 2006 Yet More Evidence That Osteoarthritis Is Not a Cartilage Disease. Annals of the Rheumatic Diseases 65(10): 1261–1264.

24. Brocklehurst, R., M. T. Bayliss, A. Maroudas, *et al.* 1984 The Composition of Normal and Osteoarthritic Articular Cartilage from Human Knee Joints. J Bone Joint Surg Am 66: 95–106.

25. Brown, Thomas D., Eric L. Radin, R. Bruce Martin, and David B. Burr 1984Finite Element Studies of Some Juxtarticular Stress Changes due to Localized Subchondral Stiffening. Journal of Biomechanics 17(1): 11–24.

26. Buehler, Markus J 2007 Molecular Nanomechanics of Nascent Bone: Fibrillar Toughening by Mineralization. Nanotechnology 18(29): 295102.

27. Buck, R. J., Wyman, B. T., Le Graverand, M. hellio, Hudelmaier, M., Wirth, W., Eckstein, F., & A9001140 Investigators. (2009). Does the use of ordered values of subregional change in cartilage thickness improve the detection of disease progression in longitudinal studies of osteoarthritis? *Arthritis & Rheumatism*, *61*(7), 917–924. doi:10.1002/art.24613

28. Buckwalter, J. A., & Mankin, H. J. (1998). Articular cartilage repair and transplantation. *Arthritis & Rheumatism*, *41*(8), 1331-1342.

29. Buehler, M. J. (2007). Molecular nanomechanics of nascent bone: fibrillar toughening by mineralization. *Nanotechnology*, *18*(29), 295102. doi:10.1088/0957-4484/18/29/295102

30. Buehler, Markus J., and Theodor Ackbarow 2008 Nanomechanical Strength Mechanisms of Hierarchical Biological Materials and Tissues. Computer Methods in Biomechanics and Biomedical Engineering 11(6): 595–607.
31. Burr, D 2004 Anatomy and Physiology of the Mineralized Tissues: Role in the Pathogenesis of Osteoarthrosis. Osteoarthritis and Cartilage 12: 20–30.
32. Burr, David B., and Maxime A. Gallant 2012 Bone Remodeling in Osteoarthritis. Nature Reviews Rheumatology 8(11): 665–673.
33. Bush, P, P Hodkinson, G Hamilton, and A Hall 2005 Viability and Volume of Bovine Articular Chondrocytes Changes Following a Single Impact and Effects of Medium Osmolarity. Osteoarthritis and Cartilage 13(1): 54–65.
34. Buschmann M, Grodzinsky A. "A Molecular Model of Proteoglycan-AssociatedForces in Cartilage Mechanics." *Journal of Biomechanical Engineering*, 1995:117: 179-192
35. Calvo, B., E. Peña, M. A. Martinez, and M. Doblaré 2007 An Uncoupled Directional Damage Model for Fibred Biological Soft Tissues. Formulation and Computational Aspects. International Journal for Numerical Methods in Engineering 69(10): 2036–2057.
36. Campbell, Sara E., Virginia L. Ferguson, and Donna C. Hurley 2012 Nanomechanical Mapping of the Osteochondral Interface with Contact Resonance Force Microscopy and Nanoindentation. Acta Biomaterialia 8(12): 4389–4396.

37. Carnelli, Davide, Riccardo Lucchini, Matteo Ponzoni, Roberto Contro, and Pasquale Vena 2011 Nanoindentation Testing and Finite Element Simulations of Cortical Bone Allowing for Anisotropic Elastic and Inelastic Mechanical Response. Journal of Biomechanics 44(10): 1852–1858.
38. Carnelli, D., P. Vena, M. Dao, C. Ortiz, and R. Contro 2013 Orientation and Size-Dependent Mechanical Modulation within Individual Secondary Osteons in Cortical Bone Tissue. Journal of The Royal Society Interface 10(81): 20120953–20120953.
39. Carpenter, R. D., & Carter, D. R. (2008). The mechanobiological effects of periosteal surface loads. *Biomechanics and modeling in mechanobiology*, *7*(3), 227-242.
40. Chan, E. F., I.-L. Liu, E. J. Semler, *et al*. 2012 Association of 3-Dimensional Cartilage and Bone Structure with Articular Cartilage Properties in and Adjacent to Autologous Osteochondral Grafts after 6 and 12 Months in a Goat Model. Cartilage 3(3): 255–266.
41. Chen, S 2007 Depth-Dependent Compressive Properties of Normal Aged Human Femoral Head Articular Cartilage: Relationship to Fixed Charge Density. Osteoarthritis and Cartilage 9(6): 561–569.
42. Chen, S. S., Falcovitz, Y. H., Schneiderman, R., Maroudas, A., & Sah, R. L. (2001). Depth-dependent compressive properties of normal aged human femoral head articular cartilage: relationship to fixed charge density. *Osteoarthritis and Cartilage*, *9*(6), 561-569.

43. Clark, John M. "The organisation of collagen fibrils in the superficial zones of articular cartilage." *Journal of anatomy* 171 (1990): 117.

44. Cowin, S. C. 1999 Bone Poroelasticity. Journal of Biomechanics 32(3): 217–238.

45. Cotofana, S., Buck, R., Wirth, W., Roemer, F., Duryea, J., Nevitt, M., … Osteoarthritis Initiative Investigators Group. (2012). Cartilage thickening in early radiographic knee osteoarthritis: A within-person, between-knee comparison. *Arthritis Care & Research*, *64*(11), 1681–1690. doi:10.1002/acr.21719

46. Curl, W. W., Krome, J., Gordon, E. S., Rushing, J., Smith, B. P., & Poehling, G. G. (1997). Cartilage injuries: a review of 31,516 knee arthroscopies. *Arthroscopy: The Journal of Arthroscopic & Related Surgery*, *13*(4), 456–460.

47. Davison, L., Stevens, A. L., & Kipp, M. E. (1977). Theory of spall damage accumulation in ductile metals. *Journal of the Mechanics and Physics of Solids*, *25*(1), 11-28.

48. Davol, A., Bingham, M. S., Sah, R. L., & Klisch, S. M. (2007). A nonlinear finite element model of cartilage growth. *Biomechanics and Modeling in Mechanobiology*, *7*(4), 295–307. doi:10.1007/s10237-007-0098-6

49. Eckstein, F., M. Hudelmaier, and R. Putz 2006 The Effects of Exercise on Human Articular Cartilage. Journal of Anatomy 208(4): 491–512.

50. Elliott, D. M., Guilak, F., Parker Vail, T., Wang, J. Y., & Setton, L. A. (1999). Tensile properties of articular cartilage are altered by meniscectomy in a canine model of osteoarthritis. *Journal of orthopaedic research*, *17*(4), 503-508.

51. Eser, A., Tonuk, E., Akca, K., Dard, M. M., & Cehreli, M. C. (2013). Predicting bone remodeling around tissue- and bone-level dental implants used in reduced bone width. *Journal of Biomechanics*, *46*(13), 2250–2257. http://doi.org/10.1016/j.jbiomech.2013.06.025

52. Famaey, N., Vander Sloten, J., & Kuhl, E. (2013). A three-constituent damage model for arterial clamping in computer-assisted surgery. *Biomechanics and Modeling in Mechanobiology*, *12*(1), 123–136. doi:10.1007/s10237-012-0386-7

53. Federico, Salvatore, and Walter Herzog 2007 The Effect of Collagen Fibres on Permeability of Articular Cartilage. *In* Proceedings of the 31st Annual Meeting of the American Society of Biomechanics. http://www.asbweb.org/conferences/2007/149.pdf, accessed September 30, 2013.

54. Ferguson, V. L., Bushby, A. J., & Boyde, A. (2003). Nanomechanical properties and mineral concentration in articular calcified cartilage and subchondral bone. *Journal of Anatomy*, *203*(2), 191–202.

55. Ferguson, V. L., Bushby, A. J., Firth, E. C., Howell, P. G., & Boyde, A. (2007). Exercise does not affect stiffness and mineralisation of third

metacarpal condylar subarticular calcified tissues in 2 year old thoroughbred racehorses.*European cells & materials*, *16*, 40-6.

56. Ferguson, S. J., J. T. Bryant, R. Ganz, and K. Ito 2000 The Influence of the Acetabular Labrum on Hip Joint Cartilage Consolidation: A Poroelastic Finite Element Model. Journal of Biomechanics 33(8): 953–960.

57. Ferguson, Virginia L., Andrew J. Bushby, and Alan Boyde 2003 Nanomechanical Properties and Mineral Concentration in Articular Calcified Cartilage and Subchondral Bone. Journal of Anatomy 203(2): 191–202.

58. Ficklin, Timothy, Gregory Thomas, James C. Barthel, *et al.* 2007 Articular Cartilage Mechanical and Biochemical Property Relations before and After *in Vitro* Growth. Journal of Biomechanics 40(16): 3607–3614.

59. Gajewski, Tomasz, Hannah Weisbecker, Gerhard A. Holzapfel, and Tomasz Lodygowski 2013 Implementation of a Hyperelastic Model for Arterial Layers Considering Damage and Distributed Collagen Fiber Orientations. http://www.ikb.poznan.pl/tomasz.gajewski/cad.put.poznan.pl/TG/cmm2013_gajewski_weisbecker_holzapfel_logydowski.pdf, accessed October 31, 2013.

60. Galbusera, Fabio, Maxim Bashkuev, Hans-Joachim Wilke, Aboulfazl Shirazi-Adl, and Hendrik Schmidt 2012 Comparison of Various Contact Algorithms for Poroelastic Tissues. Computer Methods in Biomechanics and Biomedical Engineering: 1–12.

61. Gautier, E., D. Kolker, and R. P. Jakob 2002 Treatment of Cartilage Defects of the Talus by Autologous Osteochondral Grafts. Journal of Bone & Joint Surgery, British Volume 84(2): 237–244.

62. Gautieri, Alfonso, Simone Vesentini, Alberto Redaelli, and Markus J. Buehler 2011 Hierarchical Structure and Nanomechanics of Collagen Microfibrils from the Atomistic Scale Up. Nano Letters 11(2): 757–766.

63. Genin, Guy M., Alistair Kent, Victor Birman, *et al.* 2009 Functional Grading of Mineral and Collagen in the Attachment of Tendon to Bone. Biophysical Journal 97(4): 976–985.

64. Goldring, Mary B., and Steven R. Goldring 2010 Articular Cartilage and Subchondral Bone in the Pathogenesis of Osteoarthritis: Articular Cartilage and Subchondral Bone. Annals of the New York Academy of Sciences 1192(1): 230–237.

65. Gomoll, Andreas H., Henning Madry, Gunnar Knutsen, *et al.* 2010 The Subchondral Bone in Articular Cartilage Repair: Current Problems in the Surgical Management. Knee Surgery, Sports Traumatology, Arthroscopy 18(4): 434–447.

66. Gratz, Kenneth R., Benjamin L. Wong, Won C. Bae, and Robert L. Sah 2009 The Effects of Focal Articular Defects on Cartilage Contact Mechanics. Journal of Orthopaedic Research 27(5): 584–592.

67. Grushko, G., Schneiderman, R., & Maroudas, A. (1989). Some biochemical and biophysical parameters for the study of the pathogenesis of

osteoarthritis: a comparison between the processes of ageing and degeneration in human hip cartilage. *Connective tissue research*, *19*(2-4), 149-176.

68. Grynpas, M. D., Alpert, B., Katz, I., Lieberman, I., & Pritzker, K. P. H. (1991). Subchondral bone in osteoarthritis. *Calcified Tissue International*, *49*(1), 20–26.

69. Gupta, H.S., S. Schratter, W. Tesch, *et al*. 2005 Two Different Correlations between Nanoindentation Modulus and Mineral Content in the Bone–cartilage Interface. Journal of Structural Biology 149(2): 138–148.

70. Harrigan, Timothy P., Murali Jasty, Robert W. Mann, and William H. Harris

1988 Limitations of the Continuum Assumption in Cancellous Bone. Journal of Biomechanics 21(4): 269–275.

71. Hauch, K.N., M.L. Oyen, G.M. Odegard, and T.L. Haut Donahue 2009 Nanoindentation of the Insertional Zones of Human Meniscal Attachments into Underlying Bone. Journal of the Mechanical Behavior of Biomedical Materials 2(4): 339–347.

72. Hazelwood, S. J., Bruce Martin, R., Rashid, M. M., & Rodrigo, J. J. (2001). A mechanistic model for internal bone remodeling exhibits different dynamic responses in disuse and overload. *Journal of Biomechanics*, *34*(3), 299–308.

73. Hollander, A. P., Pidoux, I., Reiner, A., Rorabeck, C., Bourne, R., & Poole, A. R. (1995). Damage to type II collagen in aging and osteoarthritis starts at the articular surface, originates around chondrocytes, and extends into the cartilage with progressive degeneration. *Journal of Clinical Investigation*, *96*(6), 2859.

74. Holmes, M. H., and V. C. Mow 1990 The Nonlinear Characteristics of Soft Gels and Hydrated Connective Tissues in Ultrafiltration. Journal of Biomechanics 23(11): 1145–1156.

75. Hosseini, S.M., W. Wilson, K. Ito, and C.C. van Donkelaar 2014 A Numerical Model to Study Mechanically Induced Initiation and Progression of Damage in Articular Cartilage. Osteoarthritis and Cartilage 22(1): 95–103.

76. Hull, M. L. 2002 A Finite Element Model of the Human Knee Joint for the Study of Tibio-Femoral Contact. Journal of Biomechanical Engineering 124(3): 273.

77. Hwang, Jennifer, Won C. Bae, Wendy Shieu, *et al.* 2008 Increased Hydraulic Conductance of Human Articular Cartilage and Subchondral Bone Plate with Progression of Osteoarthritis. Arthritis & Rheumatism 58(12): 3831–3842.

78. Hwang, J., E. M. Kyubwa, W. C. Bae, *et al.* 2010 *In Vitro* Calcification of Immature Bovine Articular Cartilage: Formation of a Functional Zone of Calcified Cartilage. Cartilage 1(4): 287–297.

79. Hyttinen, M. M., Holopainen, J., Rene van Weeren, P., Firth, E. C., Helminen, H. J., & Brama, P. A. (2009). Changes in collagen fibril network organization and proteoglycan distribution in equine articular cartilage during maturation and growth. *Journal of anatomy*, *215*(5), 584-591.

80. Jeffrey, Janet E., L. Anne Thomson, and Richard M. Aspden 1997 Matrix Loss and Synthesis Following a Single Impact Load on Articular Cartilage *in Vitro*. Biochimica et Biophysica Acta (BBA)-General Subjects 1334(2): 223–232.

81. Julkunen, Petro, Rami K. Korhonen, Walter Herzog, and Jukka S. Jurvelin 2008 Uncertainties in Indentation Testing of Articular Cartilage: A Fibril-Reinforced Poroviscoelastic Study. Medical Engineering & Physics 30(4): 506–515.

82. Kersting, Uwe G., Johann J. Stubendorff, Matthias C. Schmidt, and Gert-Peter Brüggemann 2005 Changes in Knee Cartilage Volume and Serum COMP Concentration after Running exercise1. Osteoarthritis and Cartilage 13(10): 925–934.

83. Kitahara, Sota, Koichi Nakagawa, Robert L. Sah, *et al.* 2008 *In Vivo* Maturation of Scaffold-Free Engineered Articular Cartilage on Hydroxyapatite. Tissue Engineering Part A 14(11): 1905–1913.

84. Kiviranta, P., Rieppo, J., Korhonen, R. K., Julkunen, P., Töyräs, J., & Jurvelin, J. S. (2006). Collagen network primarily controls Poisson's ratio

of bovine articular cartilage in compression. *Journal of Orthopaedic Research*, *24*(4), 690–699. doi:10.1002/jor.20107

85. Klein, Travis J., Manu Chaudhry, Won C. Bae, and Robert L. Sah 2007 Depth-Dependent Biomechanical and Biochemical Properties of Fetal, Newborn, and Tissue-Engineered Articular Cartilage. Journal of Biomechanics 40(1): 182–190.

86. Klisch, Stephen M., Silvia S. Chen, Robert L. Sah, and Anne Hoger 2003 A Growth Mixture Theory for Cartilage With Application to Growth-Related Experiments on Cartilage Explants. Journal of Biomechanical Engineering 125(2): 169.

87. Kopperdahl, David L., and Tony M. Keaveny 1998 Yield Strain Behavior of Trabecular Bone. Journal of Biomechanics 31(7): 601–608.

88. Korhonen, R. K., Laasanen, M. S., Töyräs, J., Lappalainen, R., Helminen, H. J., & Jurvelin, J. S. (2003). Fibril reinforced poroelastic model predicts specifically mechanical behavior of normal, proteoglycan depleted and collagen degraded articular cartilage. *Journal of Biomechanics*, *36*(9), 1373–1379. doi:10.1016/S0021-9290(03)00069-1

89. Kuettner, Klaus E. "Biochemistry of articular cartilage in health and disease."*Clinical Biochemistry*, 1992: 25(3): 155-163.

90. Lai, W. M., Hou, J. S., & Mow, V. C. (1991). A triphasic theory for the swelling and deformation behaviors of articular cartilage. *Journal of biomechanical engineering*, *113*(3), 245-258.

91.. Lai, W. M., Mow, V. C., & Roth, V. (1981). Effects of nonlinear strain-dependent permeability and rate of compression on the stress behavior of articular cartilage. *Journal of biomechanical engineering*, *103*(2), 61-66.

92. Lanir, Y. (1983). Constitutive equations for fibrous connective tissues. *Journal of biomechanics*, *16*(1), 1-12.

93. Laursen, Tod A., Michael A. Puso, and Jessica Sanders 2012 Mortar Contact Formulations for Deformable–deformable Contact: Past Contributions and New Extensions for Enriched and Embedded Interface Formulations. Computer Methods in Applied Mechanics and Engineering 205-208: 3–15.

94. Lei, F., & Szeri, A. Z. (2006). The influence of fibril organization on the mechanical behaviour of articular cartilage. *Proceedings of the Royal Society A: Mathematical, Physical and Engineering Sciences*, *462*(2075), 3301–3322. doi:10.1098/rspa.2006.1732

95. Lei, Fulin, and Andras Z. Szeri 2006 The Influence of Fibril Organization on the Mechanical Behaviour of Articular Cartilage. Proceedings of the Royal Society A: Mathematical, Physical and Engineering Sciences 462(2075): 3301–3322.

96. Li, Baohua, and Richard M. Aspden 1997 Mechanical and Material Properties of the Subchondral Bone Plate from the Femoral Head of Patients with Osteoarthritis or Osteoporosis. Annals of the Rheumatic Diseases 56(4): 247–254.

97. Li, Baohua, Deborah Marshall, Martin Roe, and Richhard M. Aspden 1999 The Electron Microscope Appearance of the Subchondral Bone Plate in the Human Femoral Head in Osteoarthritis and Osteoporosis. Journal of Anatomy 195(1): 101–110.

98. Li, Guoan, Orlando Lopez, and Harry Rubash 2001 Variability of a Three-Dimensional Finite Element Model Constructed Using Magnetic Resonance Images of a Knee for Joint Contact Stress Analysis. Journal of Biomechanical Engineering 123(4): 341.

99. Li, L. P., M. D. Buschmann, and A. Shirazi-Adl 2000 A Fibril Reinforced Nonhomogeneous Poroelastic Model for Articular Cartilage: Inhomogeneous Response in Unconfined Compression. Journal of Biomechanics 33(12): 1533–1541.

100. Li, L. P., Buschmann, M. D., & Shirazi-Adl, A. (2003). Strain-rate Dependent Stiffness of Articular Cartilage in Unconfined Compression. *Journal of Biomechanical Engineering*, *125*(2), 161. doi:10.1115/1.1560142

101. Li, L. P., J. Soulhat, M. D. Buschmann, and A. Shirazi-Adl 1999 Nonlinear Analysis of Cartilage in Unconfined Ramp Compression Using a Fibril Reinforced Poroelastic Model. Clinical Biomechanics 14(9): 673–682.

102. Lima, Eric G., Robert L. Mauck, Shelley H. Han, *et al.* 2004 Functional Tissue Engineering of Chondral and Osteochondral Constructs. Biorheology 41(3): 577–590.

103. Lin, P. (2004). Increased stromelysin-1 (MMP-3), proteoglycan degradation (3B3- and 7D4) and collagen damage in cyclically load-injured articular cartilage. *Osteoarthritis and Cartilage*, *12*(6), 485–496. doi:10.1016/j.joca.2004.02.012

104. Loret, B., & Simões, F. M. (2004). Articular cartilage with intra-and extrafibrillar waters: a chemo-mechanical model. *Mechanics of Materials*, *36*(5), 515-541.

105. Lories, Rik J., and Frank P. Luyten 2010 The Bone–cartilage Unit in Osteoarthritis. Nature Reviews Rheumatology 7(1): 43–49.

106. Maroudas, A., Bannon, C. Measurement of swelling pressure in cartilage and comparison with the osmotic pressure of constituent proteoglycans. Biorheology 1981: 18(3-6): 619-632

107. Maroudas A, Bullough P, Swanson SA, Freeman MA. The permeability of articular cartilage. J Bone Joint Surg Br 1968;50:166–77

108. Maroudas, A., M. T. Bayliss, and M. F. Venn 1980 Further Studies on the Composition of Human Femoral Head Cartilage. Annals of the Rheumatic Diseases 39(5): 514–523.

109. Maroudas, A., Muir, H., & Wingham, J. (1969). The correlation of fixed negative charge with glycosaminoglycan content of human articular cartilage. *Biochimica et Biophysica Acta (BBA)-General Subjects*, *177*(3), 492-500.

110. Maroudas, A., & Venn, M. (1977). Chemical composition and swelling of normal and osteoarthrotic femoral head cartilage. II. Swelling. *Annals of the rheumatic diseases*, *36*(5), 399-406.

111. Mastbergen, S. C., and F. P. J. G. Lafeber 2011 Changes in Subchondral Bone Early in the Development of Osteoarthritis. Arthritis & Rheumatism 63(9): 2561–2563.

112. McCormack, T., & Mansour, J. M. (1997). Reduction in tensile strength of cartilage precedes surface damage under repeated compressive loading *in vitro*. *Journal of Biomechanics*, *31*(1), 55–61.

113. Mente, P. L., and J. L. Lewis 1994 Elastic Modulus of Calcified Cartilage Is an Order of Magnitude Less than that of Subchondral Bone. Journal of Orthopaedic Research 12(5): 637–647.

114. Milz, S., F. Eckstein, and R. Putz 1995 The Thickness of the Subchondral Plate and Its Correlation with the Thickness of the Uncalcified Articular Cartilage in the Human Patella. Anatomy and Embryology 192(5): 437–444.

115. Minns, R. J., & Steven, F. S. (1977). The collagen fibril organization in human articular cartilage. *Journal of anatomy*, *123*(Pt 2), 437.

116. Mohan, Neethu, Nathan H. Dormer, Kenneth L. Caldwell, *et al.* 2011 Continuous Gradients of Material Composition and Growth Factors for Effective Regeneration of the Osteochondral Interface. Tissue Engineering Part A 17(21-22): 2845–2855.

117. Mononen, M. E., P. Julkunen, J. Töyräs, *et al.* 2010 Alterations in Structure and Properties of Collagen Network of Osteoarthritic and Repaired Cartilage Modify Knee Joint Stresses. Biomechanics and Modeling in Mechanobiology 10(3): 357–369.

118. Mononen, M.E., M.T. Mikkola, P. Julkunen, *et al.* 2012 Effect of Superficial Collagen Patterns and Fibrillation of Femoral Articular Cartilage on Knee Joint mechanics—A 3D Finite Element Analysis. Journal of Biomechanics 45(3): 579–587.

119. Morgan, Elise F., and Tony M. Keaveny 2001 Dependence of Yield Strain of Human Trabecular Bone on Anatomic Site. Journal of Biomechanics 34(5): 569–577.

120. Mullins, L. P., Bruzzi, M. S., & McHugh, P. E. (2009). Calibration of a constitutive model for the post-yield behaviour of cortical bone. *Journal of the Mechanical Behavior of Biomedical Materials*, *2*(5), 460–470. doi:10.1016/j.jmbbm.2008.11.003

121. Nabovati, A., Llewellin, E. W., & Sousa, A. C. (2009). A general model for the permeability of fibrous porous media based on fluid flow simulations using the lattice Boltzmann method. *Composites Part A: Applied Science and Manufacturing*, *40*(6), 860-869.

122. Nauman, Eric A., K. E. Fong, and T. M. Keaveny 1999 Dependence of Intertrabecular Permeability on Flow Direction and Anatomic Site. Annals of Biomedical Engineering 27(4): 517–524.

123. Niebur, G. L., M. J. Feldstein, J. C. Yuen, T. J. Chen, and T. M. Keaveny 2000 High-Resolution Finite Element Models with Tissue Strength Asymmetry Accurately Predict Failure of Trabecular Bone. Journal of Biomechanics 33(12): 1575–1583.

124. Norrdin, R. W., C. E. Kawcak, B. A. Capwell, and C. W. McIlwraith 1999 Calcified Cartilage Morphometry and Its Relation to Subchondral Bone Remodeling in Equine Arthrosis. Bone 24(2): 109–114.

125. Novakofski, K. D., Williams, R. M., Fortier, L. A., Mohammed, H. O., Zipfel, W. R., & Bonassar, L. J. (2014). Identification of cartilage injury using quantitative multiphoton microscopy. *Osteoarthritis and Cartilage*, *22*(2), 355–362. doi:10.1016/j.joca.2013.10.008

126. O'Hara, B. P., Urban, J. P., & Maroudas, A. (1990). Influence of cyclic loading on the nutrition of articular cartilage. *Annals of the Rheumatic Diseases*, *49*(7), 536–539.

127. Olsen, S., A. Oloyede, and C. Adam 2004 A Finite Element Formulation and Program to Study Transient Swelling and Load-Carriage in Healthy and Degenerate Articular Cartilage. Computer Methods in Biomechanics and Biomedical Engineering 7(2): 111–120.

128. Oungoulian, S. (2007). *Articular Cartilage Constitutive Modeling: A Polyconvex Strain Energy Function for Proteoglycan and Validation of a Growth Mixture Model with Collagen Remodeling: a Thesis* (Master's dissertation, California Polytechnic State University).

129. Paietta, Rachel C., Evalina L. Burger, and Virginia L. Ferguson 2013 Mineralization and Collagen Orientation throughout Aging at the Vertebral Endplate in the Human Lumbar Spine. Journal of Structural Biology. http://linkinghub.elsevier.com/retrieve/pii/S1047847713002177, accessed October 15, 2013.

130. Pan, J., Zhou, X., Li, W., Novotny, J. E., Doty, S. B., & Wang, L. (2009). In situ measurement of transport between subchondral bone and articular cartilage. *Journal of Orthopaedic Research*, *27*(10), 1347–1352. doi:10.1002/jor.20883

131. Peña, Estefanía, Begoña Calvo, Miguel Angel Martínez, and Manuel Doblaré 2007 Effect of the Size and Location of Osteochondral Defects in Degenerative Arthritis. A Finite Element Simulation. Computers in Biology and Medicine 37(3): 376–387.

132. Pierce, D. M., Ricken, T., & Holzapfel, G. A. (2013). A hyperelastic biphasic fibre-reinforced model of articular cartilage considering distributed collagen fibre orientations: continuum basis, computational aspects and applications. *Computer methods in biomechanics and biomedical engineering*, *16*(12), 1344-1361.

133. Pins, G. D., & Silver, F. H. (1995). A self-assembled collagen scaffold suitable for use in soft and hard tissue replacement. *Materials Science and Engineering: C*, *3*(2), 101-107.

134. Peerlings, R. H. J., Geers, M. G. D., De Borst, R., & Brekelmans, W. A. M. (2001). A critical comparison of nonlocal and gradient-enhanced softening continua. *International Journal of solids and Structures*, *38*(44), 7723-7746.

135. Pritzker, K. P. H., Gay, S., Jimenez, S. A., Ostergaard, K., Pelletier, J. P., Revell, P. A., ... & Van den Berg, W. B. (2006). Osteoarthritis cartilage histopathology: grading and staging. *Osteoarthritis and cartilage*, *14*(1), 13-29.

136. Puso, Michael A., and Tod A. Laursen 2004 A Mortar Segment-to-Segment Contact Method for Large Deformation Solid Mechanics. Computer Methods in Applied Mechanics and Engineering 193(6): 601–629.

137. Radin, EricL, IgorL Paul, and Robert M Rose 1972 Role of Mechanical Factors in Pathogenesis of Primary Osteoarthritis. The Lancet 299(7749): 519–522.

138. Radin, E. L., & Rose, R. M. (1986). Role of subchondral bone in the initiation and progression of cartilage damage. *Clinical orthopaedics and related research*, *213*, 34-40.

139. Rizkalla, G., Reiner, A., Bogoch, E., & Poole, A. R. (1992). Studies of the articular cartilage proteoglycan aggrecan in health and osteoarthritis. Evidence for molecular heterogeneity and extensive molecular changes in disease. *Journal of Clinical Investigation*, *90*(6), 2268.

140. Rodríguez, J. F., Cacho, F., Bea, J. A., & Doblaré, M. (2006). A stochastic-structurally based three dimensional finite-strain damage model for fibrous soft tissue. *Journal of the Mechanics and Physics of Solids*, *54*(4), 864-886.

141. Rodriguez, J. F., Alastrue, V., & Doblare, M. (2008). Finite element implementation of a stochastic three dimensional finite-strain damage model for fibrous soft tissue. *Computer Methods in Applied Mechanics and Engineering*,*197*(9), 946-958.

142. Rolauffs, B., Muehleman, C., Li, J., Kurz, B., Kuettner, K. E., Frank, E., & Grodzinsky, A. J. (2010). Vulnerability of the superficial zone of immature articular cartilage to compressive injury. *Arthritis & Rheumatism*, *62*(10), 3016–3027. doi:10.1002/art.27610

143. Saarakkala, S., P. Julkunen, P. Kiviranta, *et al*. 2010 Depth-Wise Progression of Osteoarthritis in Human Articular Cartilage: Investigation of Composition, Structure and Biomechanics. Osteoarthritis and Cartilage 18(1): 73–81.

144. Sasaki, Naoki, and Shingo Odajima 1996 Elongation Mechanism of Collagen Fibrils and Force-Strain Relations of Tendon at Each Level of Structural Hierarchy. Journal of Biomechanics 29(9): 1131–1136.

145. Sasazaki, Y., Shore, R., & Seedhom, B. B. (2006). Deformation and failure of cartilage in the tensile mode. *Journal of Anatomy*, *208*(6), 681–694.

146. Scherft, J. P. 1968 The Ultrastructure of the Organic Matrix of Calcified Cartilage and Bone in Embryonic Mouse Radii. Journal of Ultrastructure Research 23(3): 333–343

147. Schinagl, Robert M., Donnell Gurskis, Albert C. Chen, and Robert L. Sah

1997 Depth-Dependent Confined Compression Modulus of Full-Thickness Bovine Articular Cartilage. Journal of Orthopaedic Research 15(4): 499–506.

148. Schröder, J., & Neff, P. (2003). Invariant formulation of hyperelastic transverse isotropy based on polyconvex free energy functions. *International journal of solids and structures*, *40*(2), 401-445.

149. Setton, L. A., Elliott, D. M., & Mow, V. C. (1999). Altered mechanics of cartilage with osteoarthritis: human osteoarthritis and an experimentald model of joint degeneration. *Osteoarthritis and Cartilage*, *7*(1), 2-14.

150. Setton, L. A., Mow, V. C., & Howell, D. (1995). Mechanical behavior of articular cartilage in shear is altered by transection of the anterior cruciate ligament.*Journal of Orthopaedic Research*, *13*(4), 473-482.

151. Shirazi, R., and A. Shirazi-Adl 2009 Computational Biomechanics of Articular Cartilage of Human Knee Joint: Effect of Osteochondral Defects. Journal of Biomechanics 42(15): 2458–2465.

152. Shirazi, R., A. Shirazi-Adl, and M. Hurtig 2008 Role of Cartilage Collagen Fibrils Networks in Knee Joint Biomechanics under Compression. Journal of Biomechanics 41(16): 3340–3348.

153. Shirazi, R., P. Vena, R. L. Sah, and S. M. Klisch 2011 Modeling the Collagen Fibril Network of Biological Tissues as a Nonlinearly Elastic Material Using a Continuous Volume Fraction Distribution Function. Mathematics and Mechanics of Solids 16(7): 706–715.

154. Sniekers, Y. H., Intema, F., Lafeber, F. P., van Osch, G. J., van Leeuwen, J. P., Weinans, H., & Mastbergen, S. C. (2008). A role for subchondral bone changes in the process of osteoarthritis; a micro-CT study of two canine models. *BMC Musculoskeletal Disorders*, *9*(1), 20. http://doi.org/10.1186/1471-2474-9-20

155. Soltz, M. A., & Ateshian, G. A. (1998). Experimental verification and theoretical prediction of cartilage interstitial fluid pressurization at an impermeable contact interface in confined compression. *Journal of Biomechanics*, *31*(10), 927–934.

156. Sniekers, Yvonne H, Femke Intema, Floris PJG Lafeber, *et al.* 2008 A Role for Subchondral Bone Changes in the Process of Osteoarthritis; a Micro-CT Study of Two Canine Models. BMC Musculoskeletal Disorders 9(1): 20.

157. Soltz, Michael A., and Gerard A. Ateshian 1998 Experimental Verification and Theoretical Prediction of Cartilage Interstitial Fluid

Pressurization at an Impermeable Contact Interface in Confined Compression. Journal of Biomechanics 31(10): 927–934.

158. Stender, Michael E., Christopher B. Raub, Kevin A. Yamauchi, *et al*. 2012 Integrating qPLM and Biomechanical Test Data with an Anisotropic Fiber Distribution Model and Predictions of TGF- β1 and IGF-1 Regulation of Articular Cartilage Fiber Modulus. Biomechanics and Modeling in Mechanobiology. http://link.springer.com/10.1007/s10237-012-0463-y, accessed April 20, 2013.

159. Stender, M. E., Regueiro, R. A., Klisch, S. M., & Ferguson, V. L. (2015). An Equilibrium Constitutive Model of Anisotropic Cartilage Damage to Elucidate Mechanisms of Damage Initiation and Progression. *Journal of biomechanical engineering*, *137*(8), 081010.

160. St-Pierre, Jean-Philippe, Lu Gan, Jian Wang, *et al*. 2012 The Incorporation of a Zone of Calcified Cartilage Improves the Interfacial Shear Strength between *in Vitro*-Formed Cartilage and the Underlying Substrate. Acta Biomaterialia 8(4): 1603–1615.

161. Suri, S., Gill, S. E., de Camin, S. M., McWilliams, D. F., Wilson, D., & Walsh, D. A. (2007). Neurovascular invasion at the osteochondral junction and in osteophytes in osteoarthritis. *Annals of the rheumatic diseases*, *66*(11), 1423-1428.

162. Suri, S., & Walsh, D. A. (2012). Osteochondral alterations in Osteoarthritis. *Bone*, *51*(2), 204-211.

163. Swan, C. C., Lakes, R. S., Brand, R. A., & Stewart, K. J. (2003). Micromechanically Based Poroelastic Modeling of Fluid Flow in Haversian Bone. *Journal of Biomechanical Engineering*, *125*(1), 25. doi:10.1115/1.1535191

164. Tang, Y., R. Ballarini, M. J. Buehler, and S. J. Eppell 2010 Deformation Micromechanisms of Collagen Fibrils under Uniaxial Tension. Journal of The Royal Society Interface 7(46): 839–850.

165. Temple, M. M., Bae, W. C., Chen, M. Q., Lotz, M., Amiel, D., Coutts, R. D., & Sah, R. L. (2007). Age- and site-associated biomechanical weakening of human articular cartilage of the femoral condyle. *Osteoarthritis and Cartilage*, *15*(9), 1042–1052. doi:10.1016/j.joca.2007.03.005

166. Temple-Wong, M.M., W.C. Bae, M.Q. Chen, *et al.* 2009 Biomechanical, Structural, and Biochemical Indices of Degenerative and Osteoarthritic Deterioration of Adult Human Articular Cartilage of the Femoral Condyle. Osteoarthritis and Cartilage 17(11): 1469–1476.

167. Thambyah, A., & Broom, N. (2007). On how degeneration influences load-bearing in the cartilage–bone system: a microstructural and micromechanical study. *Osteoarthritis and Cartilage*, *15*(12), 1410–1423. http://doi.org/10.1016/j.joca.2007.05.006

168. Thibault, M., Robin Poole, A., & Buschmann, M. D. (2002). Cyclic compression of cartilage/bone explants in vitro leads to physical weakening,

mechanical breakdown of collagen and release of matrix fragments. *Journal of Orthopaedic Research*, *20*(6), 1265–1273.

169. Thomas, Gregory C., Anna Asanbaeva, Pasquale Vena, Robert L. Sah, and Stephen M. Klisch 2009 A Nonlinear Constituent Based Viscoelastic Model for Articular Cartilage and Analysis of Tissue Remodeling Due to Altered Glycosaminoglycan-Collagen Interactions. Journal of Biomechanical Engineering 131(10): 101002.

170. Thomopoulos, Stavros, Juan P. Marquez, Bradley Weinberger, Victor Birman, and Guy M. Genin 2006 Collagen Fiber Orientation at the Tendon to Bone Insertion and Its Influence on Stress Concentrations. Journal of Biomechanics 39(10): 1842–1851.

171. Urban, J. P. G. (1994). The chondrocyte: a cell under pressure. *Rheumatology*,*33*(10), 901-908.

172. Vahdati, Ali, and Diane R. Wagner 2009 Influence of Calcified Cartilage Zone Permeability in Mechanical Behavior of Articular Cartilage: A Finite Element Study. *In.* http://www.simulia.com/academics/research_pdfs/4_2011-04-08_163753_Vahdati%20SBC%202009.pdf, accessed October 3, 2013.

173. Van de Velde, Samuel K. 2009 Analysis of Tibiofemoral Cartilage Deformation in the Posterior Cruciate Ligament-Deficient Knee. The Journal of Bone and Joint Surgery (American) 91(1): 167.

174. Venn, M., & Maroudas, A. (1977). Chemical composition and swelling of normal and osteoarthrotic femoral head cartilage. I. Chemical composition. *Annals of the Rheumatic Diseases*, *36*(2), 121-129.

175. Wei, X., Räsänen, T., & Messner, K. (1998). Maturation-related compressive properties of rabbit knee articular cartilage and volume fraction of subchondral tissue. *Osteoarthritis and Cartilage*, *6*(6), 400–409.

176. Weightman, B. (1976). Tensile fatigue of human articular cartilage. *Journal of Biomechanics*, *9*(4), 193–200.

177. Weisbecker, Hannah, David M. Pierce, Peter Regitnig, and Gerhard A. Holzapfel 2012 Layer-Specific Damage Experiments and Modeling of Human Thoracic and Abdominal Aortas with Non-Atherosclerotic Intimal Thickening. Journal of the Mechanical Behavior of Biomedical Materials 12: 93–106.

178. Williams, Gregory M., Kristin J. Dills, Christian R. Flores, *et al.* 2010 Differential Regulation of Immature Articular Cartilage Compressive Moduli and Poisson's Ratios By *in Vitro* Stimulation with IGF-1 and TGF-ß1. Journal of Biomechanics 43(13): 2501–2507.

179. Williamson, A. K., Chen, A. C., & Sah, R. L. (2001). Compressive properties and function—composition relationships of developing bovine articular cartilage.*Journal of Orthopaedic Research*, *19*(6), 1113-1121.

180. Williamson, A. K., Chen, A. C., Masuda, K., Thonar, E. J.-M. A., & Sah, R. L. (2003). Tensile mechanical properties of bovine articular cartilage:

Variations with growth and relationships to collagen network components. *Journal of Orthopaedic Research*, *21*(5), 872–880. doi:10.1016/S0736-0266(03)00030-5

181. Wilson, W., Huyghe, J. M., & Donkelaar, C. C. (2006). Depth-dependent Compressive Equilibrium Properties of Articular Cartilage Explained by its Composition. *Biomechanics and Modeling in Mechanobiology*, *6*(1-2), 43–53. doi:10.1007/s10237-006-0044-z

182. Wilson, W., C.C. van Donkelaar, B. van Rietbergen, and R. Huiskes 2005a A Fibril-Reinforced Poroviscoelastic Swelling Model for Articular Cartilage. Journal of Biomechanics 38(6): 1195–1204.

183. Wilson, W., van Donkelaar, C. C., van Rietbergen, R., & Huiskes, R. (2005b). The role of computational models in the search for the mechanical behavior and damage mechanisms of articular cartilage. *Medical Engineering & Physics*, *27*(10), 810–826. doi:10.1016/j.medengphy.2005.03.004

184. Wilson, W., C.C. van Donkelaar, B. van Rietbergen, K. Ito, and R. Huiskes

2004 Stresses in the Local Collagen Network of Articular Cartilage: A Poroviscoelastic Fibril-Reinforced Finite Element Study. Journal of Biomechanics 37(3): 357–366.

185. Wilson, W, N Driessen, C Vandonkelaar, and K Ito 2006 Prediction of Collagen Orientation in Articular Cartilage by a Collagen Remodeling Algorithm. Osteoarthritis and Cartilage 14(11): 1196–1202.

186. Wong, Benjamin L., Won C. Bae, Kenneth R. Gratz, and Robert L. Sah 2008 Shear Deformation Kinematics during Cartilage Articulation: Effect of Lubrication, Degeneration, and Stress Relaxation. Molecular & Cellular Biomechanics: MCB 5(3): 197.

187. Wong, B.L., S.H. Chris Kim, J.M. Antonacci, C. Wayne McIlwraith, and R.L. Sah 2010 Cartilage Shear Dynamics during Tibio-Femoral Articulation: Effect of Acute Joint Injury and Tribosupplementation on Synovial Fluid Lubrication. Osteoarthritis and Cartilage 18(3): 464–471.

188. Wu, J. Z., W. Herzog, and E. M. Hasler 2002 Inadequate Placement of Osteochondral Plugs May Induce Abnormal Stress-Strain Distributions in Articular Cartilage-Finite Element Simulations. Medical Engineering & Physics 24(2): 85–97.

189. Zhang, Wei, Jialin Chen, Jiadong Tao, *et al.* 2013 The Promotion of Osteochondral Repair by Combined Intra-Articular Injection of Parathyroid Hormone-Related Protein and Implantation of a Bi-Layer Collagen-Silk Scaffold. Biomaterials 34(25): 6046–6057.